Table of Contents

Ocean Redox Evolution Past and Present

Dalton S. Hardisty[a,1] and Kimberly V. Lau[b,1]

[a]Department of Earth and Environmental Sciences, Michigan State University, East Lansing, MI, United States
[b]Department of Geosciences and Earth and Environmental Systems Institute, The Pennsylvania State University, University Park, PA, United States

Abstract

The availability and spatial landscape of marine oxygen and related redox-sensitive elemental cycles has changed dramatically over the last 4 billion years. This chapter uses a database framework to synthesize recent quantitative and conceptual advances in this story, emphasizing an integrated view of modern and ancient processes. We highlight three main timescales of marine redox evolution: modern and anthropogenic, glacial-interglacial, and geologic. On modern and anthropogenic timescales, the discussion focuses on defining redox thresholds and physical and biogeochemical mechanisms driving spatiotemporal variations. For ancient timescales, we synthesize proxy constraints on coupled ocean-atmosphere redox dynamics and feedbacks with biological and geologic evolution.

Keywords:

- Ancient seawater chemistry
- Biogeochemical cycles
- Carbon cycle
- GEOTRACES
- Oceanic Anoxic Events
- Ocean oxygenation
- Oxygen deficient zone
- Paleoredox proxies
- Redox-sensitive elements and their isotopes
- Sedimentary Geochemistry and Paleoenvironment Project
- Sediment diagenesis

Key points/objectives:

- Ocean redox on modern and anthropogenic timescales
- Origin, distribution, and characteristics of oxygen deficient zones
- Evolution of redox on glacial-interglacial timescales
- Evolution of ocean redox on geologic timescales
- Neoarchean disequilibria and oxygen oases

- The Great Oxidation Event and mid-Proterozoic redox
- Neoproterozoic through Paleozoic redox
- Deep ocean ventilation

Acknowledgements

This work is supported by grants from the Oceanographic and Earth Sciences Divisions of the National Science Foundation to DH and KL (OCE-1829406, SGP-2124802, FRES-2021324), a National Aeronautics and Space Administration Exobiology Grant to DH and KL (80NSSC22K1560), and a Sloan Research Foundation Fellowship to DH. Data compilations provided by Ben Gill (S isotopes), Ben Uveges (S-MIF), Devon Cole (Cr isotopes), and Josh Krissansen-Totton and Matt Saltzman (C isotopes). KL thanks Tamara Pico and Jerry Mitrovica for discussions about sea-level change and OMZs. This manuscript benefited from critical feedback from Tristan Horner and one anonymous reviewer. We additionally acknowledge our colleagues and collaborators at our current and past institutions—along with the oceanographic community as a whole—whose inclusiveness, countless conversations, and contagious scientific commitment and passion motivated this synthesis.

1 Introduction

A major challenge over the 21st century is documenting and predicting the impacts of ongoing climate change on Earth's atmosphere and ocean and how these changes may impact life. The ocean's dissolved oxygen (O_2) availability and its related redox state is no exception. Multiple studies since the beginning of the 21st century have documented declines in O_2 availability in the global ocean, tentatively linked to climate change, including the expansion of naturally existing O_2 deficient zones in the open ocean as well as the increased occurrence and frequency of low-O_2 waters along global coastlines. Urgent impetuses in light of these observations include: (1) understanding the mechanisms and feedbacks driving ongoing observations of marine O_2 decline; (2) incorporating these feedbacks into models intended to predict future marine O_2 decline, thus aiding strategic policy but also predicting where to look to observe and understand changes going forward; and (3) understanding the degree to which natural climate change in Earth's ancient past can provide quantitative insights into ongoing and future climate change.

Our ongoing anthropogenic experiment with climate change and the increased frequency of available data presents multiple opportunities to understand the Earth system across the past, present, and future. Indeed, we truly live in a golden age of observation, and once again, marine redox geochemistry is no exception. Modern seawater observations in databases and data products such as GEOTRACES, NOAA's World Ocean Atlas (WOA), among others (e.g., Ocean Observatories Initiative or OOI, World Ocean Climate Experiment or WOCE, Climate Variability and Predictability or CLIVAR, biogeochemical Argo), are at the forefront of calibrating models and understanding processes important for interpreting paleoredox conditions from sediment geochemistry archives—for example, cores collected through the International Ocean Discovery Program (IODP) and compilations available via the Sedimentary Geochemistry and Paleoenvironments Project (SGP; Farrell et al. (2021)). In this way, the long-established principle that the "present is the key to the past" should remain front and center; yet much of this potential currently remains untapped due to combinations of lag times and disconnects between merging insights and resources between modern and deep-time chemical oceanography research.

The goal of this synthesis is to pose and address major questions about Earth's present and past ocean redox chemistry. Why do redox states differ between modern O_2 minimum zones? How do modern O_2 spatial patterns inform the geochemical proxies that are used to interpret past ocean conditions? What was the tempo of ancient ocean oxidation and how did it relate to major tectonic and biotic changes? When did Earth's oceans transition from background reducing redox states to the background oxic conditions observed today? These are all questions at the forefront of connecting redox geochemistry across time and space. We aim to address each of them through discussion of recent breakthroughs—highlighting next steps and community challenges going forward—but also novel synthesis and discussion from integrating recent databases covering modern and ancient marine redox geochemistry. The topic of this synthesis chapter—ocean redox, past and present—is admittedly far-reaching, and hence we will not cover every aspect here. That said, there have been a range of reviews and important syntheses in the decade since the publication of the last Treatise chapter covering ancient redox (Lowenstein et al., 2013) and we will point the reader to these existing resources.

In light of these goals, we ultimately organize this synthesis into three main sections based on different time frames with distinct time-scale-dependent processes. **Modern:** An overview of emerging insights into variations in and drivers of modern spatiotemporal redox variations across the ocean's major O_2 deficient zones. This discussion is bolstered by multivariate constraints and visualizations of redox-sensitive and related elemental cycles from NOAA's WOA and GEOTRACES databases/products. **Recent:** An overview of recent findings and challenges regarding marine redox cycling on glacial-interglacial timescales. **Ancient:** An overview of recent findings and challenges regarding the oxygenation of Earth's oceans on geologic timescales, supported by explorations of novel paleoredox proxy compilations from the SGP database and other sources.

1.1 Nomenclature for tracers defining redox and O_2 levels

Modern chemical and paleo- oceanographers often use different as well as overlapping, but variably defined, nomenclature to discuss marine redox (reduction-oxidation) and O_2 levels. To circumvent this challenge, we broadly support the suggestion of Canfield and Thamdrup (2009)—i.e., that terms such as 'suboxic' are confusing and are best replaced by more specific terms defining the dominant electron acceptors in each zone. We support the continued expansion of this approach to the ancient—i.e., what major zone of electron acceptors does a given redox tracer define? We summarize these zones for common paleoredox proxies in **Figure 1**. The paleoredox proxies, which are discussed in detail in Section 4, are commonly trace elements with limited contribution to organic matter remineralization and can be directly related to the major electron acceptors to which their reduction or proxy expression most clearly overlaps. This concept applies to both water column and pore fluid redox conditions, which are distinct but represent a vertical continuum of the 'redox ladder'. We recognize that there can be significant overlap in these so-called 'zones' (for example nitrogenous and manganous), and when this is the case, this should be communicated. In alignment with previous work (Moffitt et al., 2015), we will consider "hypoxia"—a term that originated from physiological studies equivalent to 2 mg O_2 L^{-1} or ~61 µmol O_2 kg^{-1} (Hofmann et al., 2011)—as the O_2 threshold that characterizes oxygen deficient zones.

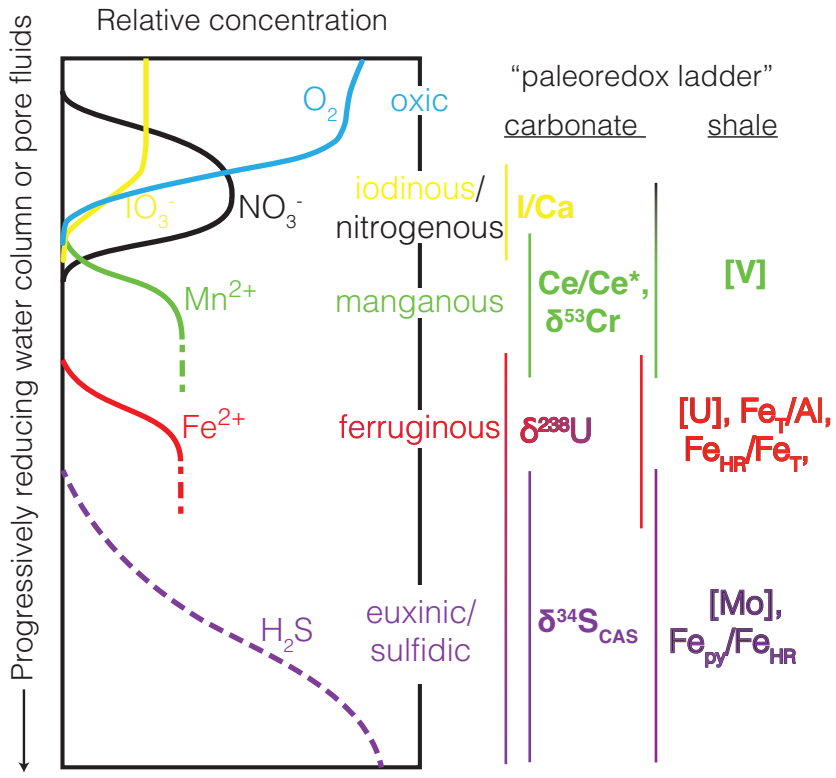

Figure 1. *Redox and paleoredox ladder. Includes redox-sensitive elements used to distinguish specific redox regimes and modern and paleoredox proxies from carbonates and shales that track those conditions. Note that the term euxinia is exclusive for water columns and 'sulfidic' is preferred for pore waters. Proxy details are discussed further in Section 4.*

Throughout this chapter, we will discuss redox dynamics of the ocean-atmosphere system using the framing shown in **Figure 2**. When and how the redox evolution of the ocean-atmosphere system proceeds through Earth history is broadly defined by four major Stages (Figure 2A-D). The key features of the oceanic redox structure include oxygenation of the atmosphere, which is described relative to present atmospheric levels (PAL). The shallow ocean generally refers to the uppermost 100-200 m (typically the photic zone) that can be influenced by atmospheric O_2 through wind-driven mixing. Vertical O_2 stratification defines much of Earth's past until the Paleozoic (Figure 2 A-C) and continues to be a feature where O_2 deficient or minimum zones develop (Figure 2C-D). The degree of O_2 consumption within these zones varies in the modern and has varied through Earth history, reaching euxinia (extreme reducing conditions where sulfide is available in the water column) further in the past (e.g., Figure 2C). Oxygen minimum zones (OMZs) differ from oxygen deficient zones (ODZs) in that the latter specifically refer to regions where O_2 levels are low enough to limit aerobic respiration, i.e. 'functional anoxia' characterized by denitrification and the presence of nitrite (generally requires sub-μM O_2; (Thamdrup et al., 2012)). In this Chapter, we generally refer to ODZs for consistency and because a key consideration for past and present marine redox conditions is the impact on marine animal habitability.

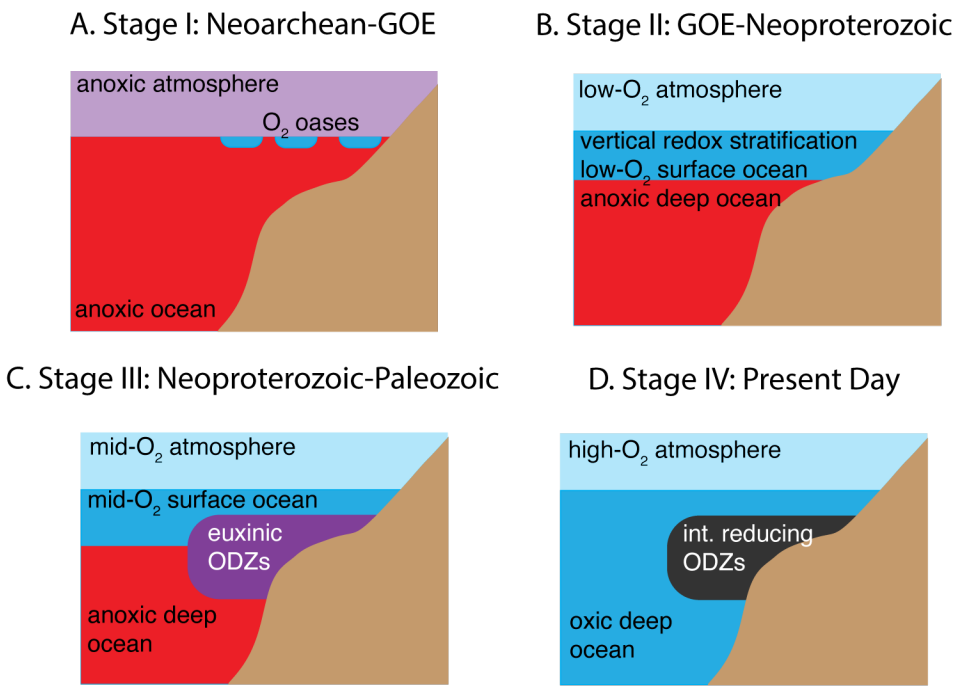

Figure 2. *Stages in oceanic redox structure through Earth history. Int = intermediate redox conditions (e.g., nitrogenous).*

1.2 Integrating mechanisms with a mass balance perspective of ocean O_2

The spatial distribution of O_2 and development of ODZs in the modern ocean highlights the processes and reactions within and between the atmosphere, surface ocean, and deep ocean reservoirs (**Figure 3**A). Today, nearly all the O_2 is present in the atmosphere (>99%) compared to the oceans (Keeling et al., 1993). In this case, air-sea exchange, temperature, and ocean circulation control the physical solubility of O_2, the physical transport of nutrients, and the biological processes that consume and produce O_2. Together, these dictate the spatial gradients of O_2 discussed in Section 2 and the temporal changes from the transition from an icehouse in Section 3. This can be considered the perspective of the O_2 system furthest from steady state, given that these processes vary on seasonal to decadal to millennial scales. Models that can simulate O_2 changes through these processes include some General Circulation Models (GCMs; e.g., Kwiatkowski et al. (2020)) and Regional Ocean Modeling System simulations (ROMS; e.g., Montes et al. (2014)).

Considerations of O_2 mass balance on longer time scales, beyond seasonal-millennial scales, are the focus of Section 4 (the ancient). On geologic time scales—which extend beyond those of the processes controlling the spatial gradients between the atmosphere, shallow ocean, and deep ocean—we can simplify the view of O_2 mass balance by focusing on a single atmosphere-ocean O_2 reservoir. Here, there are two additional time scales that are relevant to O_2 mass balance, and therefore the relationship between biogeochemical and geologic processes. The first concerns the inventory of the limiting nutrient, increases in primary productivity, and aerobic respiration/remineralization that drives O_2 demand, and is most relevant on timescales of ~10^4 years (**Figure 3**B; (Lenton et al., 2018)) and is partially discussed in Section 3. With higher nutrient delivery to the ocean-atmosphere system, primary productivity (**Equation 1**) increases, which

increases the flux of O_2 being added. This is generally balanced by an output flux where O_2 is consumed by aerobic respiration (e.g., **Equation 1**), which increases with higher primary productivity, akin to dead zones in the modern ocean that are dominated by continental runoff inputs. This simple mass balance can break down (i.e., the flux of O_2 produced from primary productivity does not equal the flux of O_2 consumed through aerobic respiration) in the case of transient increases or decreases to nutrients (primarily considered to be phosphate). Models that can simulate these processes include, but are not limited to, CANOPS (Ozaki et al., 2022), cGENIE (van de Velde et al., 2021), and LOSCAR (Zeebe, 2012); key to these are inclusion of nutrients and marine biogeochemical processes, ideally both in the water column and in the sediments.

However, it should be obvious that on long time scales and with the consideration of geologic processes, O_2 production and consumption through these two fluxes should balance (Lenton et al., 2018). When considering geologic processes, two key processes become critical (**Figure 3**C): (1) the geologic removal and exposure of organic carbon and other reductants and (2) the exogenic input of reductants. Here, the inventory of reductants encompasses organic carbon, mineral sources of electron donors (e.g., pyrite), and atmosphere- and mantle-derived reducing gases (e.g., H_2). To illustrate, the burial of organic carbon produced by photosynthesis, either on land or in the ocean, will remove a sink for O_2 consumption, resulting in a buildup of O_2 in the atmosphere-ocean reservoir (e.g., **Figure 3**). In parallel, the exposure of sedimentary organic carbon, such as through uplift and exposure of marine sedimentary rocks, would introduce an O_2 sink, resulting in lower O_2 in the atmosphere-ocean reservoir. In this view, the organic carbon cycle is considered to be the dominant control on the redox state of the ocean-atmosphere system (see *Box 1: Linking changes in redox conditions to the carbon isotope record* for discussion about C isotopes and O_2). Mass balance models that consider some of these factors include COPSE (Lenton et al., 2018) and GEOCARB (Berner, 2006b).

Other long-term processes related to changes in inputs and outputs of oxidants and reductants include fluctuations in (1) hydrothermal-derived reductants (such as Fe^{2+} or H_2S), with a key example being the Cretaceous Oceanic Anoxic Event 2 event (Jenkyns et al., 2017, Nana Yobo et al., 2022); (2) mantle-derived H_2 or CH_4 via volcanic degassing (Kasting et al., 1993, Kvenvolden and Rogers, 2005, Kadoya et al., 2020); (3) H_2 escape from the upper atmosphere (Catling et al., 2001); (4) or a change in the igneous lithology exposed through Earth's history as a result of planetary differentiation (Leong et al., 2021). On planetary timescales, a change in mantle redox chemistry and a secular decrease in atmospheric CO_2, required to balance the carbonate-silicate weathering cycle while accommodating increasing solar luminosity, would starve the biosphere, decreasing O_2 production and ultimately returning the Earth to a permanently deoxygenated state (Ozaki and Reinhard, 2021).

Ultimately, knowledge of both modern and ancient biogeochemistry play complimentary roles in the development of models used to understand mechanisms controlling ocean redox conditions on any timescale. The modern ocean-atmosphere and experimental work form the basis of models used to provide mechanisms for proxy observations across geologic time, while the geologic record provides a framework for understanding perturbations in the age of the Anthropocene.

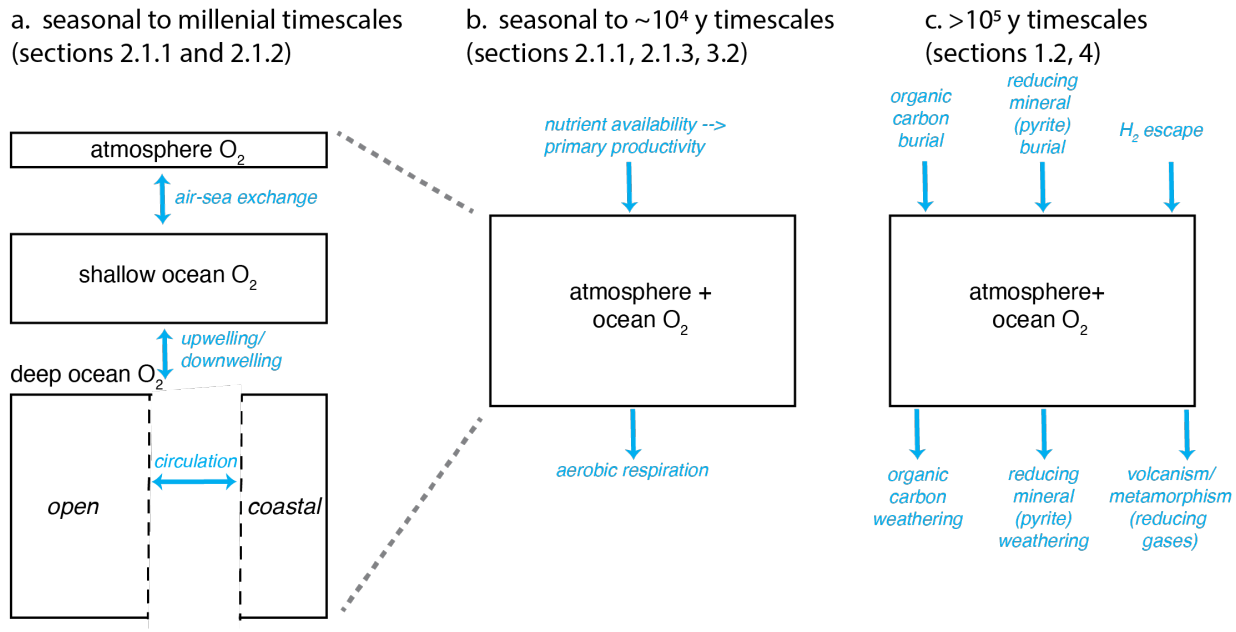

Figure 3. *Key fluxes relevant to O_2 mass balance in the ocean on different temporal and spatial scales. (A) Where spatial relationships of O_2 are critical to deconvolve, key processes between atmosphere, shallow ocean, and deep ocean O_2 reservoirs are driven by chemical properties (e.g., O_2 solubility), physical transport (upwelling, downwelling, horizontal circulation), and O_2 consumption and production within each reservoir (photosynthesis, biological and abiotic removal of O_2). (B) On longer timescales, the "average" redox state of the atmosphere-ocean system can be represented as one box. Here, the availability of nutrients drives primary productivity, the production of organic matter, and the subsequent consumption of O_2 via aerobic respiration. This can lead to "supercharged" O_2 consumption and the transient increase of marine anoxia. (C) On longer timescales, the organic carbon cycle is considered to be balanced (O_2 production via productivity and O_2 consumption via remineralization of organic matter). In this scenario, geologic processes involving sedimentation and burial of reductants (organic matter, minerals such as pyrite); tectonics, uplift, and oxidation of sedimentary reductants (organic matter, pyrite); and the balance of reducing gases entering and escaping the atmosphere/ocean through volcanism and atmospheric photochemistry become the critical sources and sinks.*

2 Modern: ocean redox on modern and anthropogenic timescales

We first provide a detailed overview of the distribution and major factors modulating marine O_2 availability in the modern ocean. We note that the O_2 cycle was reviewed in detail in the previous Treatise Edition (Petsch, 2014). We build on this here by incorporating water-column trace element data—in line with our broader theme of "redox"—but also by providing perspectives on O_2 and redox-sensitive element distribution and drivers through the lens of the NOAA World Ocean Atlas and GEOTRACES. **Figure 3** provides a synthesis of major processes impacting the distribution of marine oxygen in the modern. Below we discuss these within this context, starting with sources and sinks.

2.1 Modern O_2 inputs and outputs

2.1.1 Source: Air-sea equilibrium and marine photosynthesis at the sea surface

Air-sea gas exchange plays a fundament role in modulating marine O_2 at both the ocean surface and its deepest depths. The degree of air-sea exchange is defined by O_2 saturation—calculated as a function of the O_2 content of the atmosphere and *in situ* water specific temperature,

salinity, and pressure. Today's atmospheric pO_2 is ~21%, but this value has varied widely in the past, as is discussed in later sections. Given that atmospheric O_2 today is relatively homogenous, the *in situ* marine conditions play the biggest role in modulating absolute O_2 contents via air-sea exchange. While salinity can play an essential role in coastal, estuarine settings, there are no major salinity impacts on O_2 in the open ocean (Colt, 1985). Temperature is more spatially variable—for example across latitudinal gradients—and can vary widely temporally due to seasonal variations, thus impacting O_2 solubility.

Figure 4 shows the maximum seasonal seawater O_2 saturation within the mixed layer at a given latitude and longitude. While most of the ocean is defined by air-sea saturation broadly—or at least during some portion of the year—the most striking observation is the temporal variability at many locations. This variability is mostly defined by the Northern and Southern Hemisphere summer and winter, with oversaturation and O_2 outgassing in their respective summer and undersaturation and ingassing in their respective winter (Najjar and Keeling, 2000). Both of these endmember variations in O_2 saturation are functions of multiple processes occurring throughout the year and can be broken into two broad categories: physical processes modulating the degree of air-to-sea exchange and *in situ* marine O_2 sources via photosynthesis (reviewed in Palevsky and Nicholson (2018)).

Regarding the degree of exchange with the atmosphere, at the most basic level, physical processes—specifically sea ice—can act to block air-sea exchange. The buildup of winter sea ice can explain limited O_2 saturation at extreme latitudes seen in the winter months in **Figure 4**. Wind speed and temperature are additional examples of a physical processes that can also impact the efficiency of air-sea exchange of gases, including O_2. For example, the uptake of atmospheric O_2 to the surface ocean is modulated in part by the duration of exposure of water masses to the atmosphere—thus increasing total O_2 uptake—and the duration of their convective mixing during cold months, which leads to deeper convection (Sun et al., 2017). To a first order, lower temperatures increase O_2 solubility; however, the combination of wind speed and temperature are primary controls on mixing by impacting stratification and gas exchange velocity. Thus, increased wind speeds and decreased temperatures can lead to O_2 declines at the sea surface due to mixing with subsurface water lower in O_2. As shown in **Figure 4**, this is particularly pronounced in the winter months. Because air-sea exchange velocities are also a function of air-sea O_2 gradients, this has the impact of increasing the rate of surface O_2 uptake and thus increasing the rate of the transfer of O_2 to the subsurface. Conversely, summertime stratification directly decreases the entrainment of lower O_2 waters from the subsurface to the sea surface, which can increase surface O_2 saturation (Boyer et al., 1999). Vertical mixing is directly impacted by ocean warming by both increasing temperature—thus decreasing O_2 solubility—and stratification, limiting air-sea exchange. Together, these factors impact dissolved O_2 broadly by decreasing a primary source of O_2 to depths below the winter mixed layer (Keeling et al., 2010).

Biological activity, specifically *in situ* photosynthesis, plays a fundamental role in controlling seasonal variations in O_2 supersaturation at the sea surface (**Equation 1**). While decreases in the availability of light associated with winter months plays a primary role in modulating photosynthetic activity at high latitudes, we note that most of the variation in O_2 supersaturation occurs at mid-latitudes, with equatorial regions showing much more limited variability. This contrast is ultimately due to the importance of nutrient availability in limiting photosynthetic activity. Specifically, at mid-latitudes, ventilation during winter mixing plays a key role in re-introducing subsurface nutrients to starved surface phytoplankton communities. This ultimately leads to local photosynthetic activity increasing local O_2 and thus O_2 saturation. In

contrast, highly stratified equatorial waters have largely zonal flow and are nutrient-limited due to limited supply from deep subsurface waters.

$$CO_2 + H_2O \underset{\text{respiration}}{\overset{\text{energy}}{\longleftrightarrow}} CH_2O + O_2 \quad \text{(photosynthesis} \rightarrow\text{)}$$

Equation 1

It is important to note that, in addition to a source of O_2, primary production is an important catalysis for biogeochemical reactions and therefore a sink for a multitude of nutrients and related trace elements, including redox-sensitive elements. Horner et al. (2021) provide an extensive review of the impacts of productivity on trace element signatures, including their use as paleoproductivity proxies. Additionally, cycling of key trace elements (and their isotopes) is discussed in a complementary Chapter in this Treatise (Little et al., this issue; Farmer et al., this issue). A key take home point is that the canonical Redfield Ratio (C:N:P of 124:16:1) can be used to determine which nutrients are limiting (as well as the stoichiometry from the simplified expression for organic carbon shown in **Equation 1**). The Redfield ratio can also be extended to include many non-limiting trace elements still essential to primary production (adapted from (Ho et al., 2003, Martin and Knauer, 1973, Elderfield and Truesdale, 1980)). In **Equation 2**, note that we have bolded redox-sensitive elements also commonly used as redox tracers in modern and ancient marine systems, including throughout this Chapter. The implication is that a multitude of processes beyond redox, including productivity and related biogeochemical reactions, are important for the cycling of these trace elements and their isotopes in the ocean (Janssen et al., 2020).

$$C_{124,000}\boldsymbol{N_{16,000}}P_{1,000}\boldsymbol{S_{1,300}}K_{1,700}Mg_{560}Ca_{500}\boldsymbol{I_{19}}Sr_{5.0}\boldsymbol{Fe_{7.5}Zn_{0.8}Cu_{0.38}Cr_{0.33}Co_{0.19}Cd_{0.21}Mo_{0.03}}$$

Equation 2

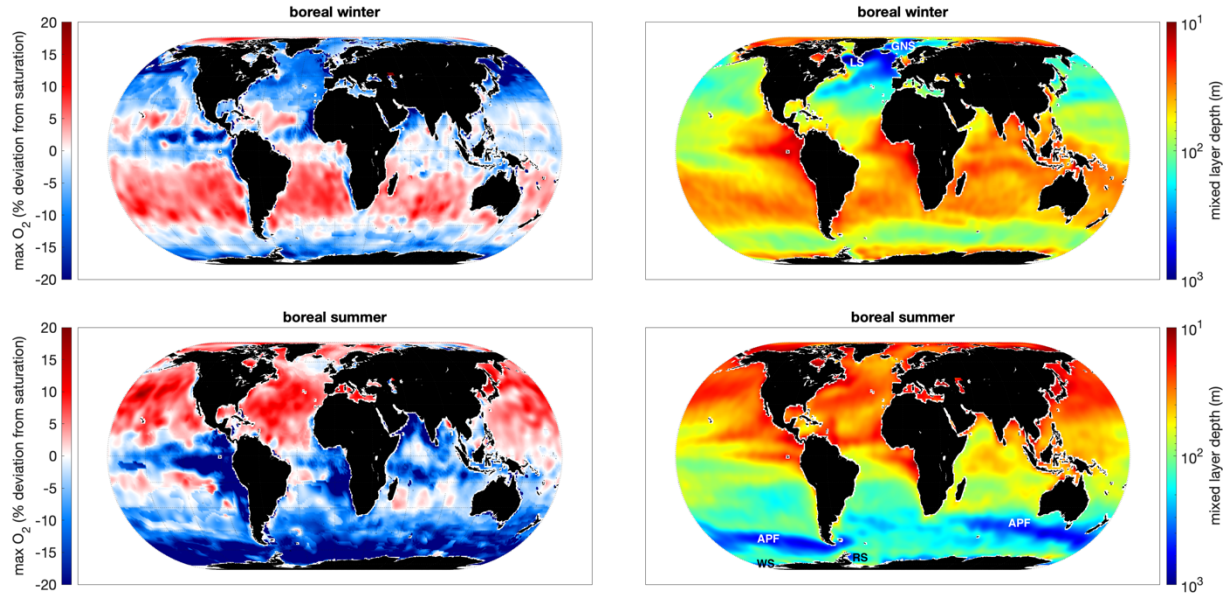

Figure 4: Left: *Seasonal variations in maximum O_2 saturation within the mixed layer for boreal winter and summer.* ***Right:*** *Mixed layer depth for boreal winter and summer. Note that each panel shows maximum O_2 saturation for a given latitude and longitude*

based on calculations of O_2 saturation from temperature, pressure, depth, and observed O_2 from the seasonal 1 deg gridded WOA 2018 (Boyer et al., 2018). Labels on right hand panels mark important areas of bottom or intermediate water formation (Weddell Sea (WS), Ross Sea (RS), Greenland-Norwegian Sea (GNS), Labrador Sea (LS)), Antarctic Polar Front (APF)).

2.1.2 Source: Circulation transports O_2 to the ocean interior

The sole source of O_2 to the ocean interior is vertical mixing and the formation and subduction of sea-surface water masses. As discussed in the previous section, winter mixing plays a key role in introducing O_2 to the subsurface, as deep as 1000 m or more in some localities (**Figure 4**). However, subducting water masses are critical for ventilation of O_2 to intermediate and deeper depths. Specifically, water masses formed at the surface at high latitudes are subducted where weather fronts and related sea ice formation combine to force subduction via density increases and/or wind patterns. For example, the Sub-Antarctic Mode Water (SAMW) and Antarctic Intermediate Waters (AAIW) form and subduct at the Antarctic Polar Front (APF) (labeled in **Figure 4**). Because of local biogeochemical processes at the site of water mass formation, these water masses can have distinct pre-formed O_2, nutrient (commonly denoted as PO_4* or NO), and related trace element signatures that together can be used as tracers of individual water masses throughout the subsurface oceans.

As discussed in later sections and recently reviewed (Reinhard and Planavsky, 2022), ancient atmospheric O_2 was not always high enough to supply surface waters with O_2 levels sustainable for preservation to the ocean interior during subduction. However, in today's well oxygenated atmosphere, the O_2 levels, nutrients concentrations, and other geochemical signatures are often considered semi-conservative, and thus largely unchanging from their pre-formed values along and within the ocean's subsurface. For this reason, an increasingly used and powerful tool in ocean transect studies is an Optimum Multi-Parameter Analysis (OMPA) to quantify the contribution of individual water masses at a given location (Shrikumar et al., 2022, Peters et al., 2018, Jenkins et al., 2015, Evans et al., 2020b). An OMPA uses pre-defined conservative physical properties (e.g., potential temperature, salinity, potential density anomaly, silicate, PO_4* or NO) of individual water masses and then applies a least-squares solution to determine the contributions of these water masses to a given sample. The combination of water mass analyses and applications of atmosphere-sourced geochemical dating tools (e.g., CFCs, SF_6) can be used to determine the age of a water mass in a given location—i.e., how long since water mass formation and subduction occurred. Importantly, while OMPA parameters are chosen because of semi-conservative behavior, these parameters themselves or additional geochemical signatures may evolve along with circulation patterns of the water mass circulation due to biogeochemical impacts (e.g., respiration, discussed in detail in the next section) and/or benthic and hydrothermal fluxes (e.g., Fe, discussed in detail in Section 2.2.4). In these cases, an OMPA can be a powerful tool to deconvolve and isolate the roles of conservative water-mass mixing and these non-conservative processes (Fitzsimmons et al., 2016, Le Roy et al., 2018, Roshan and Wu, 2015a, Roshan and Wu, 2015b). One ultimate implication is that subsurface features in geochemical profiles may reflect an integration of the pre-formed chemistry, post-subduction biogeochemical evolution, and then the conservative mixing of variable water masses with likely differences in each of the former.

Other key advances on the frontier of understanding near-surface O_2 sources include the incorporation of bubbles into models for air-sea exchange (Sun et al., 2017). Bubbles are created during wind-driven convection at the surface and provide gases, including O_2, independent of their saturation in local waters. We note as well that, while recent studies have explored geochemical applications of machine learning—for example, I, C, Ba, and N (Huang et al., 2021, Sherwen et

al., 2019, Tang et al., 2019, Mete et al., 2023)—there have been no studies to date exploring machine learning as a tool to predict marine O_2 availability and co-varying parameters.

2.1.3 Sink: Respiration

Respiration during the remineralization of organic carbon is the primary consumption process of O_2 in the modern ocean. Oxidants are sequentially reduced in the order of the highest to lowest free energy change per mole of organic carbon oxidized (**Figure 3**) (Froelich et al., 1979). This is referred to as the redox ladder and approximates redox states by describing the relative abundance of oxidants with known energetic yields at a given time or location. When O_2 is widely available, like in today's well-oxygenated ocean, aerobic respiration is the most favorable metabolism—yielding nearly an order of magnitude more energy per mole of carbon than anaerobic metabolisms—and O_2 abundance in the modern ocean is responsible for the overwhelming majority of organic matter remineralized within the water column. Ultimately, <1% of organic matter is exported to the deep sea and potentially preserved in the sediments (Hedges and Keil, 1995).

In addition to O_2 saturation, another important measure of O_2 cycling is apparent O_2 utilization (AOU), which describes O_2 loss via the difference of measured and predicted O_2 at saturation. Respiration of organic carbon in well-oxygenated seawater is an essential component of the biological pump cycling of C and nutrients from the surface to deeper waters and sediments. Specifically, the remineralization of organic carbon consumes ambient O_2 but releases CO_2, N, P—as well as the trace elements shown in **Equation 2**—to intermediate-depth waters (Shankle et al., 2021). Respiration contributes to the non-conservative behavior of O_2, nutrients and trace elements during water-mass evolution, which is essential to consider in addition to ocean circulation when viewing and interpreting any vertical profiles. For example, changes in pH, CO_2, and related parameters provide a metric for the age of deep waters in the global ocean. Interactions with sediments in bottom waters hosting remineralization of organic carbon and diffusion across the sediment water interface provides an additional opportunity for the evolution of water-mass geochemistry.

Although only a fraction of organic carbon makes it to the seafloor and through burial (e.g., remineralization in the sediment column), it is important to remember that the long-term burial and sequestration of organic carbon in sediments is among the key drivers of O_2 accumulation in our atmosphere and oceans (**Figure 3**c). Specifically, as outlined in **Equation 1**, when organic carbon is buried it is removed from potential respiration, and thus O_2 accumulates. Organic carbon burial, along with pyrite formation, are key components of mass balance models considering O_2 accumulation on geologic timescales (Berner and Raiswell, 1983, Berner, 1982). An illustration of this process comes from real-time observations of O_2 decline in the atmosphere associated with the recent oxidation of fossil fuels (Battle et al., 1996, Bender et al., 1994b, Bender et al., 1994a).

An exciting frontier is determining the impact of reactive O_2 species (ROS)—e.g., hydrogen peroxide (H_2O_2) and superoxide ($O_2^{\bullet-}$)—on the marine O_2 cycle and in the cycling of carbon and trace elements (Hansel and Diaz, 2021). For example, a recent study identified extracellular superoxide production via the reduction of O_2 as a sink corresponding to as much as 5-19% of the global O_2 budget (Sutherland et al., 2020). Further, superoxide has been demonstrated to play an essential role in Mn^{2+} (Learman et al., 2011) and perhaps I^- (Li et al., 2014) oxidation, acts as both an oxidant and reductant for Cu and Fe (Hansard et al., 2011, Rose, 2012, Voelker and Sedlak, 1995, Voelker et al., 2000), and reacts with dissolved organic matter (Heller and Croot, 2010, Wuttig et al., 2013).

2.1.4 *What is the distribution of bottom water O_2?*

Figure 5 shows a map of global bottom water O_2 concentrations and demonstrates clear variations within and between ocean basins. Like that of ODZs discussed in Section 2.2, bottom-water O_2 is largely a function of the length of time water masses have been isolated from O_2 recharge from the atmosphere, or O_2 age. We note two prominent observations from **Figure 5**: low O_2 levels around the "rim" of ocean basins, particularly the Indian and Pacific Oceans, as well as lower overall bottom water O_2 in the Pacific and Indian relative to the Atlantic Ocean.

The O_2-depleted waters at intermediate depths within the rims of the Pacific and Indian Oceans and in the Eastern Atlantic can be explained by the presence of ODZs at intermediate depths within these basins (**Figure 6**). As shown in **Figure 7**, the ODZs are developed in regions dominated by upwelling along the eastern boundary currents, and O_2-depleted water then extends laterally at intermediate depths. For the Pacific and Indian Oceans, **Figure 7** and Error! Reference source not found. show that the ODZs can extend across the ocean basins, intersecting with the shelfs along the opposite margins. As discussed in the Section 2.2, shorter thermocline ventilation timescales and thus O_2 ages in the Atlantic prevent the formation of expansive low O_2 bottom waters relative to the Pacific and Indian Oceans.

A similar explanation accounts for the higher overall bottom water O_2 observed in the Atlantic relative to the Pacific and Indian Oceans. Specifically, downwelling and bottom water formation at high latitudes of the Atlantic and Southern Ocean are the ultimate source of bottom waters to the Pacific and Indian Oceans (**Figure 5** and Error! Reference source not found.). The Atlantic is most proximal to these bottom water formation sites, with the flushing from the nutrient poor, but O_2 rich, North Atlantic Deep Water (NADW) resulting in relatively higher O_2. In contrast, similar sites of intermediate or deep water flushing are not present in the Pacific or Indian Oceans. Accordingly, longer O_2 age for ocean basins furthest along the flow path from these sites of ventilation—i.e., the Pacific and Indian Oceans—results in lower overall O_2 due to integrated consumption along the flow path.

Although there are large variations in bottom water O_2 globally, we note that <1% of seafloor area is estimated to be characterized by anoxia. As discussed in the Section 2.2, bottom-water O_2 levels or redox conditions play an important role regulating global trace element fluxes to and from the sediments. The resulting isotope composition or trace element concentrations of sediments are commonly used in models estimating the global seafloor area of various redox states in Earth's past. For example, using Cr, Mo, and Re mass balance models, the modern redox distribution of the seafloor has been estimated as 0.11% by area anoxic and 1-5% reducing or suboxic (Reinhard et al., 2013c, Sheen et al., 2018). Anoxia in these studies is typically defined by the presence of sulfide in bottom waters or the benthic boundary layer and reducing/suboxia is defined by low O_2 levels preventing the burial of Mn and Fe oxides (typically 10-100 μM), all of which can have major implications for isotope fractionations or authigenic burial rates for redox-sensitive trace elements.

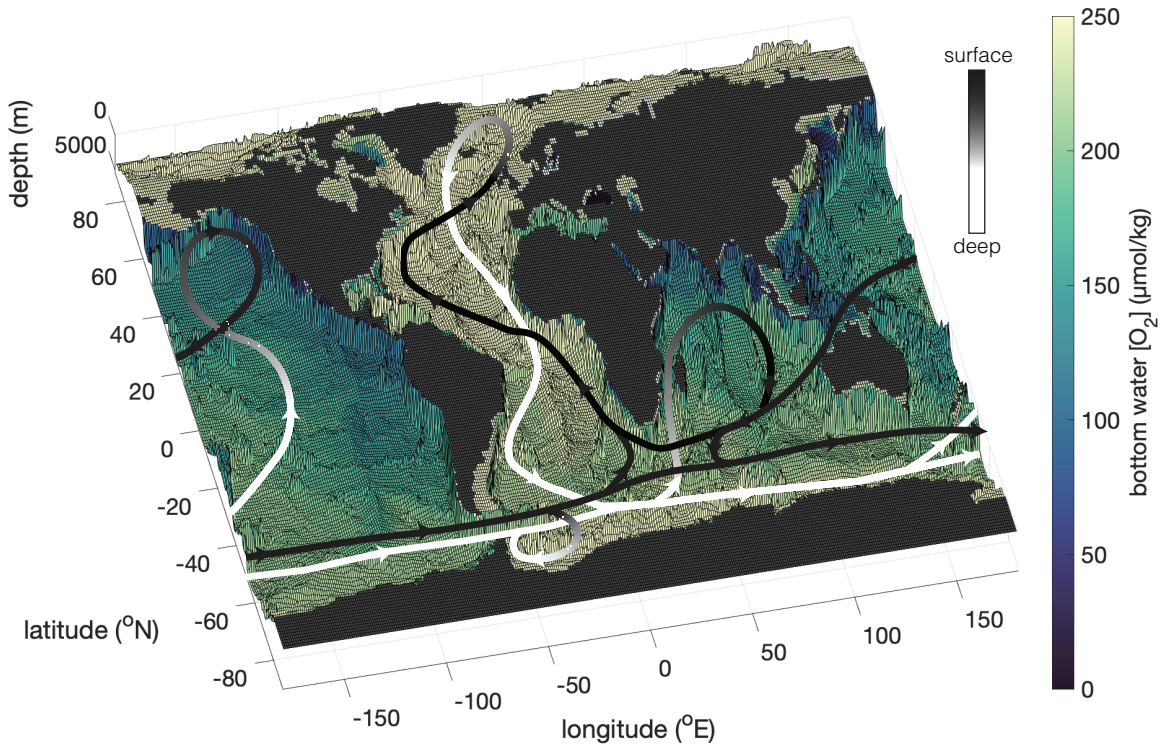

Figure 5. *Concentrations of bottom water O_2 from WOA18 (Boyer et al., 1999). The Z-axis shows the depth at which the O_2 concentrations are from, which represents the closest depth to the seafloor available from the WOA18. We note that the WOA18 does not contain data below 5500 m, thus in deeper areas the plot misrepresents seafloor features. Note that the z-axis is not fully resolvable here and is simply intended to show the depth range and basic seafloor feature. The lines and arrows show generalized patterns of thermohaline circulation and areas of deep-water formation.*

2.2 Origin, characteristics, and distribution of O_2 deficient zones

Figure 6 summarizes the physical, chemical, and biological factors, discussed in detail in this subsection, that result in vertical redox gradients of present-day ODZs. Many of these factors are also important for ancient upwelling regions, but with a greater diversity of atmospheric, ODZ, and bottom-water redox states (e.g., oxic, ferruginous, euxinic, anoxic, etc).

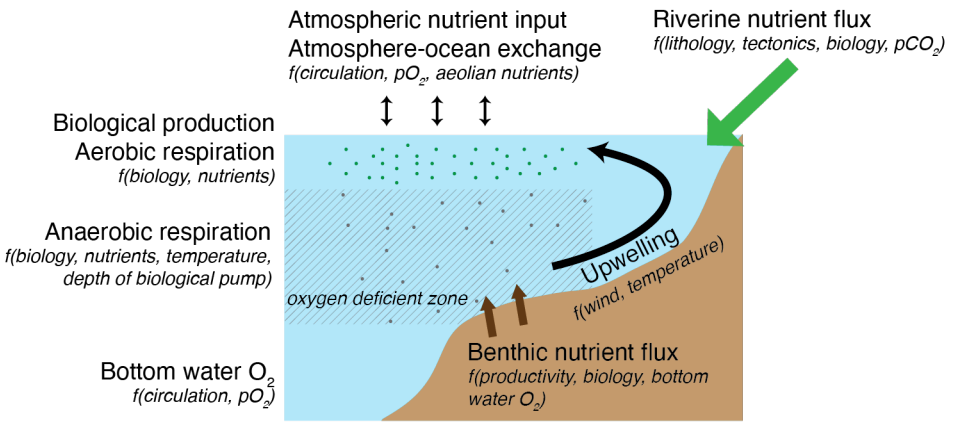

Figure 6: *Cartoon of modern O_2 deficient zone emphasizing the controls on redox conditions, including the major factors modulating each control. For example, the riverine nutrient flux is a function of the riverine bedrock lithology, uplift and other tectonic parameters, climate – pCO_2—that drives local hydrology and biospheric weathering.*

2.2.1 The general origin and redox characteristics of O_2 deficient zones

Whereas air-sea exchange buffers the impacts of respiration on O_2 accumulation through most of the ocean, ODZs represent expansive regions where O_2 concentrations are depleted, thus excluding macrofauna and supporting diverse microbial metabolisms. The most extreme ODZs are found in the Eastern Tropical North Pacific (ETNP), Eastern Tropical South Pacific (ETSP), Arabian Sea, Bay of Bengal, and the Benguela and Mauritania Upwelling zones (all labeled in **Figure 7**a). The total volume of ODZ cores (where O_2 <20 µmol kg^{-1}) has been estimated as 102 ± 15 x 10^6 km^3, or ~7% of the total ocean volume (Paulmier and Ruiz-Pino, 2009).

Sources and sinks necessary for the formation and maintenance of ODZs are not different from the processes described above for the marine O_2 cycle broadly, but instead represent an extreme endmember where O_2 demand exceeds supply (as discussed above, ultimately from air-sea exchange and *in situ* production in surface waters). Specifically, ODZs are poorly ventilated water masses found in upwelling regions characterized by a combination of sustained O_2 depletion and increased nutrients and CO_2. Both upwelling and air-sea exchange can be impacted by wind: higher winds would increase mixing in the upper ocean, and intensifying wind stress can strengthen upwelling (Bakun and Weeks, 2004, Deutsch et al., 2006, Deutsch et al., 2014, Friedrich et al., 2006, Lovenduski et al., 2008). As described above, the O_2, nutrient levels, and CO_2 concentrations of water masses together represent the evolution of deep and intermediate waters removed from exchange with the atmosphere and are products of respiration of organic carbon over variable timescales. While the burial of organic carbon represents one endmember of the biogeochemical carbon pump, providing O_2 to the atmosphere, these ODZ regions also represent pathways of return and outgassing for older CO_2 (Siani et al., 2013, Anderson et al., 2009, Broullon et al., 2020) and nutrients (e.g., Si, N, P, Fe, others in **Equation 2** and **Figure 9**) back to surface waters via upwelling. Upwelling of these remineralized nutrients contributes to enhanced primary production, seen through global maps of chlorophyll in marine surface waters, which can contribute to O_2 supersaturation in local surface waters (**Figure 4**); however, the more pronounced impact is the contribution of carbon export to respiration in subsurface waters. Together, this local O_2 demand and the circulation of poorly ventilated subsurface waters are the drivers of ODZ development.

An important research direction going forward is increasing our understanding of O_2 variability at sub-μmol kg^{-1} levels in and between ODZs. Water column O_2 concentrations are most commonly characterized by *in situ* CTD measurements or Winkler titration, which both have lower-end detection limits near 1 μmol kg^{-1}; however, multiple recent studies over the last decade have utilized STOX sensors—with O_2 at detection limits closer to 10 nmol kg^{-1}—which have revealed O_2 variations at sub-μmol kg^{-1} levels that are important catalysts and limitations for metabolisms (Revsbech et al., 2009, Ulloa et al., 2012). These studies also reveal important differences between the ODZs in terms of background O_2 levels. Specifically, O_2 surveys in the ETNP and ETSP found O_2 commonly below detection limits (as low as <10 nmol kg^{-1}) within the ODZ core—termed functional anoxia—but in some localities up to 400 nmol kg^{-1} (Canfield et al., 2019, Larsen et al., 2016, Tiano et al., 2014, De Brabandere et al., 2014, Padilla et al., 2016, Thamdrup et al., 2012, Thamdrup et al., 2019, Tsementzi et al., 2016, Kalvelage et al., 2015, Penn et al., 2016, Sun et al., 2021, Gazitua et al., 2021). In contrast to the widespread functional anoxia of the ETSP and ETNP, a study from the Benguela Upwelling zone found below detection O_2 (≤100 nmol kg^{-1}) along the shelf but also elevated O_2 near 2-6 μmol kg^{-1} in nearby stations (Kalvelage et al., 2015). In a further contrast, a Bay of Bengal study found persistent detectable O_2 in the 10-200 nmol kg^{-1} range (Bristow et al., 2017, Larsen et al., 2016).

Understanding the distribution of O_2 at sub-μmol kg^{-1} levels is important for interpreting variations in microbial metabolisms, discussed in detail below. O_2 levels commonly reported at <1 μmol kg^{-1} are in fact overlooking O_2 variations important for understanding biogeochemical and related mixing dynamics within the ODZ. For example, N and Mn redox cycling has been demonstrated to be sensitive to O_2 at levels of 5-30 and 100 nmol kg^{-1}, respectively (Thamdrup et al., 2012, Bristow et al., 2016, Clement et al., 2009). Other N redox cycling pathways—e.g., annamox and N_2 and N_2O production—as well as CH_4 cycling, are also sensitive to sub-μmol kg^{-1} O_2 variations (Dalsgaard et al., 2014, Thamdrup et al., 2019). While some quantifiable sub-μmol kg^{-1} O_2 concentrations within ODZs are interpreted as reflecting the transient intrusion of external water masses (Thamdrup et al., 2012), other studies have also demonstrated evidence for the *in situ* creation of "aerobic" zones within functionally anoxic areas via diurnal photosynthetic O_2 production or nitrous oxide disproportionation (Canfield et al., 2019, Kraft et al., 2022, Garcia-Robledo et al., 2017). We also note, as discussed in detail in later sections, that these sub-μmol kg^{-1} O_2 levels are relevant to what has been constrained or predicted for much of Earth's oceans in the geologic past. This implies that relating geochemical proxy variations to specific sub-μmol kg^{-1} O_2 levels requires modern field or experimental studies characterizing the thresholds relevant for redox-active geochemical cycling.

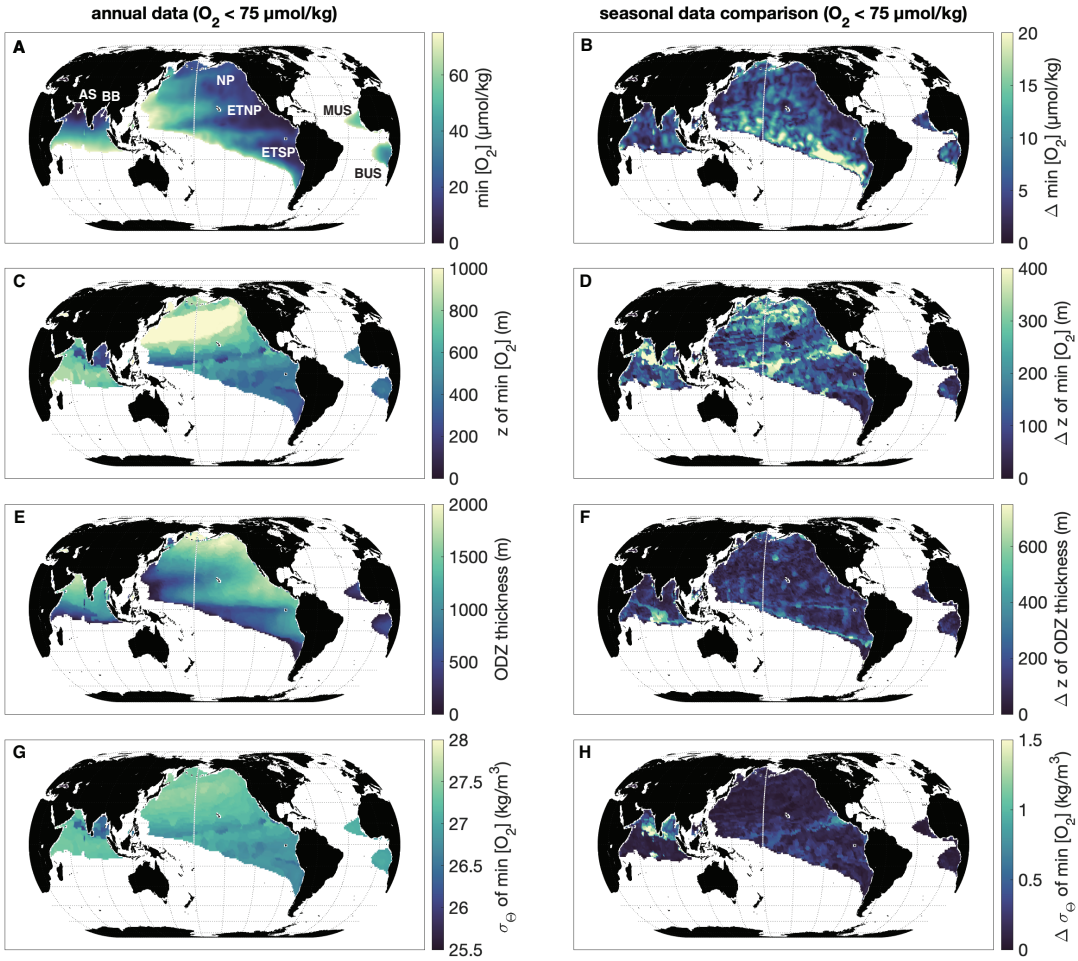

***Figure 7**: Characterization of minimum O_2 from the 2018 WOA (Boyer et al., 2018). **A.)** Minimum O_2 concentrations across the global ocean for the annually averaged WOA data. **B.)** The difference between the highest and lowest minimum O_2 concentration between the winter, spring, summer, and autumn WOA datasets. **C.)** Depth of minimum O_2 concentrations for the annually averaged WOA18. **D.)** The difference between the highest and lowest depth of minimum O_2 concentration between the boreal winter, spring, summer, and autumn WOA18. **E.)** Thickness of ODZ with O_2 < 75 µmol kg^{-1} based on annual WOA18 for the annually averaged WOA18. **F.)** The difference in ODZ thickness with O_2 < 75 µmol kg^{-1} between the boreal winter, spring, summer, and autumn WOA18. **G.)** The potential density anomaly at the depth of minimum O_2 concentration for annually averaged WOA18. **H.)** The difference between the highest and lowest potential density anomalies from the depths of minimum O_2 concentration between the boreal winter, spring, summer, and autumn WOA18.*

Modern O_2 deficient waters support diverse metabolisms and redox reactions and can be characterized by combinations of nitrogenous, iodinous, manganous, and to a lesser extent ferruginous conditions (**Figure 1**). An example is shown in **Figure 8** for the ETSP. Most prominently, anaerobic N cycling dominates in ODZs and is an important contributor to global N cycling, accounting for at least 33% of the loss of fixed nitrogen from the global oceans (Codispoti et al., 2001, Galloway et al., 2004). Specifically, secondary NO_2^- maxima—that below the primary maxima from nitrification observed in surface waters—formed from the reduction of NO_3^- are a global feature of ODZs. Nitrite is further reduced to N_2 through heterotrophic denitrification and/or annamox or to NH_4 through dissimilative reduction. In addition, intermediate reduction can form

N_2O gas, a greenhouse gas contributing to global warming (Babbin et al., 2015). Iodine cycling in ODZs has received increased recent attention, including detailed transect studies (Moriyasu et al., 2020, Rapp et al., 2019, Rapp et al., 2020, Cutter et al., 2018) and identification of genes specific to dissimilatory IO_3^- reduction (Reyes-Umana et al., 2022, Saunders et al., 2022). Because I is a trace element in seawater—with a mean concentration of ~0.45 μM (Chance et al., 2014)— the reduction of IO_3^- to I^- is not a major contributor to organic matter remineralization. Nonetheless, the pronounced I^- maxima occurs at depths in the water column that typically overlap with that of NO_2^- in ODZs and therefore can be applied as a redox tracer.

Ferruginous and manganous conditions—or elevated water-column dissolved Fe^{2+} and Mn^{2+}—may best track benthic reductive fluxes maintained within ODZ water columns. Dissolved Fe and Mn concentrations have been studied extensively in several ODZs, including the ETNP (Hopkinson and Barbeau, 2007, Bian et al., 2023, Rue et al., 1997), ETSP (Noffke et al., 2012, Vedamati et al., 2014, Cutter et al., 2018), the Benguela Upwelling Current (Noble et al., 2012, Liu et al., 2022), and the Arabian Sea in the Indian Ocean (Moffett et al., 2007, Moffett and German, 2020, Singh et al., 2023). In shelf sediments located within the upper part of ODZs, the reduction of Fe and Mn oxides, delivered via Fe and Mn "particulate shuttles"—the transport of oxidized Fe- and Mn-bearing particles from the more oxygenated upper water column (Scholz et al., 2014a)—results in a benthic flux of reduced Fe and Mn from sedimentary pore fluids into the water column. This effect, which is identified by peaks in Fe^{2+} at water depths where NO_2^- concentrations are high (Heller et al., 2017, Cutter et al., 2018, Bolster et al., 2022) results in the covariation between Fe and Mn in the water columns of the ETNP, Benguela, and the Arabian Sea (discussed further in Section 2.2.3; (Resing et al., 2015, Noble et al., 2012, Bolster et al., 2022, Liu et al., 2022, Moffett and German, 2020)). Lower Fe concentrations at greater depths has been interpreted to reflect NO_2^- or NO_3^- scavenging and export of Fe (Lam et al., 2020). Though this redox-sensitive cycling can maintain Fe and Mn levels necessary for biological processes, it does not reflect productivity nor respiration. We note that additional sources of Fe and Mn include hydrothermal inputs, which can even be an important source to mid-ocean oligotrophic surface waters (**Figure 8**) (Fitzsimmons et al., 2014).

Although euxinia is not a prominent feature of modern ODZs, multiple recent works have provided evidence of active S cycling. This includes likely SO_4^{2-} reduction within anaerobic microniches but also sulfidic plumes sourced from local benthic fluxes. For example, plumes of hydrogen sulfide within the ETSP (Schlosser et al., 2018) and Benguela Upwelling Zone (Lavik et al., 2009, Bruchert et al., 2003, Ohde and Dadou, 2018) have been documented to have concentrations as high as 6 and 40 μM, respectively. We note that the highest water column sulfide concentrations are typically associated with bottom waters and—similar to dissolved Fe and Mn—elevated hydrogen sulfide is likely sustained via benthic fluxes. Indeed, these sulfidic plumes can also contain elevated dissolved Fe and may themselves be important for benthic Fe mobilization (Schlosser et al., 2018). While likely not the primary source of dissolved water column sulfide (Lavik et al., 2009), we also note that S cycling within anaerobic microniches of sinking organic particles has recently been documented to play an important role in the global C and N cycles (Raven et al., 2021, Bianchi et al., 2018, Carolan et al., 2015, Canfield et al., 2010), and hence likely others. Specifically, sulfurization of organic particles may enhance organic carbon burial fluxes and consideration of anaerobic microniches nearly doubles global estimates of denitrification rates. Anaerobic microniches have also been observed even within oxic water columns and sediments (Shanks and Reeder, 1993, Jorgensen, 1977, Cutter and Krahforst, 1988), thus further expanding their potential global importance to the cycling of organic carbon and of

redox-sensitive elements. However, research to date is lagging in demonstrating the potential diversity of other particle-hosted metabolisms and their significance to broader ocean chemistry. For example, given the fast reaction between IO_3^- and sulfide (faster than that of O_2 and sulfide; e.g., Jia-Zhong and Whitfield (1986)), sulfide production may contribute to the IO_3^- minima observed in global ODZs, but this has yet to be investigated.

ODZ formation is initiated along productive coastlines, but their extensive lateral open ocean area is the result of continued, offshore subsurface circulation of these semi-conservative O_2 deficient water masses. As discussed above, productive continental margin sediments are the primary source of Fe and Mn within ODZ water columns. Similarly, I and N redox chemistry initiated in the water columns and sediments of these upwelling zones may be the primary sources of I^- and NO_2^- that are retained in offshore reducing waters. One of the most prominent examples is the 13CW water mass, which is linked to the formation and circulation of ODZ waters from both the ETNP and ETSP within the ~26.25 kg m^{-3} potential density anomaly (Peters et al., 2018, Evans et al., 2020b). In offshore transects, semi-conservative mixing between the 13CW and adjacent water masses has been demonstrated to play an essential role in I distribution (Evans et al., 2020b, Hardisty et al., 2021). An important area of study going forward is the quantification of water mass contributions to global ODZ transects along with redox-sensitive elements, thus allowing for better quantification of the role of *in situ* vs. *ex situ* geochemistry in relation to ODZ chemistry.

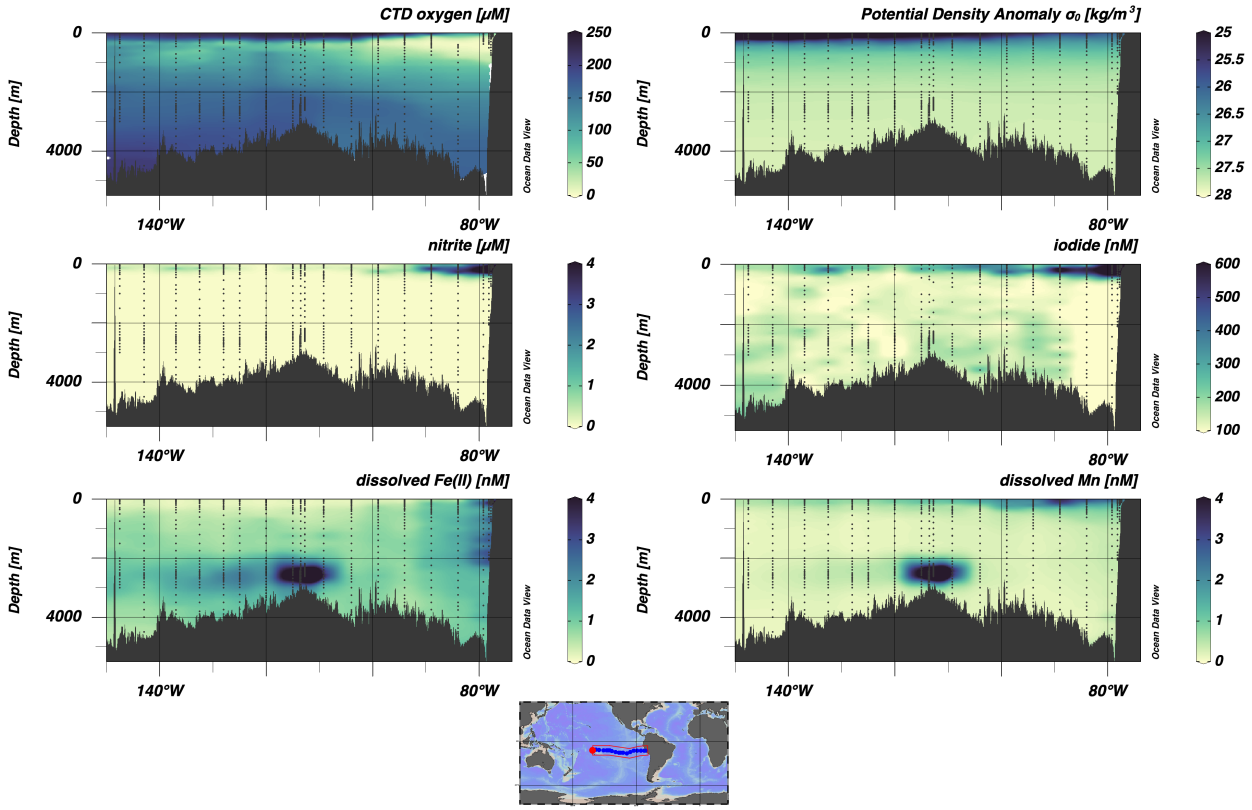

***Figure 8**. Select geochemical data from GEOTRACES GP16 cruise transecting the Eastern Tropical South Pacific ODZ from Peru to Tahiti (Cutter et al., 2018, Schlitzer et al., 2018, GEOTRACES Intermediate Data Product Group, 2021). Figure made in Ocean Data View.*

2.2.2 What are drivers of inter- and intra- O_2 spatiotemporal variations?

Not all ODZs are created equally. Notable differences include the spatial variability in sub-μmol kg^{-1} O_2 concentrations that were already discussed in Section 2.2.1. Ultimately, several factors can influence O_2 availability in ODZs. As reviewed in Oschlies et al. (2018), O_2 sources can be impacted by temperature effects on O_2 solubility, increased stratification limiting the exchange of O_2-rich surface waters and O_2-poor subsurface waters, wind-driven changes in overturning circulation, and freshwater inputs decreasing deep meridional overturning at high latitudes. O_2 consumption can be impacted by temperature effects on metabolic rates, the quality and/or quantity of sinking particles, and nutrient supply from the ocean interior, land, or the atmosphere.

Figure 7 demonstrates spatial and temporal variations in the minimum O_2, depth, thickness, and potential density anomaly (sigma-theta) of modern ODZs. As reviewed extensively in previous works (Paulmier and Ruiz-Pino, 2009, Karstensen et al., 2008), these characteristics provide basic constraints on the source of water masses hosting ODZs. The most prominent observation is that the most extensive and intense ODZs are observed in the Pacific and Indian Oceans. In contrast, the Benguela and Mauritanian ODZs of the South and North Atlantic, respectively, occupy limited water column areas and have less reducing cores, with higher O_2 concentrations compared to their Pacific and Indian counterparts. Another prominent observation is that ODZ thickness and depth is greatest in the North Pacific relative to other ODZs. The drivers of these observations are discussed in more detail below.

The Atlantic and Pacific ODZs are located in regions not reached by the equatorward flow of oxygenated waters from the subtropics—or shadow zones (Luyten et al., 1983). These sluggish flow regimes result in a similar pattern of Eastern Boundary Current distribution in the North and South Pacific and Atlantic Oceans. However, the lesser extent of ODZs and higher maximum O_2 values in the Atlantic relative to the Pacific distinguishes the two basins. On a first order, these differences are related to the relative size of the ocean basins themselves compared to their thermocline ventilation rates (Karstensen et al., 2008). Specifically, the thermocline volume in the Pacific is three times larger than that of the Atlantic and is renewed at a substantially slower rate, thus impacting the rate of O_2 replenishment vs loss and acting as a primary control on ODZ extent. The limited ventilation in the Pacific vs the Atlantic can be quantified via their O_2 ages, which also differ between the North and South for the two basins (Karstensen et al., 2008). The Atlantic is overall best ventilated. In the Pacific, more limited ventilation, and a larger water volume result in much older O_2 ages and thus more extensive volume of and lower O_2 within ODZs. This situation is particularly exacerbated in the North Pacific, which occupies approximately $1/4^{th}$ of the thermocline volume of the Atlantic and Pacific but is characterized by $1/8^{th}$ of the renewal rate (Karstensen et al., 2008).

The ODZs in the Indian Ocean are most similar to the Pacific, with extensive volumes of water with $O_2 < 20$ μmol kg^{-1}. While the O_2 ages and renewal rates for the Indian Ocean have not been estimated to our knowledge, the ODZs are similarly regulated by sluggish ventilation of the thermocline (Tomczak and Godfrey, 2003). A front at 15 ºS is created by the inflow of the Australasian Mediterranean Water (AAMW) mass from the Pacific to the Indian Ocean (Quadfasel and Schott, 1982). At the front, an intense O_2 gradient is formed, creating the ODZ in the Arabian Sea. Active deoxygenation does not extend into the Bay of Bengal (Howell et al., 1997), likely contributing to the higher minimum, yet still sub-μmol kg^{-1}, O_2 values and more limited active N cycle in this region.

A seasonal comparison of ODZ properties demonstrated that permanent ODZs may contract/expand by as much as 10-15% annually (Paulmier and Ruiz-Pino, 2009). We also present visualizations of seasonality in Error! Reference source not found. by comparing the minimum and maximum properties of ODZs at the depth of minimum O_2 across the four seasons. Winter mixing in the Gulf of Alaska and West Bering Sea contributes to a strong seasonal dynamic of the ODZ (Paulmier and Ruiz-Pino, 2009). The West Bering Sea and Gulf of Alaska ODZs develop mostly in the boreal winter and in the fall-to-spring, respectively, with O_2 fluctuations in the ODZ core above and below 20 µmol/kg in many locations (Paulmier and Ruiz-Pino, 2009). For other ODZs, the cores are relatively stable while the fringes, particularly in the South Pacific, have the potential to be seasonally dynamic and show the largest seasonal variations (**Figure 7**).

In the Arabian Sea, the seasonal Asian monsoon has a strong impact on the ODZ, which is reflected in part in Error! Reference source not found. by the large seasonal swing in the depth and sigma-theta of minimum O_2 (Schmidt et al., 2020). The ODZ vertical expansion is highest during the boreal winter monsoon, with the most seasonal O_2 concentration along the 27 kg m^{-3} isopycnal due to ventilation from the Persian Gulf and Red Sea water masses (Schmidt et al., 2020, Banse et al., 2014). Other factors contributing to seasonal variations in ODZs generally include seasonal wind patterns impacting upwelling rates, eddy fluxes on the ODZ fringes introducing O_2 and often hosting denitrification, and associated nutrient feedbacks impacting primary production and zooplankton biomass (Bhaskar et al., 2021, Wishner et al., 2013, Vergara et al., 2016, Margolskee et al., 2019, Evans et al., 2020b). Beyond seasonal timescales, the ETSP ODZ has also been reported to show as much as a 60% reduction in the sea floor *area* characterized by O_2 levels <20 µmol kg^{-1} during El Niño years (Helly and Levin, 2004).

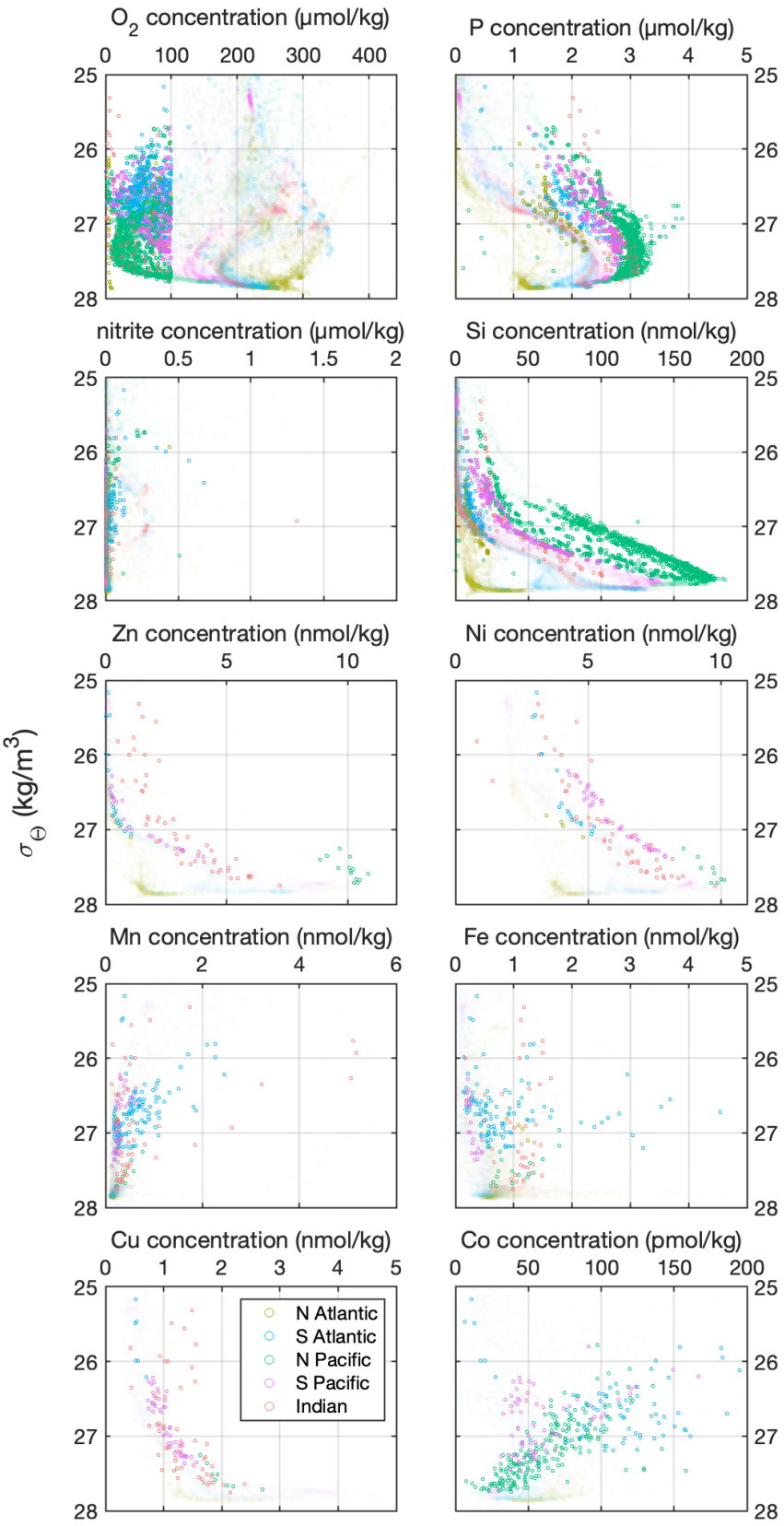

Figure 9. A.) Plot of potential density anomaly (sigma-theta) vs. O_2, nutrient, and trace element concentrations for different ocean basins for the entire GEOTRACES database (Schlitzer et al., 2018, GEOTRACES Intermediate Data Product Group, 2021). These are the same data evaluated using the PCA in **Figure 10**. The transparent data points represent data at depths with O_2 concentration >100 µmol kg^{-1} while the opaque data points are from depths with O_2 concentrations <100 µmol kg^{-1}. The elements are shown in order of descending maximum concentration.

2.2.3 Patterns of dissolved O_2, trace elements, and nutrients in modern water columns

A current frontier is fingerprinting variable ODZ controls via their trace element compositions. The GEOTRACES data provide the opportunity to explore the relationship between the processes impacting O_2-deficient waters and biogeochemically relevant elemental concentrations and by extension, their geochemical cycles. Trace element and isotope data from GEOTRACES were introduced in the last Treatise Edition (Bruland et al., 2014) and cycling of many key elements are discussed in this Treatise Edition (Little et al., this issue; Farmer et al., this issue).

Here we focus on ocean redox controls on trace element distributions. To investigate the controls on the variability of the data shown in **Figure 9**, we conducted Principal Component Analysis (PCA), a statistical tool that allows us to evaluate differences in key data from the GEOTRACES 2021 database (GEOTRACES Intermediate Data Product Group, 2021) between different ODZs as well as between O_2-deplete and O_2-replete water masses (**Figure 10**; e.g., Bolster et al., 2022). We limited our analysis to samples that contained all of the parameters shown in **Figure 10**. Due to this limitation and the limited data availability for low O_2 waters, we use a higher cutoff of $[O_2] < 100$ µM for identifying ODZ water masses and refer to samples where $[O_2] > 100$ µM as well-oxygenated waters. Therefore, some of these waters have O_2 levels above the hypoxia threshold and expand into regions that technically are not considered ODZs.

Water mass characteristics (depth, sigma-theta, and dissolved O_2 recorded as "O_2"), dissolved macronutrient concentrations (P), dissolved micronutrient concentrations (Fe, Mn, Zn, Ni), and dissolved concentrations of other essential nutrients (Si, Cd, Co) can be compared across ocean basins where ODZs can be observed. Fe-limitation is a well-recognized phenomenon in oligotrophic settings (Martin et al., 1994, Fitzsimmons and Conway, 2023); Si and Cd are critical elements for diatoms and Co and Mn can limit primary productivity. Bioessential elements such as Fe, Mn, Co and Zn are also redox sensitive and therefore trace metal patterns in ODZs can reflect not just biogeochemical cycling (e.g., productivity and remineralization) but also abiotic redox and non-redox processes (reviewed in Horner et al. (2021)).

Though these variables are all treated as independent, there are likely co-dependencies that can be observed in the relationships in **Figure 9** and **Figure 10**. For example, in all analyses, depth and sigma-theta are closely aligned, which is logical given that density is a function of temperature and pressure, which changes with water depth. In sum, the PC1 and PC2 for these data describe most of the variance observed in the global datasets (~60% and 15-22%, respectively). The main observations from the PCA are:

1. The PCA for the global dataset (**Figure 10A**) strongly reflects the differences between ocean basins (**Figure 10B** vs. **Figure 10C**). Within the global dataset and for well-oxygenated regions, the largest sources of variance between ocean basins are the distribution of nutrients and O_2 concentrations, which are inversely related. The North Atlantic is generally best oxygenated, followed by the South Atlantic, South Pacific, Indian, and North Pacific regions. As discussed previously, this reflects the development of young, well-oxygenated sub-surface waters in the Atlantic. Similarly, the concentrations of nutrients, as well as average water depth/sigma-theta, increase in the order listed above.
2. For the PCAs of the global dataset and well-oxygenated water masses (**Figure 10A,B**), the distribution of Mn is inverse to Fe and the other micronutrients discussed above, highlighting Mn cycling in well-oxygenated waters that broadly reflects well known, non-redox-based processes such as photoreduction and/or external fluxes.

3. The PCA for O_2-depleted waters (**Figure 10C**) also shows a strong correlation with depth/sigma-theta and nutrients (Cd, P, Zn, Si), which are the variables most closely aligned with PC1 (59.1%). The different ocean basins are arrayed along PC1, and primarily reflect differences in nutrient availability. The relative abundance of nutrients in the O_2-depleted waters of these ocean basins is also similar to the order observed in the global dataset, with higher concentrations in the North Pacific and decreasing in the Indian, South Pacific, North Atlantic, and South Atlantic basins. Note that we did not perform an ANOVA or other test of the significance of these difference in concentrations. Compared to the global PCA, however (**Figure 10A and B**), the relationship between O_2 and nutrients is weak in O_2-depleted waters (O_2 is more closely aligned with PC2 instead of PC1).
4. Although most of the variance between O_2-depleted waters of different basins is attributed to nutrients, PC2 (22.3%) reflects different controls on redox-sensitive elements and O_2 compared to the global dataset. Specifically, PC2 identifies Mn and Fe as behaving roughly similar and inversely with O_2 concentrations. In other words, higher Mn and Fe are found to correspond to lower O_2 concentrations, and this appears to be most important for the North Pacific and Indian Ocean basin data. This relationship is reasonable because the dissolved forms of Mn and Fe are expected in low-O_2 water masses due to their redox-dependent solubility. This is supported by a PCA of GEOTRACES data from the ETNP that shows a strong correspondence of Mn and Fe with nitrite (Bolster et al., 2022).

This analysis identifies a few key features that define the major redox controls in the modern ocean and potential geochemical signals that record this behavior. First, there is a clear grouping of nutrients and bioessential elements (Cd, Ni, P, Si, Zn) whose cycling is similar and whose concentrations can pinpoint well-oxygenated, high-density waters. We suggest that these are linked via water mass age. As discussed above in Section 2.2.1, variation in O_2 ages is an important control on bottom water O_2 as well as O_2 within ODZs, ultimately resulting in the differences in O_2 seen between ocean basins and across N-S transects (**Figure 8**). Elevated nutrients are also closely tied to O_2 ages because they reflect similar inputs from remineralization (**Equation 1** and **Equation 2**) as well as limited ventilation or re-supply from nutrient-starved surface waters.

In O_2-depleted waters, however, the relationship between nutrients and O_2 is weaker. The correlation between the bioessential elements and depth/sigma-theta in **Figure 10** reflects the increase of dissolved concentrations from remineralization via the biological pump (Liu et al., 2022). Importantly, the concentrations of these nutrient-type trace elements are typically much more elevated in ODZ regions relative to oxygenated regions (**Figure 9**). Differences in concentrations of bioessential elements and/or the depth of the O_2 minima drive the differences between O_2-depleted waters of different ocean basins, which are arrayed along the PC1 axis: water depths and nutrients are both highest in the North Pacific (also seen in **Figure 9**), followed by the Indian, South Pacific, North Atlantic, and South Atlantic basins. This generally corresponds to the age of upwelling water-masses, with the oldest, most nutrient-replete waters found in the Pacific and relatively younger, more nutrient-deplete waters in the Atlantic (Karstensen et al., 2008). As discussed previously, the PCA therefore provides further evidence that the geochemical composition of trace elements—in addition to O_2 levels, CO_2, pH—are related to water-mass age (Section 2.1.3).

For water masses with O_2 concentrations >100 μM, Fe and Mn diverge (**Figure 10B**). In the global dataset, Mn is positively correlated with O_2 whereas it is negatively correlated with O_2

892 in O_2-depleted waters. Dissolved Fe is generally inversely correlated with oxygen, regardless of
893 whether O_2 is high or low. We hypothesize that the Fe-O_2 inverse relationship reflects that Fe is a
894 limiting nutrient for primary productivity in many modern ocean basins (Martin et al., 1994).
895 Additionally, inputs of total dissolved Fe (dominantly Fe^{2+}) in well-oxygenated waters below
896 ODZs in the Arabian Sea and Peru Margins are sourced by hydrothermal plumes as well as
897 dissolution and desorption from slope sediments (Moffett and German, 2020, Resing et al., 2015,
898 Horner et al., 2015) (**Figure 8**). In the South Atlantic, dissolved Fe and Co are both elevated, even
899 under oxic conditions below the ODZ core, because they can be stabilized in the upwelling zone
900 by abundant organic ligands and subsequently transported laterally into oxygenated waters (Liu et
901 al., 2022).
902 The inverse correlation between Mn and O_2 is important because Mn is not a limiting
903 nutrient and its cycling reflects more than redox processes. For example, nutrient profiles are
904 characterized by very low concentrations in the eutrophic zone from uptake during primary
905 productivity, but elevated dissolved Mn concentrations at the same depths can result from supply
906 from continental runoff near the mouths of rivers and dust inputs near continental margins. This is
907 observed off the coast of the ETNP, such as near the mouth of the Río Balsas, Mexico (Bolster et
908 al., 2022, Landing and Bruland, 1987). Additionally, photoreduction of Mn oxides can result in
909 higher Mn in surface waters than expected (Sunda et al., 1983). Below ODZs, where dissolved O_2
910 concentrations are elevated from old intermediate and bottom waters, elevated Mn is observed
911 from hydrothermal seafloor activity that result in high fluxes of Mn but low dissolved Fe, which
912 in contrast is quickly oxidized and titrated out of solution. Compared to Fe, oxidation of Mn is
913 kinetically slower (Moffett and German, 2020) and hydrothermal Mn plumes can persist (e.g., the
914 East Pacific Rise in **Figure 8**). High Mn concentrations in deep, well-oxygenated waters have also
915 been observed in the Arabian Sea (Moffett and German, 2020) and in the ETNP (Bolster et al.,
916 2022).
917 Therefore, the combination of bioessential elements, Fe, and Mn in a given water mass can
918 be useful for characterizing the productivity and redox dynamics of a given region. First, a
919 correlation between Fe and Mn is a good indicator of O_2-deficient conditions, whereas the lack of
920 a correlation may indicate other non-redox processes and therefore are more likely to represent
921 waters with more O_2. Higher concentrations of bioessential elements (P, micronutrients) primarily
922 reflect water mass age and ocean-scale circulation patterns. These patterns have potential promise
923 for more nuanced understanding of redox in ancient oceans, if some assumptions are made about
924 how these signals are transferred to marine sedimentary records.

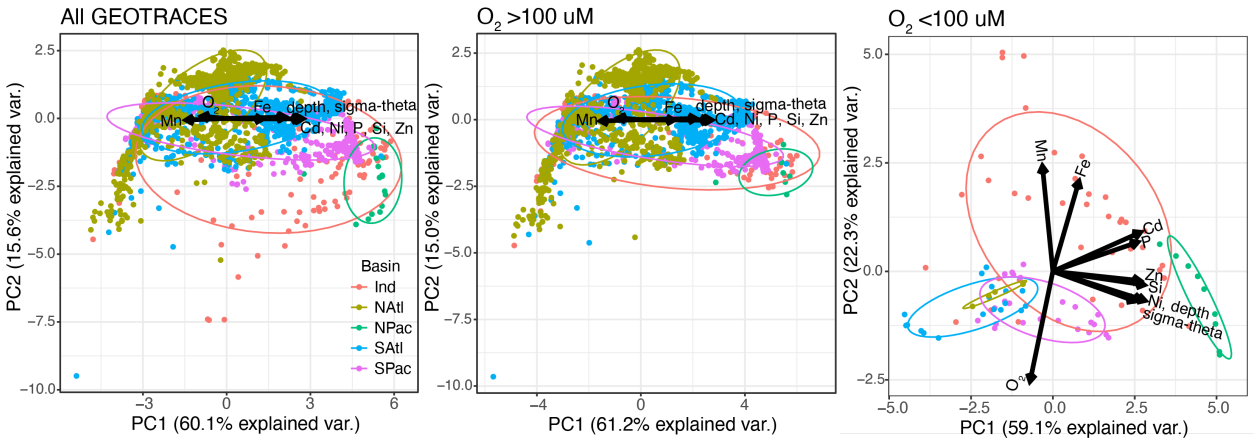

Figure 10: *Principal component analysis of GEOTRACES data (GEOTRACES Intermediate Data Product Group, 2021), including depth, sigma-theta, CTD-collected O_2 concentrations, and Cd, Mn, Fe, Ni, Zn, Si, and P concentrations. (A) PC1 and PC2 of all data for the Indian (Ind), North Atlantic (NAtl), North Pacific (NPac), South Atlantic (SAtl), and South Pacific (SPac). (B) PC1 and PC2 for samples where O_2 concentrations are > 100 uM. (C) PC1 and PC2 for samples where O_2 concentrations are < 100 uM as a rough filter for ODZs. Note that the axes scales differ for each plot.*

2.2.4 Implications for fingerprinting ancient redox processes

In the last decade, there has been a broad push to advance paleoredox proxy calibrations beyond the Black Sea and other modern euxinic basins, and to better understand our ability to recognize ODZ-like settings in the ancient past. Targeted sediment and water column studies from individual ODZs, as well as data collection programs like GEOTRACES have played a major role in this important frontier. To be clear, the translation between water column geochemistry and sedimentary geochemistry is not straightforward. Nonetheless, the use of proxies necessitates understanding the links and limitation for the application of redox-sensitive and/or bioessential elements from sediments as a reflection of water column concentrations and/or processes.

An important finding from the PCA results and recent studies is a reminder of the strong link that benthic and diagenetic processes also have on water column geochemistry, which must be integrated into paleoredox interpretation. The geochemical cycles of Fe and Mn are often interpreted as paleoredox proxies, as the burial of Fe-Mn oxides—linked to the areal extent of oxygenated bottom waters—is an important sink for many redox-sensitive trace elements, impacting their availability and isotopic compositions in seawater. Iron cycling is more directly traced via Fe isotopes and the abundance of Fe within specific mineral fractions, i.e. Fe speciation used to distinguish between euxinic from ferruginous conditions (Raiswell et al., 2018). The PCA in **Figure 10** indicates a strong link between O_2 and Mn and Fe cycling within ODZs. As reviewed in Section 2.2.1, the concentrations of Fe and Mn are primarily sourced from benthic fluxes, and thus reflect diagenetic processes, but their accumulation and transport within the water column are related to water column redox conditions allowing for their persistence.

We suggest that there is an important need to more specifically calibrate the integrated impact of benthic processes on Fe and Mn-based paleoredox proxies. The GEOTRACES analyses builds on recent studies suggesting that Fe speciation ratios, and particularly those intended to characterize ferruginous conditions—can be complicated by sedimentary transformation of Fe-bearing mineral phases. Indeed, ODZs offer the only modern marine analogue of so called 'ferruginous' conditions, but multiple lines of evidence suggest that ferruginous conditions may

have been widespread in the past and likely characteristically different than today. Modern ferruginous lakes may actually represent the best analogues for ancient ferruginous marine settings because modern high marine SO_4^{2-} limits Fe mobilization due to pyrite formation (Swanner et al., 2020). That said, modern studies can provide a framework for interpreting ancient Fe/Mn cycling while simultaneously constraining the limitations of these proxies for understanding ancient paleoredox environments lacking true modern analogues (Pasquier et al., 2022, Hepburn et al., 2020, Slotznick et al., 2020, Slotznick et al., 2022).

Specifically, early diagenetic processes readily impact the distribution of Fe-bearing phases, including redox reactions involving Fe(III)-(oxyhydr)oxide under oxic or anoxic water columns. As discussed in Section 2.2.3, the impact of this can be observed in elevated Mn and Fe concentrations in low-O_2 waters (**Figure 10**). As a result, Fe speciation may be most strongly linked to benthic Fe fluxes which remobilize Fe across redox gradients (Scholz et al., 2011, Moffett and German, 2020, Bolster et al., 2022). For example, **Figure 8** shows elevated bottom water Fe along the Peru margin slope both within and outside the ODZ, which is supported by Fe speciation data indicating sedimentary remobilization within the ODZ and deposition along the ODZ fringes (Scholz et al., 2014a, Scholz et al., 2014b, Lam et al., 2020). The sediment-water interface is also itself a redox gradient, with Fe (and Mn) mobilization from anoxic pore fluids to the water column and deposition downslope (Severmann et al., 2006). Ultimately the extent of the effect of the benthic Fe flux on Fe speciation ratios is determined by the abundance of sulfide, which in turn is related to the degree of organic carbon loading. Because ODZs are commonly loci of high organic carbon burial, where some Fe(II) diffuses from the pore fluids to the water column, a significant portion of Fe(II) must also be stabilized by sulfide during early diagenesis. Regardless, the net effect of reduction of Fe(III)-minerals in reducing sediments is to decrease highly reactive pools of Fe (e.g., Fe_{HR}/Fe_T) (Pasquier et al., 2022).

Similar benthic fluxes for Mn (Scholz et al., 2014a), Co (Liu et al., 2022), I (see excess I^- > 500 nM in **Figure 8**) and likely other trace metals also indicate that analogous combinations of diagenetic fluxes and low water-column O_2 are expected to also impact concentrations, enrichment factors, and normalized ratios (e.g., [metal]/[Al]) of redox-sensitive elements in the sedimentary record more broadly. Diffusive benthic fluxes of other elements such as sulfide and U are also expected in ODZs due to the concentration gradients that form during early diagenesis (Lau et al., 2020). Notably, the GEOTRACES data suggest that high productivity regions where oxidized solid phases can be transported downslope may result in lower-than-expected proxy ratios for a low-O_2 setting.

This discussion is an important reminder that early and late diagenetic processes can strongly impact the sedimentary geochemical record post-depositionally but also more directly impact water column conditions that are critical for linking environmental and biotic change through time. Therefore, mechanistic studies that probe the relative roles of water-column and sedimentary geochemical processes on proxy records continue to be a major area of research in understanding past ocean redox.

2.3 Anthropogenic impacts on ocean redox

The evidence for anthropogenic impacts on ocean redox conditions indicates significant declines in dissolved O_2 concentrations for much of the ocean (Keeling et al., 2010, Breitburg et al., 2018, Oschlies et al., 2018). Since 1950, a 2% decline in marine O_2 has been observed (Schmidtko et al., 2017, Stramma et al., 2008). Supporting this, a decrease in atmospheric potential O_2 (APO), which reflects exchange of O_2 with the oceans, was observed from 1990 to 2010 in the

northern and southern hemisphere (Keeling et al., 2010). Based on this measure, the oceans are estimated to be losing ~40 Tmol O_2 yr^{-1}. In the 2014 Intergovernmental Panel on Climate Change (IPCC) report (Hoegh-Guldberg et al., 2014), decreases in dissolved O_2 were recognized that are consistent with warming temperatures, increased stratification and microbial respiration, coastal eutrophication, and drawdown of O_2 in semi-enclosed seas, coastal boundary systems, some eastern boundary upwelling ecosystems, subtropical gyres, and the deep sea. From 1970 to 2010, the upper 1000 m of the ocean lost 0.5 to 3.3% of its dissolved O_2 content (Bindoff et al., 2019), with the magnitude of decrease modulated by interannual and inter-decadal climate variability (Cooley et al., 2022). The area of expanded OMZs since the 1950s is approximately equivalent to the area of the European Union, with the volume of completely anoxic waters quadrupling over that time span (Breitburg et al., 2018). The expansion of coastal waters that are now hypoxic includes a compilation of 500 sites, more than 90% of which were previously not known to be hypoxic (Breitburg et al., 2018).

This trend toward more extensive and more severe hypoxia is expected to continue over the next century. Community Earth System Models suggest that O_2 may decrease in the subsurface by approximately 0.05 to 0.15 mmol m^{-3} (equivalent to a 4 to 11% decrease compared to 1995-2014 levels) by 2100 depending on the model boundary conditions and the assumed emission scenario (Kwiatkowski et al., 2020). Spatially dissolved O_2 was modeled to decrease most significantly in the North Pacific and in parts of the Southern Ocean (Kwiatkowski et al., 2020). Model predictions for globally decreasing O_2 are in strong agreement with each other, but vary regionally depending on changes in wind stress, coastal processes, and organic matter supply. Confidence that ODZs and seasonally hypoxic waters will expand is high but changes in productivity from climate- and wind-driven upwelling is less clear. There is high confidence that future predicted hypoxia will impact commercial fisheries and habitat loss. Additive effects on ecosystems between ocean acidification, warming, and hypoxia, especially in productive upwelling regions, have been recognized to be a growing concern for marine environments and impacts on humans (Bindoff et al., 2019, Cooley et al., 2022).

The direct anthropogenic effects on ocean redox conditions are myriad (Breitburg et al., 2018, Cooley et al., 2022). Direct effects on solubility (i.e., higher temperatures decreasing O_2 saturation) account for ~15% of total global oxygen loss, with a significant impact (~50%) in the upper 1000 m (Helm et al., 2011, Schmidtko et al., 2017). The burning of fossil fuels has decreased atmospheric O_2 (Keeling and Manning, 2014), leading to lower O_2 dissolved in seawater. In shelf seas, seasonal bottom-water hypoxia occurs due to warming thanks to riverine nutrient loading and freshwater input, leading to stratification, which reduces O_2 penetration into deep waters, and productive conditions, which increases O_2 demand. In eastern boundary upwelling systems, intensification of ocean upwelling leads to enhanced anoxia and acidification, but uncertainty remains for specific regions due to contradictory observations. Anthropogenic eutrophication, including organic matter addition and pollution-induced atmospheric inputs of iron, have enhanced deoxygenation (Breitburg et al., 2018, Cooley et al., 2022). By 2100, dissolved O_2 is expected to decrease in critical marine biomes, including coastal seas, coral reefs, kelp systems, upwelling zones, and polar regions, with varying severity (Kwiatkowski et al., 2020).

Indirect mechanisms of warming temperatures, including greater stratification and changes to circulation patterns, are more difficult to accurately represent and predict (Oschlies et al., 2018) but are significant (Breitburg et al., 2018). Understanding the mechanisms linking surface winds to upwelling in key productive regions of the ocean, mainly in coastal regions, is a critical need for predicting the extent and severity of future hypoxia (Hoegh-Guldberg et al., 2014). Model

improvements that are needed include better representation of transport processes, higher spatial resolution, and a focus on wind forcings and overturning of the deep ocean (Oschlies et al., 2018). Another key need is to better understand how microbial metabolic feedbacks will respond to changing temperature, which will ultimately drive O_2 concentrations in the deep ocean. Where nutrient trends (e.g., nitrate) regionally lead to redox stratification is another area of needed future study, with significant uncertainty in how warming will result in ocean deoxygenation in subtropical oceans, especially for major ODZs (Cooley et al., 2022). Additionally, incorporation of improved biogeochemical schemes, including redox-dependent nutrient stoichiometries, would improve GCM predictions of anthropogenic effects on ocean O_2 distributions (Oschlies et al., 2018).

3 Recent: Evolution of ocean redox on glacial-interglacial timescales

Quaternary climate changes, marked by glacial-interglacial cycles driven by shifts in Earth's orbital parameters, extend the timescale of processes impacting ocean redox described above in Section 2. These processes can include broader changes in climate that drive fluctuations in the O_2 sources and sinks (**Figure 3**). Previous research on ocean O_2 change on glacial-interglacial timescales has focused predominantly on the deglaciation since the Last Glacial Maximum (LGM; ~27 to 20 ka). Reconstructions of changes in the ocean redox state, including changes in ODZs, over this interval are instructive because the deglacial period (18 to 11 ka) represents a relatively rapid and major global climate warming event, punctuated by shorter-lived cooling and warming periods (**Figure 11**). Over this time, sea surface temperatures are estimated to have increased by ~ 4 to 8 ºC (Osman et al., 2021) and atmospheric pCO_2 by ~80 ppm (Petit et al., 1999, Monnin et al., 2001, Lüthi et al., 2008).

In this section, we summarize changes in ocean O_2 and ODZs that reflect aggregated climatic signals from major changes in orbital parameters and specifically the warming from a world with extensive continental ice sheets through the Holocene (last 10 ka) to a period of relative climate stability. The examples in this section can provide useful insight into the future of ocean oxygenation from anthropogenic warming and climate change. Therefore, research in developing qualitative and quantitative O_2 proxies, reconstructing O_2 depth gradients, and increasing spatial sampling of sites important for ODZ and water-mass redox reconstructions are all critical needs (Section 3.1). Further, integrating oceanographic, climatic, and modeling constraints are necessary to understand how regional and global climate factors compete or balance to impact the overall redox landscape, including ODZ development (Section 3.2). Last, we discuss the role of sea-level change on redox conditions—a factor that can be overlooked for this time period (Section 3.3).

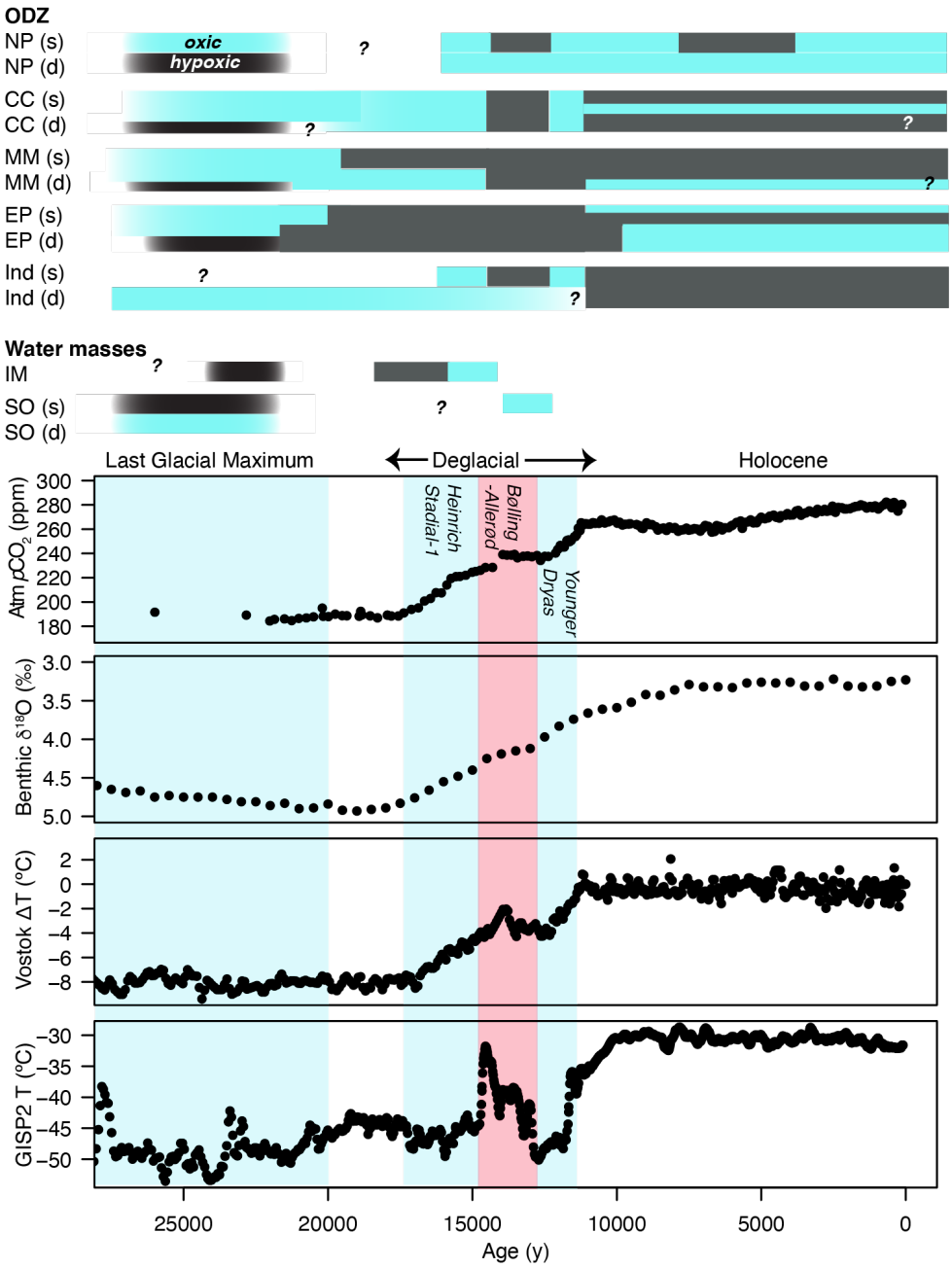

Figure 11. *Overview of redox and climate reconstructions from the Last Glacial Maximum (LGM), through the Deglacial, and into the Holocene. The Deglacial was punctuated by the Bølling-Allerød warming event and the Younger Dryas cooling event. Relative changes in oxic (blue) and intermediately/severely hypoxic (gray) conditions are shown for ODZs and key water masses (summarized from Moffitt et al., 2015 and other sources in text). (s) indicates shallow and (d) indicates deep. NP = North Pacific/Subarctic Pacific, CC = California Current, MM = Mexico Margin, EP = Equatorial Eastern Pacific, Ind = Indian Ocean, IM = Iberian Margin, SO = Southern Ocean. Benguela Current not shown due to lack of glacial-interglacial variability. Climate proxy records, top to bottom: atmospheric pCO_2 (Lüthi et al., 2008), global benthic $\delta^{18}O$ stack (Lisiecki and Stern, 2016), Vostok surface temperature changes calculated from snow δD (Petit et al., 1999), and Greenland Ice Sheet Project 2 (GISP2) temperature reconstructed from snow $^{18}O/^{16}O$ (Grootes and Stuiver, 1997).*

3.1 Patterns of ocean O_2 change since the Last Glacial Maximum

Globally, shallow-marine O_2 is higher during the LGM compared to the deglaciation, whereas the deep ocean was less well oxygenated (**Figure 11**) (Lu et al., 2020a, Jaccard and Galbraith, 2011). Similarly, reconstructions of O_2 during older Pleistocene periods suggest cooling is broadly associated with low O_2 in intermediate and deep waters—e.g., the Amundson Sea of the Southern Ocean (Lu et al., 2016), the Iberian Margin (Hoogakker et al., 2015), and North Atlantic (Hoogakker et al., 2016). These broad redox shifts are also observed in ODZs during the LGM, but regional variability exists that reflects both differences between northern and southern hemisphere warming and cooling over the deglaciation as well as regional climate (**Figure 11**; e.g., upwelling strength). The extent of ODZs since the LGM has been reconstructed for the Subarctic Pacific, California Current, Baja and Mexico Margins, the Equatorial Pacific and Humboldt Current, the Benguela Current, and the Oman/Pakistan Margin (Moffitt et al., 2015). Using sediment core logs from continental margins (within 400 nautical miles of the continental coastline, plus the Galapagos Islands), evidence for various degrees of hypoxia, relative to the impact on bilaterian behavior and habitability, were compiled from: (1) sedimentary data, and specifically the presence of laminations that form from the absence of bioturbation; (2) benthic foraminiferal diversity, density, and abundance, based on thresholds defined by specific taxa; and (3) geochemical proxies, including N isotopes that trace water masses and nutrients, redox-sensitive trace elements that record redox and/or productivity (Re, Cr, U, Mo, Cd), and C isotopes of planktonic forams that track productivity and carbon export. Evaluating the compilation as a whole, and accounting for the incomplete temporal and spatial coverage of the sediment core records, ODZs exhibited a trend toward more anoxic conditions during the deglaciation and toward the present (Moffitt et al., 2015). Actual trends in redox conditions vary between ODZs, with some reflecting larger scale climatic changes and others modulated by regional processes. Below, we briefly summarize the synthesis from Moffitt et al. (2015). We refer the reader there for additional details and references therein and include more recent studies where applicable (**Figure 11**).

Subarctic (North) Pacific: the extensive, intermediate water ODZ here is controlled by poorly ventilated, nutrient-rich and O_2-depleted North Pacific Deep Water. Today, there is a seasonal ODZ in the Gulf of Alaska, with expansion of hypoxic waters toward Russia in the winter ((Paulmier and Ruiz-Pino, 2009); **Figure 7**). During the LGM, the deep North Pacific was ferruginous and became more oxic during the deglaciation (Jaccard et al., 2009), with greatest O_2 depletion during peak Bølling-Allerød warming (~14 ka). The region overall experienced more extensive and severe hypoxia during warming periods (intensified at 14 ka), with relatively shallow hypoxia (~600 mbsl), attributed to lower O_2 solubility and higher respiration rates (Praetorius et al., 2015). The absence of hypoxia during Younger Dryas cooling (~12.9 to 11.7 ka) suggests a high sensitivity to global climate trends. This ODZ became relatively well oxygenated at 10 ka, but the return of hypoxia at 4 ka throughout the region also supports a global climate control. Recent investigations of the stratigraphic relationships between ash, volcanic fractions (εNd), redox-sensitive trace metals, and benthic foraminifera in the Gulf of Alaska suggest that regional volcanism, stimulated by ice unloading of the Cordilleran ice sheet, resulted in iron fertilization that led to deoxygenation (Du et al., 2022). This mechanism is proposed to have acted to further enhance and sustain deoxygenation resulting from broader deglacial warming trends.

California Current region: the ODZ here reflects seasonal upwelling that intensifies in the boreal spring, with accompanying high productivity. Today the loci of O_2 depletion occurs within 200 km of the coastline and within relatively deep waters (~600 mbsl) extending almost 1.5 km deep (**Figure 7**). O_2 is replenished by North Pacific Intermediate Water which is mixed with

poorly oxygenated southern-sourced intermediate waters. During the LGM, intermediate waters (~1000 mbsl) were oxygenated whereas deep waters were hypoxic. During the Bølling-Allerød, intermediate to severe hypoxia occurred at all depths, with a respite to oxic conditions at 12 ka, midway through the deglaciation and synchronous with Younger Dryas cooling observed throughout the Northern Hemisphere. During Termination 1B (11.7 ky), regional hypoxia returned, especially at shallower depths (400-600 mbsl), that continued through the deglaciation.

Mexico Margin: the ODZ in this region is modulated by high productivity, a sharp pycnocline, and slow circulation. The upper boundary of the ODZ is shallow (up to 100 mbsl in the south; **Figure 7**) due to the intrusion of intermediate waters with low O_2. During the LGM, only the deepest waters were depleted in O_2. Bottom-water oxygenation increased through the deglaciation to the present day, though the timing is spatially variable. Changes in redox are potentially linked to the depth of the thermocline and nutricline, as well as relatively low productivity during the LGM because of reduced upwelling. In sum, regional controls appear to modulate ODZ variability in the Mexico Margin, compared to the other sites that more strongly reflect northern hemispheric climatic changes.

Humboldt Current and Eastern Equatorial Pacific: the ODZ in this region (roughly equivalent to the ETSP) is driven by upwelling of nutrient-rich southern hemispheric intermediate waters and extreme productivity, resulting in a thick, intense, and shallow ODZ (up to 50 mbsl and ~500 m thick zone of extremely O_2-depleted waters; **Figure 7**). During the LGM, only deep waters were characterized by mild hypoxia with surface and intermediate waters well-oxygenated. Deep waters became oxygenated from 10 to 5 ka, depending on the depth and spatial location. Shoaling of the ODZ began ~17 ka with severe hypoxia present at the upper boundary of the ODZ. Hypoxia at intermediate depths persisted throughout the deglaciation but attenuated at shallow depths by 10 ka, returning to oxic conditions. Changes in redox through the deglaciation follow Southern Hemisphere patterns instead of Northern Hemisphere patterns. More recently, qualitative and quantitative constraints from planktonic foraminiferal I/(Ca+Mg) (to constrain the upper water column) and a benthic foraminiferal $\delta^{13}C_{carb}$ isotope gradient (to constrain bottom water O_2) from cores off the coast of Costa Rica and offshore in the eastern equatorial cold tongue of the eastern tropical Pacific indicate relatively low O_2 (40-60 μmol kg^{-1}) in intermediate and deep waters during the LGM and during the early deglaciation (Hoogakker et al., 2018). In contrast to previous studies, surface O_2 at these sites is reconstructed to be relatively low during the LGM.

Indian Ocean: this vertically extensive ODZ (>1000 m; **Figure 7**) is controlled by nutrient delivery, ventilation by intermediate and deep waters, and mixing of deep waters. The ODZ is seasonally dynamic due to monsoonal patterns that control upwelling of nutrient-rich waters. Changes in the ODZ reflect changes in productivity, potentially due to climate-driven monsoons. Therefore, ODZ weakening is observed during cooling events (Heinrich 1 and the YD); changes here are rapid. More recent constraints on the Arabian Sea ODZ from benthic forams, I/(Ca+Mg), and authigenic U records indicate that bottom-water oxygenation was higher during the glaciation and then steadily decreased during deglaciation into the Holocene (Lu et al., 2020a). Estimates of bottom water O_2 concentration indicate that it has remained below 30 μmol kg^{-1} over the last 30 ka, reaching modern levels of ~5 μmol kg^{-1} around 11 ka (Lu et al., 2020a, Lu et al., 2022).

Benguela Current: Compared to the above examples that track major hemispheric climate trends, the Benguela Current ODZ is interpreted to reflect regional climatic controls. This ODZ is associated with high productivity and seasonal upwelling. It is shallower and more spatially limited compared to other ODZs (**Figure 7**). Hypoxic waters are relatively shallow, reaching depths up to 50 m. During the LGM, bottom-waters were continuously anoxic (Riedinger et al., 2021). The

proxy records here do not suggest a change in oxygenation driven by deglaciation but instead regional changes in productivity and upwelling (Mollenhauer et al., 2002, Moffitt et al., 2015). However, the role of deep-water circulation patterns has recently been argued to impact productivity and thus ODZ severity during the deglaciation (Riedinger et al., 2021).

Southern Ocean: The Southern Ocean plays an important role in controlling O_2 concentrations in deep waters that subsequently ventilate the ocean elsewhere. Records of redox-sensitive trace metals (Mn/Al, authigenic U) and reconstructions of opal burial fluxes, collected from two sediment cores near the Weddell Sea where the Antarctic Bottom Water forms **Figure 4**, suggest that during the LGM, low organic carbon supply to the seafloor corresponded to poorly oxygenated deep waters (Jaccard et al., 2016). Semi-quantitative constraints on surface-water O_2 from I/(Ca+Mg) planktonic foram records collected from a sediment core in the Amundson Sea suggest upper ocean O_2 was below 70 µmol kg^{-1} during the LGM (Lu et al., 2016). During cold phases of the deglaciation (identified in the Northern Hemisphere, e.g., Younger Dryas), Weddell Sea records indicate higher bottom-water O_2 concentrations (Jaccard et al., 2016). This is attributed to a decrease in iron fertilization by dust and enhanced ventilation of the deep ocean. Differences in O_2 concentrations in the Southern Ocean compared to the deep North Atlantic during Heinrich Stadial 1 (17.5-14.7 kyr) suggest hemispheric differences in ventilation and a larger influence of Fe supply in this site. However, during Younger Dryas cooling the Southern Ocean experienced a transient increase in ventilation also observed in records globally. This example reflects the potential for individual water masses to reflect both global and regional processes controlling redox conditions—and that they can sometimes conflict.

In addition to reconstructions of major ODZs, proxy records have also been implemented to track O_2 content variability for other key water masses. For example, O_2 of bottom waters along the Iberian Margin track northward recirculating North Atlantic Deep Water. Reconstructions of bottom-water O_2 using a calibrated carbon isotope gradient reconstructed with infaunal and epifaunal benthic forams suggest levels were below 200 µmol kg^{-1} during the LGM and as low as 160 µmol kg^{-1} during Heinrich-1 (~15 ka), after which O_2 increased rapidly to levels well above 230 µmol kg^{-1} (Hoogakker et al., 2015). Reconstructions of bottom-water O_2 from the deep northeast Atlantic obtained using the same method also indicate that O_2 was lower during the LGM (Hoogakker et al., 2015).

3.2 Mechanisms linking deglacial warming with ODZ change

Deoxygenation of deep waters during glacial intervals may be linked to a combination of reduced ventilation and slower circulation that impact O_2 resupply as well as higher productivity rates (Lu et al., 2020). Warming during interglacial intervals can impact ocean oxygenation through: (1) direct solubility effects of higher ocean temperatures; (2) changes in O_2 demand, and (3) changes in ocean circulation patterns (Jaccard et al., 2014). Lower solubility of O_2 from warming results in expansion of ODZs (Jaccard et al., 2014, Keeling et al., 2010, Praetorius et al., 2015). Further, photosynthetic and microbial respiration rates are argued to be temperature dependent (Eppley, 1972, Matsumoto, 2007, Boscolo-Galazzo et al., 2021), and so warming also increases O_2 demand in ODZs (Matear and Hirst, 2003, Bograd et al., 2008). The processes described here illustrate how global climate changes can be connected to parallel patterns in oxygenation or deoxygenation in ODZs, which are also subject to regional controls and variability.

Following ODZ expansion, the release of iron from hypoxic sediments has been proposed to act as a positive feedback to sustain hypoxic conditions (Davies et al., 2011, Praetorius et al.,

2015, Du et al., 2022). Similarly, enhanced nutrient delivery from eutrophication due to a more vigorous terrestrial hydrologic cycle can intensify O_2 demand during warming intervals (Keeling et al., 2010). Conversely, a database of sediment nitrogen isotopes indicate a substantial increase in the rates of denitrification through the deglaciation (Galbraith and Kienast, 2013). Coupled with lower dust fluxes during interglacial periods (Winckler et al., 2008), nutrient limitation may have dominated most areas of the ocean (i.e., outside of ODZs and river mouths).

Global changes in ocean circulation during deglaciation are hypothesized to have resulted in ventilation of the deep sea that would have increased O_2 concentrations in intermediate and deep waters. A key example is the strengthening of the Atlantic Meridional Ocean Circulation (AMOC) during the Bølling-Allerød Antarctic Cold Reversal (14.5 to 12.5 ka), associated with warming in the Northern Hemisphere. This is associated with a major expansion of oxygen-deficient waters in the Northern Hemisphere and in the Indian Ocean (Jaccard and Galbraith, 2011, Jaccard et al., 2014). This can reflect the rapid delivery of freshwater to the surface ocean during warming that decreased O_2 supply to the thermocline and resulted in greater stratification, especially at locations key to subsurface water formation (Jaccard and Galbraith, 2011). Conversely, in the ETNP, a weakening of the AMOC during early deglaciation (~16 to 18 ka) intensified upper water column O_2 depletion, perhaps with greater productivity from higher nutrient delivery from southern deep waters and higher upwelling rates (Hoogakker et al., 2018).

Additionally, the O_2 content in upwelling eastern boundary currents varied during deglaciation, also due to warming and cooling on large spatial scales. Changes in upwelling strength of these boundary currents, which control O_2 resupply, predominantly reflects land-ocean temperature differentials and associated wind regimes (Deutsch et al., 2014, Wang et al., 2015). For example, a decrease of wind-driven upwelling since the late Holocene has been reconstructed in the eastern equatorial Atlantic (Kohfeld et al., 2005).

As discussed in Section 2.3, areas of future work include further characterizing the mechanistic relationships between temperature, microbial rates and O_2 demand, and circulation patterns and O_2 resupply. Such relationships are critical for model predictions of future and past ocean redox changes.

3.3 Sea-level change: does oxygen rise or fall?

Many studies of modern and recent anoxia do not consider sea level as a major control on the ODZ and instead favor explanations involving processes on shorter timescales. However, there remain many unanswered questions regarding the importance of sea level in controlling ODZs that are relevant on glacial-interglacial as well as geologic timescales, a pressing gap in the context of future global warming and sea-level rise. Specifically, sea-level rise (*i.e.*, marine transgression) is speculated to have increased anoxic conditions via expansion of ODZs during many of the mass extinctions in the Paleozoic and Mesozoic (Hallam, 1989, Hallam and Wignall, 1999). For example, sea-level rise has been associated with the organic-rich black shales of the Cretaceous Oceanic Anoxic Events (OAEs) (Jenkyns, 1980, Leckie et al., 2002, Voigt et al., 2006). Indeed, sea level has varied dramatically over the Phanerozoic, as reflected in sequence stratigraphic patterns (Hallam, 1989, Haq et al., 1987, Vail et al., 1984). Ice volume fluctuations and mantle processes drive this variability—the latter including changes in plate spreading and subduction rates, as well as more general dynamic topography linked to mantle flow—and it is characterized by regional and global scale geometries.

Multiple mechanisms linking sea-level rise to fluctuations of the ODZ have been suggested that rely on changes in the demand of O_2 in the ocean via variations in nutrient cycling (**Figure**

12); yet, these proposed conceptual models do not make consistent predictions for changes in oxygenation. Several models suggest that a sea-level rise would lead to shoaling of anoxic waters (**Figure 12**B), resulting in inhospitable continental shelves (Hallam, 1989, Saltzman et al., 2015, Lau et al., 2016). Moreover, marine transgression would result in a larger continental shelf area influenced by wind- or tidal-mixing (**Figure 12**C), leading to greater recycling of sediment-sourced nutrients that increase productivity and O_2 utilization (Jenkyns, 1980). Finally, enhanced evaporation during transgressions has been proposed to generate oxygen-poor warm and salty waters (**Figure 12**D) that stimulate circulation and upwelling (Arthur et al., 1987). In contrast, other models link higher sea levels with a diminished ODZ and a more ventilated ocean: greater shelf area has been proposed to act as a nutrient buffer (**Figure 12**E), sequestering phosphate and reducing productivity and thus O_2 utilization (Bjerrum et al., 2006, Ozaki and Tajika, 2013). In addition to nutrient cycling, changes in the continental shelf area from glacial regression and interglacial transgression are expected to also impact the export of organic carbon to the deep ocean, resulting in lower and higher oxygenation of deep water, respectively (Wallmann, 2003). Incorporating these nutrient effects, modeling results suggest sea-level change is a primary factor on primary production, and therefore deep ocean O_2, during deglaciation but is also modulated by changes in circulation and weathering of nutrients (Tsandev et al., 2008).

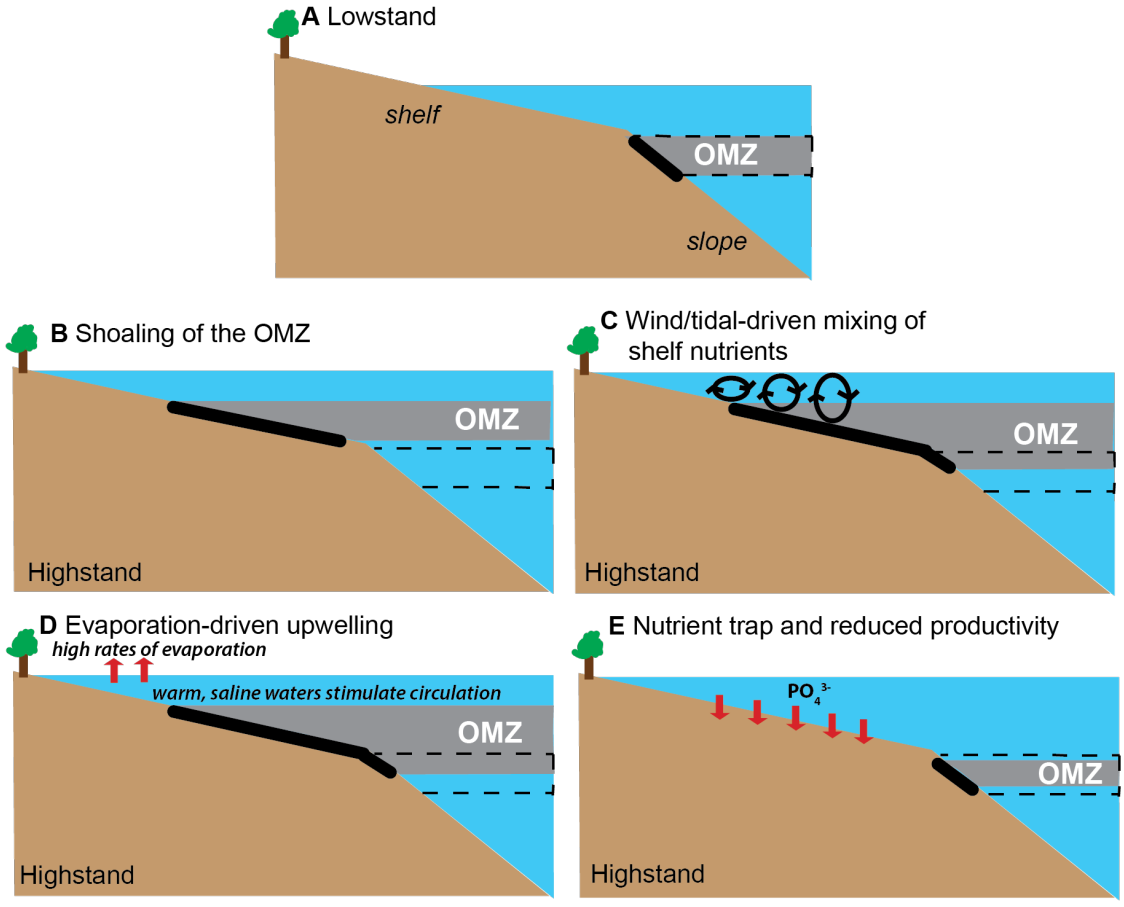

Figure 12. *Potential effects proposed on a generic O_2 minimum zone due to a transition from a (A) lowstand to (B-E) highstand. See text for further details for each scenario. These changes could occur concurrently with changes in temperature-driven O_2 solubility, increased stratification or changes in circulation due to global climate, or temperature-dependent changes to the biological pump.*

Many of the mechanisms that have been proposed to link sea-level rise with expanded ODZs (**Figure 12**) are challenging to support directly by observations. Biogeochemical models that suggest that the size of the phosphate nutrient reservoir may reduce drastically with sea-level rise, limiting deoxygenation (Bjerrum et al., 2006, Ozaki and Tajika, 2013), also lack geological evidence from redox proxies. Because sea-level change occurs alongside major climate change, it is not straightforward to directly link sea level with ocean redox changes (e.g., Tsandev et al., 2008). In comparison, studies of recent changes to ODZs do not consider local sea level. Studies that compile sediment data to reconstruct changes in the depth and intensity of OMZs (such as those discussed above) either use a simple or no eustatic adjustment to correct for changes in depth and shoreline location (Reichart et al., 1998, Cannariato and Kennett, 1999, Jaccard and Galbraith, 2011, Moffitt et al., 2015). However, regional sea level change can vary dramatically (by 30 to 50 m), and sediment-water column feedbacks, including redox-dependent burial and benthic diffusive fluxes, may play an unrecognized role in modulating ODZs. Therefore, this represents an important frontier in future research of past and future redox change.

4 Ancient: Evolution of ocean redox on geologic timescales

The history of oxygenation of the atmosphere is intrinsically linked to the oxidation of the ocean, and vice versa. For ancient studies, atmospheric O_2 thresholds are commonly referenced as percent of atmospheric levels (PAL), which relates pO_2 levels back to that relative to the modern atmosphere, or 21%. For marine oxygen, the PAL definition requires determining the atmospheric O_2 level required to sustain a specific distribution of marine O_2.

When possible, it is important to link a given proxy or zone to specific O_2 levels, allowing diverse element cycles to act as O_2 tracers in modern and ancient systems. These thresholds can be difficult or not realistic to define for major redox zones or specific proxies. Therefore, often proxies and tracers are referenced back to the "paleoredox ladder" shown in **Figure 1**. Further, the O_2 thresholds may vary depending on multiple factors (e.g., pH, competing oxidants/reductants, biotic vs abiotic reactions). In **Table 1** we summarize O_2 and/or redox thresholds for a suite of commonly applied paleoredox proxies. These constraints are based on combinations of modeling studies, modern field observations, and experiments. For redox-sensitive elements, these thresholds can be defined for both oxidation—for example, at what O_2 levels does IO_3^- form—or, conversely, reduction—for example, at what O_2 levels does IO_3^- reduction occur?

Importantly, as many thorough and recent reviews for modern and ancient tracers already exist, it is not our aim to replicate those here. Citations are given to these reviews and syntheses and appropriate details are given to provide context for discussion and interpretations.

Table 1. Summary of proxies with binary shifts related to O_2 evolution. For proxies relevant for the GOE (S-MIF, red beds, redox-sensitive detrital minerals, and I/(Ca+Mg)), the timing of change is based on detailed analysis of median last/first occurrence from Hodgkiss and Sperling et al. (2022), while other proxies are derived from the discussion of change point analysis results in Section 4.

Interval of change	Proxy	O_2 implications	Timing of change (Ga)	Proxy review citation
Stage 1: Neoarchean oxygen oases	Geochemical proxies for	Local marine O_2 <10 μmol kg^{-1}	Oldest at 2.9 Ga	(Olson et al., 2013)

	aerobic Fe/Mn cycling			
Stage 2: Great Oxidation Event and mid-Proterozoic	S-MIF	Disappearance associated with $>10^{-3}$ % PAL	2.19 (CPA = 2.51)	(Poulton et al., 2021, Uveges et al., 2023)
	Red beds	Deposition associated with 3×10^{-2} % PAL	2.48	(Farquhar et al., 2011)
	Redox sensitive detrital minerals	Disappearance from sedimentary record suggestive of 5 % to 5×10^{-4} % PAL	2.22	(Johnson et al., 2014)
	I/(Ca+Mg)	Increase suggestive of >1 µmol kg^{-1} local marine O_2	2.45	(Lu et al., 2020b, Hardisty et al., 2014)
	$\delta^{34}S_{CAS}$	Increase suggestive of presence of SO_4^{2-} reservoir and $>10^{-3}$ % PAL	2.38	(Johnson et al., 2021, Johnson et al., 2019)
	$\delta^{238}U_{shale}$	Variability from crustal values indicates oxidative weathering of uraninite	2.35	(Kendall et al., 2013)
Stage 3: Neoproterozoic Oxidation Event and a persistently stratified ocean	$\delta^{53}Cr_{shale}$	Variability from crustal values suggestive of >1 % PAL	0.83	(Planavsky et al., 2014b)
	$[Re]_{shale}$	Higher values → Decrease in euxinic/ferruginous seafloor area	0.59	(Sheen et al., 2018)
	$[V]_{shale}$	Higher values → Decrease in euxinic/ferruginous/manganous seafloor area	0.54	(Nielsen, 2020)
	$[Mo]_{shale}$	Higher values → Decrease in euxinic seafloor area	0.54	(Algeo and Lyons, 2006, Hlohowskyj et al., 2021)
Stage 4: OOE-to-OAE transition and ventilation of the deep ocean	Ce/Ce*	Lower values → Decreased redox stratification	0.43	(Wallace et al., 2017)
	$\delta^{34}S_{py}$	Higher values → Decrease in euxinic seafloor area	0.38	(Canfield, 2001)
	$[U]_{shale}$	Higher values → Decrease in euxinic/ferruginous seafloor area	0.37	(Partin et al., 2013)
	$\delta^{238}U_{CAS}$	Higher values → Decrease in euxinic/ferruginous seafloor area	0.39	(Zhang et al., 2020, Lau et al., 2019)
	I/(Ca+Mg)	Decreased redox stratification	0.21	(Lu et al., 2020b, Lu et al., 2018)

In **Figure 13** we provide a synthesis of the relationship between atmospheric, surface ocean, and deep ocean redox through geologic time, which considers both PAL and the dominant marine redox zones based on the available electron acceptors (e.g., **Figure 1**). This synthesis is in part bolstered by an evaluation of data from the Sedimentary Geochemistry and Paleoenvironments (SGP) database (Farrell et al., 2021) and determining changes through time via a change point analysis (CPA) (Cole et al., 2020). We use this analysis to support the reconstruction of timing of ocean redox changes over Earth history and implications of these changes on geobiological events in **Figure 13** and **Figure 14**. Specifically, we separate atmosphere-ocean oxidation into four distinct

eras distinguished by a combination of steady states and transitions in atmospheric oxygenation (**Figure 2**).

Stage I: An anoxic atmosphere-ocean system, with isolated O_2 oases present in the Neoarchean.

Stage II: Initial atmosphere and near-surface oxidation at the Great Oxidation Event. Stage II includes the middle Proterozoic. Oxidative weathering on land increased the sources of redox-sensitive elements to the ocean, thus increasing their reservoir sizes. Atmospheric O_2 may still be at levels allowing for marine O_2 oases.

Stage III: Increase in atmospheric oxygenation in the Neoproterozoic and into the early Paleozoic transitioning to an air-sea equilibrium regime. While widespread deep ocean anoxia and vertical/lateral redox stratification was maintained, a shift toward less reducing seafloors decreased the sinks of many redox-sensitive elements, thus increasing their reservoir sizes.

Stage IV: Increase in atmospheric oxygenation in the late Paleozoic leading to deep ocean ventilation. A shift toward more oxidizing seafloors decreased the sinks of many redox-sensitive elements, further increasing their reservoir sizes.

We note that the transition into Stage IV ushers the marine redox state from the era of so-called 'Oceanic Oxic Events' (OOE), where broad marine anoxic conditions are episodically punctuated by oxygenation events, to the 'Oceanic Anoxic Event' (OAE) era, where broadly oxic marine conditions are episodically punctuated by anoxic events.

Importantly, the CPA used to define these stages broadly shows consistent patterns of redox evolution. As shown in Table 1, the change points occur for groups of proxies that require analogous redox thresholds. That said, we note that the timing of transitions between the stages remain poorly defined and that the CPA results for a given element are partially dependent on the availability of data. In many cases, data availability is biased toward oxygenation or anoxic events and thus there are limited constraints on baseline redox conditions, which is an important frontier for improving confidence in defining the timing and nature of redox transitions. Future studies might use mass balance models of Re, Cr, Mo, and U to link the timing of their relative change points to reservoir size increases driven by dynamic ferruginous and euxinic conditions; however, here, due to data limitations for some elements, we more conservatively interpret their changes across the Neoproterozoic and Paleozoic to reflect shrinking seafloor area characterized by both ferruginous and euxinic conditions due to progressive oxygenation of the deep ocean during the transition between Stages III and IV.

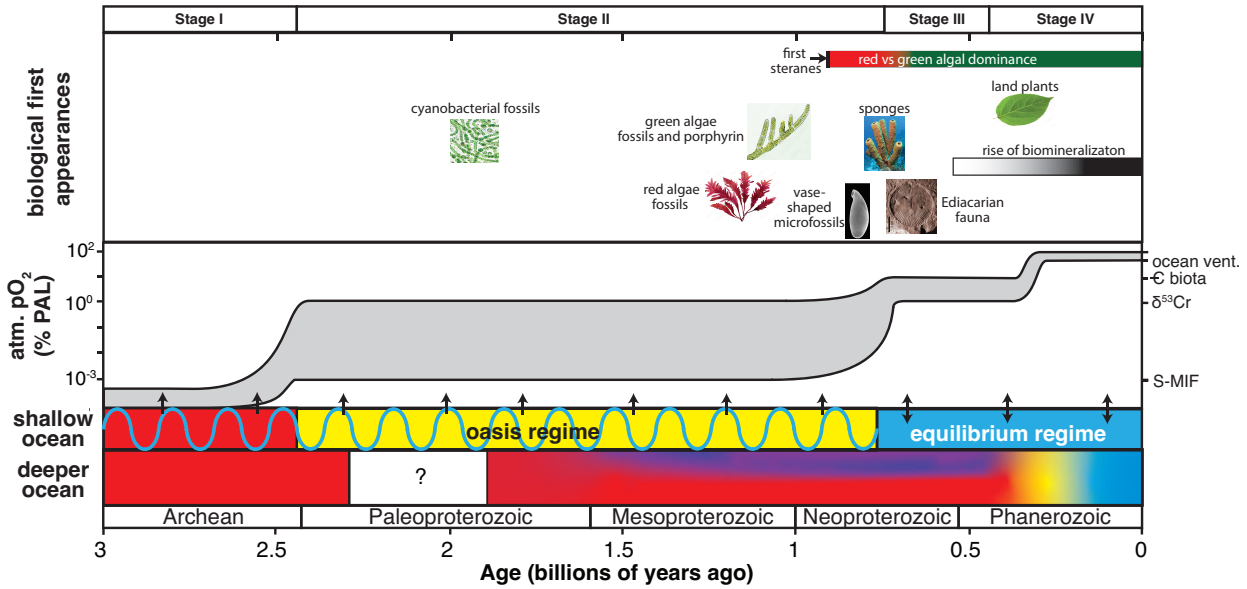

Figure 13. *Top Panel: Important evolutionary first appearances from the geologic record. Further descriptions and citations are described in the text (specifically Section 4.3.2). Middle Panel: Reconstruction of atmospheric O_2 concentrations through time in percent present atmospheric levels (PAL). Axes on right shows the proposed O_2 levels for proxies used to reconstruct the O_2 curve. Є refers to Cambrian biota (Sperling et al., 2015a). Bottom Panel: Representation of shallow and deep ocean redox regimes. Colors correspond to Figure 1. Red is indicative of ferruginous conditions, purple indicative of euxinic conditions, yellow indicative of iodinous conditions, and blue indicative of oxic conditions. Oscillating blue line indicates shallow variability linked to oxygen oases.*

4.1 Stage I: Neoarchean Disequilibria and O_2 oases

4.1.1 What is an O_2 oasis?

Most models for the oxygenation of Earth's atmosphere include marine O_2 oases—isolated hot spots of local O_2 production at levels above that expected from equilibrium with the atmosphere—as a precursor or contemporary phenomenon (Fischer, 1965, Kasting, 1992, Olson et al., 2013). Specifically, the main source for O_2 in the atmosphere both today and in the ancient past is via oxygenic photosynthesis. Models of ancient oceans predict similar regions of marine O_2 sources and sinks to and from the atmosphere as that observed today (Olson et al., 2013), but these trends are exacerbated by several important factors.

First, a key characteristic of ancient O_2 oasis is O_2 concentrations in excess of that sustainable through sea-air equilibrium. O_2 oasis models suggest the potential for O_2 concentrations from *in situ* production alone as high as 10 µmol kg^{-1} even if the atmosphere is completely anoxic. These maximum values can vary according to a number of factors, discussed below, but are also important in setting the threshold at which the atmospheric O_2 concentrations transition from an O_2 oasis to an equilibrium ocean where air-sea exchange of O_2 determines stable shallow marine O_2 levels (Reinhard and Planavsky, 2022).

Second, anoxic oceans allowed for the accumulation of relatively high concentrations of dissolved Fe, Mn, and sometimes sulfide, sourced from combinations of continental, sediment, and hydrothermal fluxes and local biogeochemistry (e.g., sulfate reduction). These reductants would act as O_2 titrants that limited the spatial extent of marine O_2 accumulation both laterally and vertically. O_2 oasis models (Reinhard et al., 2016b) explicitly consider Fe as the primary marine O_2 titrant. In oligotrophic areas beyond these O_2 oases, local O_2 sources are mostly limited to air-

sea exchange, meaning the maximum O_2 concentrations are set by equilibrium with the atmosphere. Importantly, the flux of reduced titrants can result in estimated minimum O_2 concentrations well below the value set by air-sea exchange.

The third key feature of O_2 oasis is their spatiotemporal instability driven by daily and/or seasonal availability of nutrients and sunlight. Specifically, O_2 concentrations would have varied along with seasonal changes in light and upwelling intensity—a key driver of nutrient sources to shallow waters—that impact primary production and thus local O_2 concentrations even today (**Figure 4**). During periods of minimum biological O_2 production, local O_2 concentrations would have trended toward air-sea equilibrium.

4.1.2 What is the geochemical evidence for O_2 oases?

While O_2 oases are a predicted feature for the transition period between the emergence of oxygenic photosynthesis and the oxygenation of Earth's atmosphere, direct geochemical evidence for their existence is limited and often controversial (reviewed in Reinhard and Planavsky, 2022). Frankly, this is not surprising—even if they were common—given the challenges toward recognizing O_2 oases with proxy records. These include but are not limited to: their spatially isolated nature, limited geologic preservation of shallow open ocean environments, contamination of oxidant signals given the long period of atmospheric oxygenation since the Great Oxidation Event (GOE, section 4.2), and the limited availability of sedimentary archives without significant high-temperature alterations that complicate clear interpretations of proxy evidence.

While O_2 oases may have persisted well into the Proterozoic (see Section 4.2.6), the clearest evidence for their existence comes from the Archean, with the oldest dating back to nearly 3.0 Ga. Two key basic observations are necessary to demonstrate an O_2 oasis: contemporary evidence for low atmospheric O_2—most prominently the presence of sulfur mass-independent fractionation (S-MIF; (Uveges et al., 2023))—and evidence for redox-active marine geochemical cycles requiring dissolved O_2 availability. The majority of this evidence is linked to oxidative cycling of Fe and Mn. Active Fe cycling is consistent with evidence for background ferruginous oceans during this time, and consequently, Fe fluxes from surrounding ferruginous waters are incorporated into O_2 oases models as the primary marine O_2 sink. Relevant proxies include δ^{98}Mo, rare earth element (REE) pattern changes and the cerium anomaly (Ce/Ce*), and δ^{56}Fe anomalies that are all linked to oxidative cycling of Fe and/or Mn in the ~2.9 Ga Sinqeni formation (Planavsky et al., 2014a, Ossa et al., 2018, Riding et al., 2022), ~2.8 Ga Steep Rock Formation (Riding et al., 2014) and 2.5-2.68 Ga Campbellrand-Malmani platform (Czaja et al., 2012), respectively. While Fe isotope fractionations can be specifically linked to oxidation-reduction reactions, δ^{98}Mo and REE shifts are linked to Fe and Mn cycling through isotope fractionations and uptake specific to sorption on Fe/Mn oxides. Other interpretations of O_2 oases comes from putative evidence for methane oxidation—also in the ~2.8 Ga Steep Rock (Hayes, 1994)—and for local N oxidation in the ~2.7 Ga Jeerinah formation and Campbellrand-Malmani platform (Godfrey and Falkowski, 2009, Koehler et al., 2018).

4.1.3 'Whiffs' vs O_2 oases

So-called "whiffs" of O_2 are distinct from marine O_2 oases in that they specifically imply accumulation of O_2 in the *atmosphere* at some combination of levels, time, or spatial scales below that required for the effective elimination of the S-MIF. Indeed, transient or low, but non-zero, levels of atmospheric O_2 are predicted to result from sea-to-air fluxes in association with O_2 oases. Thus, like O_2 oases, 'whiffs' are a pre-GOE phenomenon expected perhaps as early as the advent

of oxygenic photosynthesis. Again similar to O_2 oases, direct evidence for 'whiffs' are controversial (Slotznick et al., 2022, Ostrander et al., 2019) and require the presence of S-MIF alongside evidence for weathering of redox-sensitive minerals and elemental cycles, but in this case linked to *terrestrial* environments.

The earliest claims of 'whiffs' of atmospheric O_2 date back to 3 Ga and are evidenced from $\delta^{53}Cr$ fractionations requiring Mn and hence O_2 cycling on land (Crowe et al., 2013). These isotope fractionations may require as much as 1% PAL, or three orders of magnitude more than the pre-GOE O_2 concentration constrained by the S-MIF record (Cole et al., 2016). Given the presence of the S-MIF and lack of $\delta^{53}Cr$ fractionations beyond the rocks examined, this evidence requires temporally limited or strictly local atmospheric O_2 fluxes. Beyond $\delta^{53}Cr$ isotopes, most evidence for pre-GOE atmospheric O_2 fluxes comes indirectly from increases in the marine reservoir sizes of redox-sensitive metals—chiefly, S, Mo, and Re, but also N, Tl, Se, and U—sourced from oxidative weathering of terrestrial sulfides in the ~2.7 Ga Jeerinah formation and ~2.5 Ga Mt. McRae shale (Scott et al., 2011, Duan et al., 2010, Reinhard et al., 2009, Kaufman et al., 2007, Anbar et al., 2007, Ostrander et al., 2019, Stueeken et al., 2015, Kendall et al., 2013, Garvin et al., 2009). Indeed, modeling and experimental studies predict oxidative sulfide dissolution at $pO_2 < 10^{-3}$ % PAL—the threshold required for termination of the S-MIF (Johnson et al., 2021, Johnson et al., 2019, Reinhard et al., 2013a). An alternative hypothesis to transient and/or limited O_2 increases is that O_2 oases may have existed in association with microbial mats in freshwater benthic and soil environments (Planavsky et al., 2021, Wilmeth et al., 2022, Lalonde and Konhauser, 2015).

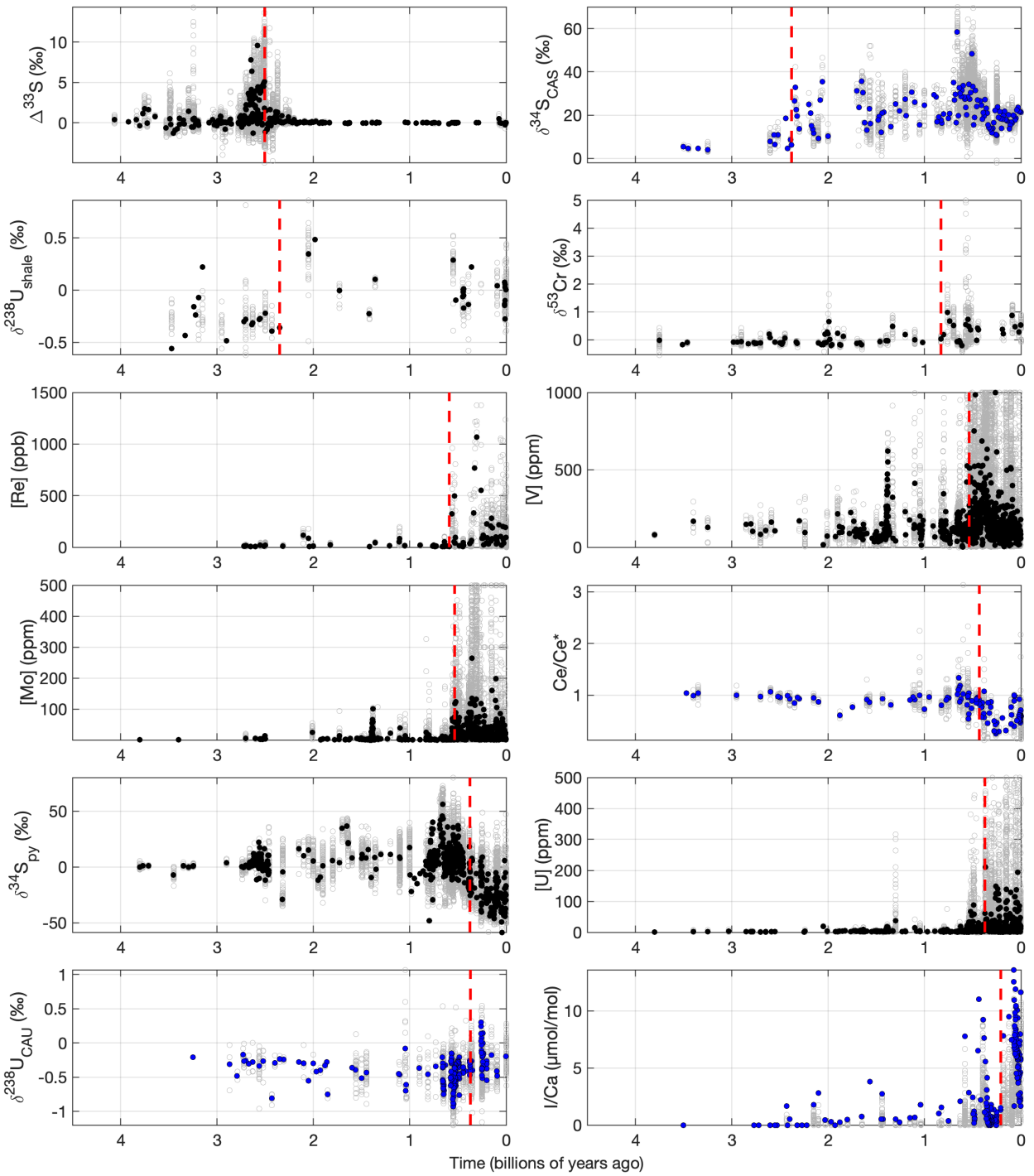

Figure 14. *Proxy compilations averaged at 1 million year-bin intervals and listed in the order of their corresponding change point (vertical red lines). Carbonate records are shown in blue and shale records in black. The shale [Mo], [V], and [U] records are derived from the SGP database (Farrell et al., 2021), filtered to only include samples where $Fe_{HR}/Fe_T < 1$, [Mo] < 500 ppm, [U] < 500 ppm, and [V] < 1000 ppm. Other records come from independent sources, including [Re] (Sheen et al., 2018), Ce/Ce* (Wallace et al., 2017), I/(Ca+Mg) (Lu et al., 2018), $\delta^{238}U$ (Chen et al., 2021), and Cr isotopes (Cole et al., 2020, Mänd et al., 2022). S isotope compilation courtesy of B.C. Gill and additional sources (Present et al., 2020). S-MIF record from Uveges et al., (2023). Note that the binned data for I/(Ca+Mg) show the maximum values of each 1 million year-bin interval and the corresponding change point. A paired t-test of the pre- and post- change point data populations revealed p-values are < 10^{-5} for all proxies except for $\delta^{238}U_{sh}$ and [Re] (p values equal $3.3x10^{-5}$ and $1.1x10^{-3}$, respectively). A note about compilations that are not depicted: a compilation of Fe speciation was recently published and is not included here (Pasquier et al., 2022). As of this review,*

the δ^{98}Mo and ^{205}Tl compilations exhibit significant temporal gaps and therefore are not suitable for similar statistical treatment as the records shown above.

4.2 Stage II: The Great Oxidation Event and mid-Proterozoic

4.2.1 What geochemical evidence is there for the GOE?

The Great Oxidation Event (GOE) was originally recognized from broad shifts in redox-sensitive minerals in sedimentary rocks. Specifically, the loss of detrital pyrite and other reduced minerals (e.g., uraninite, siderite; Johnson et al., 2014) and the appearance of red beds, gypsum deposits, and Superior-type iron formations, all mark the broad oxidation of S and Fe exposed to the atmosphere (reviewed in Farquhar et al. (2011)). Since then, multiple lines of geochemical evidence have been generated that support the GOE. Most prominently, the disappearance of S-MIF is well accepted as a marker for a transition to an atmosphere with $pO_2 > 10^{-3}$ % PAL (**Table 1**). Other proxy records specific to the GOE include the transition from the absence to the presence of IO_3^- (Hardisty et al., 2014), increases in marine SO_4^{2-} (Blättler et al., 2018), transitions to aerobic N cycling (Zerkle et al., 2017), and increases in marine U concentrations (Partin et al., 2013).

The combination of the disappearance of S-MIF and the sustained lack of Cr isotope fractionations constrain atmospheric O_2 to have increased from $<10^{-3}$ % PAL to a range of $\sim10^{-3}$ to 1 % PAL at the GOE. Unlike "whiffs" or O_2 oases, these geochemical transitions are broad and perhaps unidirectional and are thus less disputed as representing atmospheric O_2. Part of the challenge for future work is providing quantitative constraints on the other oxidative cycles initiated at the GOE. For example, the O_2 concentrations necessary to support oxidative cycles for I and N are not well quantified and may help refine constraints on GOE atmospheric O_2 concentrations.

4.2.2 Great Oxidation Event or Great Oxidation Transition?

The GOE is debated to be a sharp binary switch in atmospheric O_2 at 2.33 Ga (Luo et al., 2016) versus a broad transition spanning >300 My (Gumsley et al., 2017, Poulton et al., 2021, Hodgskiss and Sperling, 2022). There are three primary issues that complicate our understanding of the length and timing of the GOE: (1) Poor age constraints, sampling biases, and differential timing among variable proxies (Hodgskiss and Sperling, 2022); (2) Recent evidence suggesting that the S-MIF transition was not binary and included multiple reversals over a prolonged period (Poulton et al., 2021); and (3) Sedimentary recycling of S-MIF that implies the potential for a lag time, by as much as 10-100 My, between the loss of S-MIF in the atmosphere and the preservation of the full transition in the geologic record (Reinhard et al., 2013b).

In essence, the GOE is bookmarked by the initial and final loss of the S-MIF, occurring from 2.5-2.43 Ga initially and permanent loss near 2.22 Ga (Poulton et al., 2021). Importantly, given the potential for sedimentary recycling of pyrite retaining the presence of S-MIF even after its loss in the atmosphere, this could put the initial loss of the S-MIF closer to 2.6 Ga—hence overlapping with some so-called "whiffs" of O_2. These interpretations of an earlier initiation of the GOE are also supported by both the initial transition in the I/(Ca+Mg) record (**Table 1**) and the appearance of red beds. The late complete disappearance of S-MIF puts the end of the GOE as late as 2.19 Ga, which implies potential overlap with the Lomagundi-Jatuli carbon isotope excursion, which has itself has been linked to oxygenation (Section 4.2.4).

We note that the I/(Ca+Mg) record presents a significant opportunity to expand our understanding of the GOE (Hodgskiss and Sperling, 2022, Hardisty et al., 2014). Specifically, the current record across the GOE is from a coarse survey of Archean to Paleoproterozoic carbonate successions and analysis of more sections or stratigraphic analyses of individual sections spanning proposed GOE initiations could likely provide more insight into the timing of the first carbonate-bound I—i.e., dissolved marine IO_3^-—appearance in the rock record.

4.2.3 What caused the GOE?

Given uncertainty of the timing and duration of the GOE, it is not surprising that a clear driving mechanism of the GOE has not been resolved. That said, multiple plausible candidates have been suggested, all linked in part to the inputs of O_2 to the atmosphere necessary to overcome the addition and large reservoir of reductants that titrate O_2 (reviewed in Lyons et al. (2014))—sources vs sinks. The proposed mechanisms for the GOE are outlined in **Figure 16**, with an emphasis on indirect geologic and biological mechanisms acting as initial drivers of geochemical evolution. On the source side, these drivers include, but are not limited to the biological advent of oxygenic photosynthesis, large igneous provinces, widespread glaciation, the initiation of plate tectonics, hydrogen escape, and a decrease in reductant fluxes related to impactors from space and abiotic and biotic methane formation.

The simplest explanation for the GOE is that it marks the advent and/or proliferation of oxygenic photosynthesis (Fischer et al., 2016). Indeed, a fundamental question at the heart of the investigation of early O_2 is understanding when oxygenic photosynthesis itself evolved. If the GOE is the advent of oxygenic photosynthesis, this requires that pre-GOE evidence of aerobic processes record late-stage alteration or are non-specific to O_2 (Slotznick et al., 2022). Though molecular clocks support a pre-GOE origin for cyanobacteria and diversification at the GOE (Schirrmeister et al., 2013, Fournier et al., 2021), we also note that the earliest fossil evidence for cyanobacteria comes from 1.9 Ga (Hofmann, 1976). Sterane biomarkers previously interpreted to indicate pre-GOE oxygenic photosynthesis (2-methyl-hopanes; (Brocks et al., 1999)) are non-diagnostic (Rashby et al., 2007) and records of these steranes in pre-GOE rocks have been re-interpreted to reflect younger contaminants (French et al., 2015). In this view, the rise of O_2 at the GOE itself is the clearest proxy for the emergence of cyanobacteria.

Other models also link the GOE to enhanced O_2 production at this time—regardless of whether oxygenic photosynthesis may have existed prior to the GOE—with limited marine productivity maintaining low O_2 relative to reductant fluxes in the atmosphere/ocean. Specifically, a proliferation of oxygenic photosynthesis is tied to enhanced nutrient delivery to the oceans at the GOE (Gumsley et al., 2017). Importantly, this hypothesis builds on the likely temporal overlap between the GOE and Paleoproterozoic glaciation and low-latitude large igneous provinces (LIPs). Specifically, low latitude LIPs documented from this period are hypothesized to have triggered enhanced chemical weathering of continental flood basalts. Chemical weathering resulted in CO_2 drawdown, ushering in the documented low-latitude glaciation but also supplying extensive nutrients. A nutrient-based origin to the GOE and other oxidation events is supported by increases in P contents of igneous rocks and sedimentary rocks at the GOE and later oxidation events (Cox et al., 2018, Alcott et al., 2022, Bayon et al., 2022). The increase in nutrients fueled photosynthetic activity which in turn increased O_2 fluxes to the atmosphere, initiating the GOE. Further, tectonic forcing—the initiation of plate tectonics in the Paleoproterozoic—may have resulted in greater subduction of carbon into the mantle as graphite or increased burial in association with Fe-oxides,

which both could have led to an increase in atmospheric O_2 accumulation (Duncan and Dasgupta, 2017, Zhao et al., 2023).

The coincidence of the GOE with low latitude glaciation during the first great 'Snowball Earth' in the Paleoproterozoic also provides evidence for a potential tipping point with O_2 overcoming reductive fluxes of methane (CH_4) at this time (Goldblatt et al., 2006, Pavlov et al., 2000). Similar to P, a change in marine Ni fluxes—a key micronutrient for methanogens—may have also played a role in limiting CH_4 fluxes (Wang et al., 2019). Other positive feedbacks leading to higher net O_2 export include the titration of reductants resulting from increasing the competitive niches of oxygenic over anoxygenic photosynthesizers (Ozaki et al., 2019) and increases in SO_4^{2-} fluxes that supplied O_2 via pyrite formation and limited atmospheric CH_4 fluxes (Heard et al., 2020).

On the flip side, a second model more explicitly ties the GOE to a decrease in reductants relative to O_2 sources. Such a process could have been protracted, with O_2 production via oxygenic photosynthesis predating the GOE but limiting atmospheric pO_2 to trace levels. For example, rapid crustal growth at 2.7 Ga may have resulted in an increase in subaerial relative to submarine volcanism leading to higher CO_2/H_2O and SO_2/H_2O ratios of volcanic gases compared to reduced C and S equivalents (Gaillard et al., 2011, Kump and Barley, 2007, Meng et al., 2022, Kadoya et al., 2020, Holland, 2009). Related mechanisms tie the development of an O_3 layer at the GOE as a new irreversible state (Goldblatt et al., 2006). More recently, models and spherule-bed records suggest oxygenation at the GOE was linked to lower reductant fluxes from impactors particularly prevalent during the late Archean (Marchi et al., 2021).

4.2.4 Lomagundi-Jatuli O_2 overshoot: Fact or fiction?

The Lomagundi-Jatuli event, or LJE, is the most positive and longest-lived carbon isotope excursion in Earth history. It lasted from 2.3-2.1 Ga and $\delta^{13}C_{carb}$ values often reach +10‰, with extreme values above +20‰ (Karhu and Holland, 1996, Prave et al., 2022). In the context of traditional carbon isotope interpretations (see ***Box 1: Linking changes in redox conditions to the carbon isotope record***)—where positive $\delta^{13}C_{carb}$ excursions reflect increased organic carbon burial and thus an increase in marine and atmospheric O_2 budgets—the LJE has traditionally been interpreted to reflect a major increase in atmospheric O_2 (Karhu and Holland, 1996). As mentioned above, it remains unclear whether such an oxygenation event is coupled to the GOE or stands as a separate event. Follow up work in the last decade testing hypotheses of atmospheric/marine O_2 increases has yielded mixed results, thus forcing reconsideration of the origins and interpretations of the carbon isotope excursion (Fakhraee et al., 2023).

Beyond the carbon isotopes themselves, the strongest supporting evidence for oxygenation comes from the S and Cr isotope records. This includes both the S concentration and isotope composition of carbonate-associated sulfate (CAS) as well as records of S minerals, specifically gypsum and anhydrite, over this interval. Collectively, these widespread observations point to a large increase in the concentrations of dissolved SO_4^{2-} in the ocean over this interval (Blättler et al., 2018, Planavsky et al., 2012), which is consistent with atmospheric oxidation and increased weathering of terrestrial pyrite yielding higher SO_4^{2-} fluxes to and preservation within the ocean. Specifically, higher [CAS] point to increased dissolved ambient SO_4^{2-} abundance. Importantly, [CAS] is often overprinted to lower values during diagenesis (Gill et al., 2008, Lau and Hardisty, 2022), so there is not currently a well-accepted explanation for how these increases might have resulted from any post-depositional alterations. Further, observed positive excursions in $\delta^{34}S_{CAS}$

are linked to increases in pyrite formation and burial sourced from a relatively large marine SO_4^{2-} pool (Planavsky et al., 2012). Sulfate reduction to sulfide within larger SO_4^{2-} pools sustain larger Raleigh fractionations than smaller SO_4^{2-} pools, thus increasing $\delta^{34}S_{sulfate}$ as reduction continues. Notably, these $\delta^{34}S_{CAS}$ values track that of coeval $\delta^{34}S$ in evaporites, again making diagenetic interpretations difficult. The increase in the evaporite minerals gypsum and anhydrite during the LJE also independently point to an increase in marine SO_4^{2-} availability, and thus oxygenation to some degree, at least in shallow water settings (Blättler et al., 2018).

More recently, positive Cr isotope values from 2.1–2.0 Ga mudstones of the Onega Basin provide strong evidence for atmospheric oxygenation exceeding 1.0% PAL (Mänd et al., 2022). We note that there is limited evidence for positive Cr isotope fractionations prior to 0.8 Ga, suggesting a baseline of atmospheric O_2 levels below this low O_2 threshold. Because mudstones and black shales—often necessary for the application of trace metals and their isotopes as paleoredox proxies—are relatively limited during the LJE excursion, the temporal extent of Cr isotope records—especially to older intervals—is currently limited. Future studies should focus on expanding the Cr isotope and related records to better understand oxygenation across the duration of the LJE.

Other geochemical records fall short of identifying unambiguous oxidation during the LJE compared to preceding and subsequent time intervals. For example, there are I/(Ca+Mg) values higher than the Proterozoic baseline across the LJE (Hardisty et al., 2017), but relatively higher values are not uncommon in later Proterozoic intervals where widespread oxygenation is not invoked (**Figure 14**). Importantly, even the highest I/(Ca+Mg) values are still within a range observed within or adjacent to modern low O_2 zones. It might be easy to dismiss these observations—given that, like [CAS], I/(Ca+Mg) is easily diagenetically overprinted to lower values (Lau and Hardisty, 2022)—but they are consistent with other proxies as well. For example, the [U] record from black shales provides evidence for a larger U reservoir from greater surface oxidation of uraninite (Partin et al., 2013); however, this increase is small relative to later intervals and is also not resolvable with binned averages (**Figure 14**). Other trace element records in shales that similarly reflect reservoir sizes linked to broader oxidizing conditions (e.g., Mo, Cr) do not show clear increases across the LJE.

Together, these records suggest oxidation concurrent with the LJE—which may or may not be linked with the GOE itself—but not to the degree implied by traditional interpretations of the carbon isotope record. This obviously points to a need to resolve the degree in which feedbacks linked to oxidation may have propagated and exacerbated such a long-lived and positive carbon isotope excursion in a Proterozoic world very different than today. A recent study provides intriguing evidence that the $\delta^{13}C_{carb}$ excursion may be facies dependent and found nearly exclusively in shallow marine deposits (Prave et al., 2022). This finding indicates the possibility that local processes, akin to that already observed in modern shallow marine environments, could be responsible for the LJE (Swart and Eberli, 2005, Geyman and Maloof, 2019). Still, these models require an answer to why such large positive $\delta^{13}C_{carb}$ values are not found during surrounding time intervals. An additional hypothesis for the LJE is local methane oxidation tied to an increase in marine SO_4^{2-}, which would cause higher $\delta^{13}C_{DIC}$ values in pore waters hosting carbonate precipitation (Hayes and Waldbauer, 2006). Alternatively, local SO_4^{2-} reduction tied to methane oxidation may play a role, but on a global instead of local scale, thus altering the DIC composition of seawater (Schrag et al., 2013). To be clear, however, for both methane-related models, the negative $\delta^{13}C$ sink is still physically missing from the observed sedimentary record and

presumably would be hosted in organic-rich deposits that are either not preserved or not yet identified.

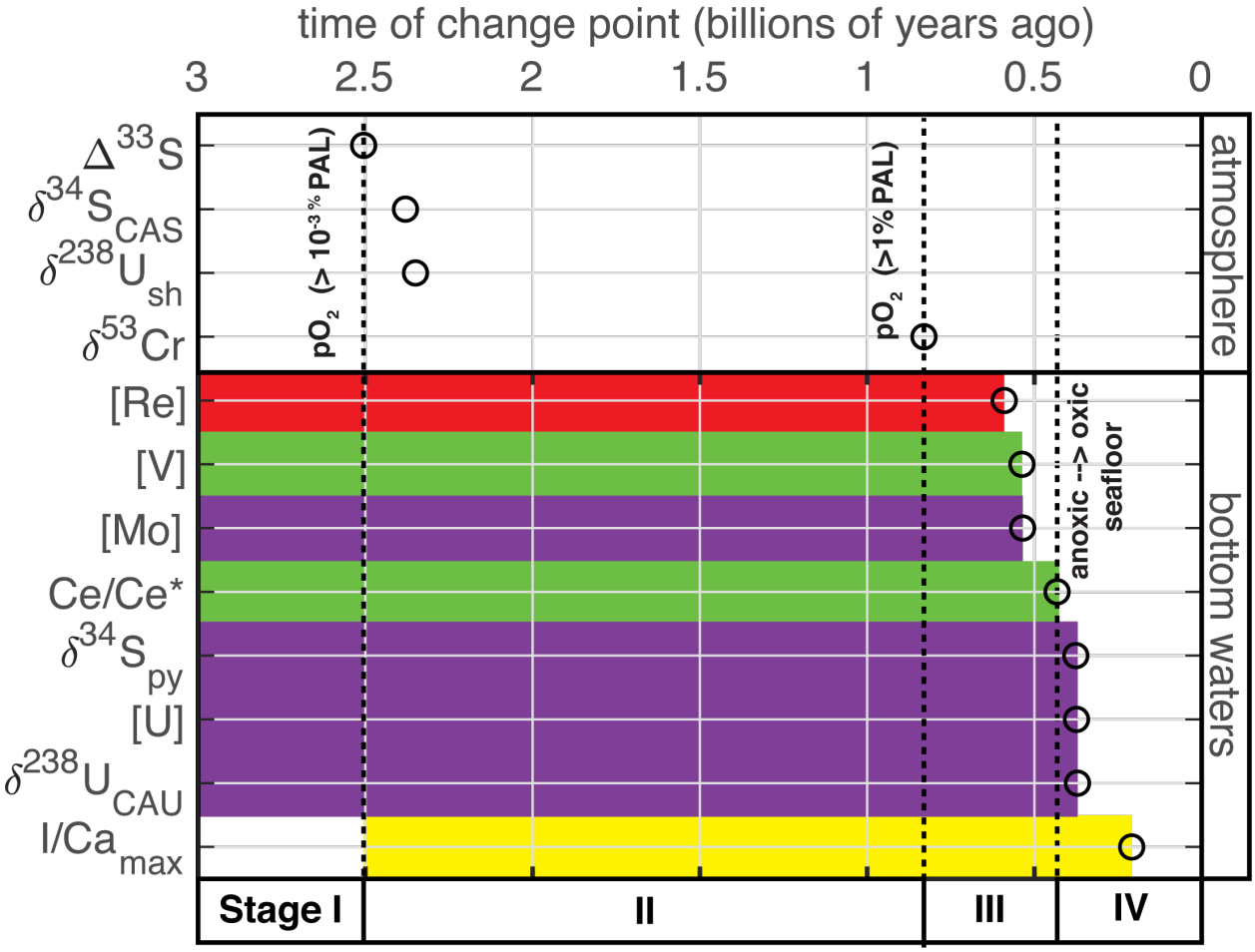

Figure 15. *Change point analyses of redox proxy records. The analysis is based on data averaged for 1 million year-binned intervals. For I/(Ca+Mg), the analysis also considered the maximum values at 1 million year-bin intervals $(I/(Ca+Mg)_{max}$. A paired t-test of the pre- and post- change point data populations revealed p-values < 10^{-5} for all proxies except for $\delta^{238}U_{sh}$ and [Re] (p = $3.3x10^{-5}$ and $1.1x10^{-3}$, respectively). Colors correspond to that in Figures 1 and 13 (red = ferruginous; green = manganous; purple = euxinic; yellow = iodinous) and indicate least reducing water column redox conditions leading to proxy change.*

4.2.5 Mid-Proterozoic biogeochemical stasis?

Following the LJE, multiple lines of evidence point to a long-term decline in atmospheric O_2 and biogeochemical stasis (1.8-0.8 Ga; e.g., Hodgskiss et al. (2019)). The middle Proterozoic is so famous for stasis—both in redox conditions and for eukaryotic life and biological evolution—that the term "boring billion" has become a cliché for describing this interval. The most prominent evidence for biogeochemical stasis through the middle Proterozoic is the relatively invariant records of carbon isotopes (which rarely deviate from 0‰) and concentrations and isotopes of redox-sensitive trace elements (**Figure 14** and **Figure 17**). However, several recent studies have challenged this premise, including that of stasis and that of low O_2.

Importantly, the Cr isotope record provides a key set of evidence for a long-term baseline of O_2 as low as <1% PAL, but there is some evidence for punctuated oxygenation. For example, positive Cr isotope anomalies from shales of the ~1.4 Ga Shennongjia Group in South China provide some evidence for an oxygenation event during this time (Canfield et al., 2018). We note that increases in I/(Ca+Mg), some trace metals, and Ce/Ce* anomalies from nearby intervals collectively point to oxygenation against a backdrop of low O_2 conditions—i.e., an OOE. Less convincing, in our view, is Cr isotope evidence from carbonates for oxygenation during this interval and other portions of the mid-Proterozoic. The Cr isotope record in carbonates suggests O_2 >1% PAL in every section analyzed to date (Gilleaudeau et al., 2016). This may represent a more detailed view of redox with ocean depth—with carbonates and shales archiving shallow and deeper waters, respectively—but other evidence suggests the potential for diagenetic alterations to have a potentially major effect on interpretations of these data (Wang et al., 2021). Regardless, going forward it will be important to demonstrate the reliability of the carbonate Cr record, such as via a lack of fractionations in Archean carbonates where the S-MIF is consistent with atmospheric O_2 <0.001% PAL.

A recent review paper highlights the potential for multiple mid-Proterozoic OOE's, including at 1.4 Ga (as highlighted above) but also at 1.1 Ga (Diamond and Lyons, 2018). This in part relies on the $\delta^{53}Cr$ record of carbonates discussed above, but also on evidence for increased Mn deposition (Spinks et al., 2023) as well as higher Re concentrations (**Figure 14**). Some tentative evidence for a broader shift in redox conditions starting at 1.1 Ga—as opposed to a discrete event—is a shift toward a more positive baseline in $\delta^{13}C_{carb}$ (Kah et al., 2004). This transition can be generally observed in **Figure 17**.

4.2.6 Proterozoic O_2 oases?

Model reconstructions of marine O_2 constrained by atmospheric redox proxies predict the persistence of O_2 oases well into the Proterozoic, but clear marine geochemical evidence for oases is still lacking. Specifically, Cr isotope predictions for a mid-Proterozoic atmosphere with O_2 concentrations <1% PAL imply marine O_2 concentrations sustained via air-sea exchange to be <2.5 μmol kg^{-1} (Planavsky et al., 2014b). This value is below the maximum of 10 μmol kg^{-1} possible in local areas of high photosynthesis predicted in models considering mid-Proterozoic and Archean constraints (Reinhard et al., 2016a).

One of the major challenges in recognizing mid-Proterozoic O_2 oases is that, unlike the Archean, evidence of oxidative geochemical cycles is widespread, but the dissolved O_2 thresholds for these proxies are not well defined. For this reason, distinguishing between background O_2 of <2.5 μmol kg^{-1}—that possible from air-sea exchange—vs values up to 10 μmol kg^{-1}—that possible from localized photosynthesis—is challenging with current paleoproxy constraints. For example, the I/(Ca+Mg) record suggests a distinct redox landscape pre vs post GOE (absence vs presence of IO_3^-, respectively), indicating a clear increase in oxidizing capacity (Hardisty et al., 2014, Hardisty et al., 2017). However, estimates of the O_2 thresholds for IO_3^- formation or persistence range from <1 μmol kg^{-1} to 30 μmol kg^{-1} (Hardisty et al., 2014, Lu et al., 2016). Importantly, the shift in I/(Ca+Mg) at the GOE cannot currently be used to determine if O_2 oases were present pre- or post-GOE. In this conceptual model, IO_3^- may have formed at local O_2 oasis pre-GOE, but Archean air-sea O_2 exchange and extremely low O_2 values at oases led to rapid IO_3^- reduction, thus limiting its spatiotemporal accumulation and retention in the carbonate record. Alternatively, the elevated post-GOE marine O_2 concentrations sustained via air-sea exchange may have risen above values important for IO_3^- accumulation, thus minimizing the role of O_2 oases in IO_3^-

formation. Further, O_2 oases after the GOE could have acted as geochemical hotspots for the formation of low levels of IO_3^- while the increase in minimum O_2 values from air-sea exchange could have sustained the circulation of IO_3^- in oligotrophic regions beyond the oases (Hardisty et al., 2021). Regardless, we note that there are limited I/(Ca+Mg) records prior to the GOE and thus it remains tentative to rule out pre-GOE marine IO_3^- accumulation.

4.2.7 What was the redox state of the mid-Proterozoic Ocean?

Against the backdrop of low O_2—potentially punctuated by infrequent OOEs, if any—there has been much focus on understanding the background redox states of the Proterozoic ocean. Efforts to quantify the amounts and stability of near-surface O_2 are important given their implications for early animals (Section 4.3.2). Beyond this, however, what were the redox states with respect to the paleoredox ladder shown in **Figure 1**? Did the redox states vary over time? Are there clear spatial differences between near-surface and deep ocean redox conditions? These outstanding questions remain unaddressed.

Starting with near-surface conditions, some of the clearest constraints come from carbonate I/(Ca+Mg) ratios, which provide abundant evidence for iodinous conditions—or those supporting partial IO_3^- reduction (**Figure 14**). Specifically, I/(Ca+Mg) ratios point to low IO_3^- abundances throughout the mid-Proterozoic that are similar to that observed in modern low O_2 zones. We note that diagenesis can decrease primary I/(Ca+Mg) ratios (Hardisty et al., 2017, Lau and Hardisty, 2022)—which amplifies the significance of non-zero iodine values in carbonate—but this is unlikely to explain the lack of any known elevated modern-like values until the Neoproterozoic. In addition to preservation, more constraints are needed to connect the presence of low but non-zero IO_3^- to specific O_2 levels or timescales of accumulation. Beyond I/(Ca+Mg), REE anomalies (i.e., Ce/Ce*) provide additional evidence for redox stratification and prevalent manganous conditions in the Proterozoic (Wallace et al., 2017).

Further, combinations of [Cr], [U], [Mo], and Fe speciation in shales are consistent with widespread low O_2 conditions maintaining small marine reservoir sizes and short residence times. The combined redox sensitivities of Cr to anoxic (ferruginous + euxinic) and Mo to euxinic conditions have been used to constrain 30-40% of the seafloor as anoxic and 1-10% as euxinic (Reinhard et al., 2013c). Importantly, Fe speciation data indicate that conditions were more broadly ferruginous. A statistical assessment of Fe speciation data through the Proterozoic provides evidence that ferruginous conditions dominated the deep ocean until well into the Paleozoic (Sperling et al., 2015b). Together these trace element and Fe speciation observations support widespread ferruginous relative to euxinic conditions (Planavsky et al., 2011) in contrast to previous models that predicted widespread euxinia during this interval (i.e., the ‘Canfield Ocean’; (Canfield, 1998)).

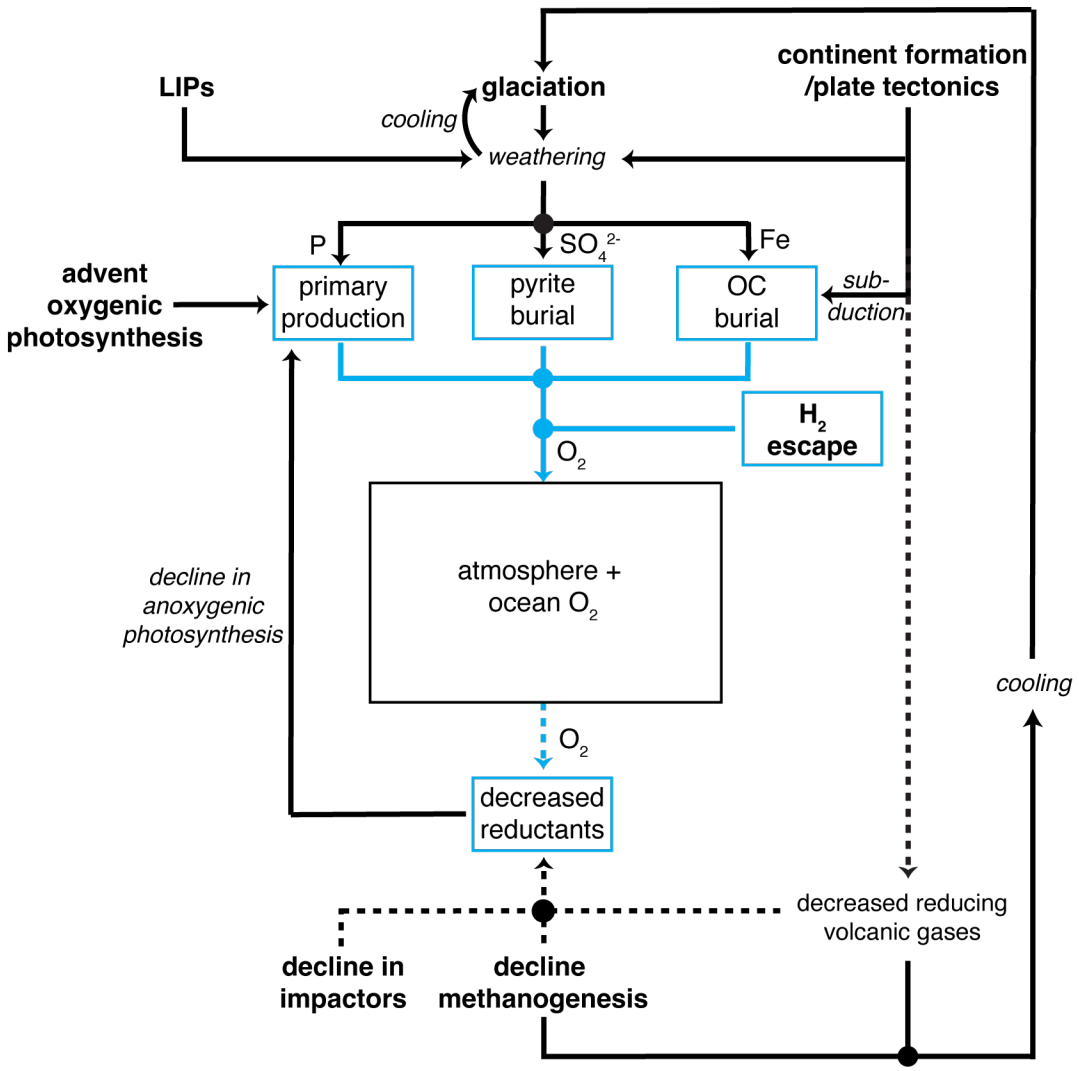

Figure 16. *Synthesis of proposed mechanisms driving the Great Oxidation Event as summarized in Section 4.2.3. Direct O_2 sources and sinks are highlighted in blue. Sources are filled lines and sinks are dashed lines. Geological and biological drivers are bolded. Indirect feedbacks are shown as black arrows.*

4.3 Stage III: Neoproterozoic through Paleozoic: a protracted transition?

4.3.1 Neoproterozoic redox landscape

The Neoproterozoic is considered a major transition in the evolution of life and environment. Chief amongst geobiological changes is a multitude increase in the evidence for eukaryotic life, biomarker sterane-based evidence for early sponges, increases in fossil abundance, as well as the first ichnofabrics indicative of complex organisms, including their movement (discussed in detail in Section 4.3.2). Further, like many of the redox transitions before it, the environmental perturbations of the Neoproterozoic are characterized by large carbon isotope excursions. Indeed, a new backdrop of positive $\delta^{13}C_{carb}$ starts as early as 1.1 Ga and persists into the Paleozoic (Kah et al., 2004). However, the Neoproterozoic is unique in that the baseline $\delta^{13}C_{carb}$ is punctuated by multiple extreme negative $\delta^{13}C_{carb}$ events, including the largest and longest in

Earth history (the Shuram-Wonoka excursion). Hypothesis specific to the origins of these carbon isotope excursions are discussed in detail in Section **Error! Reference source not found.**, but we highlight below their association with variations in redox-sensitive trace elements indicative of a baseline shift in oxygenation.

The change point analysis in **Figure 15** provides evidence from multiple proxies for a change in baseline redox conditions spanning the Neoproterozoic and into the Paleozoic. Most prominently, the Cr isotope record shows a shift to positive values as the new baseline, providing quantitative evidence for an increase in atmospheric O_2 levels near 0.8 Ga. Coinciding with this shift and subsequently in the Neoproterozoic, multiple other trace element proxies have change points indicative of higher marine and atmospheric O_2 levels—specifically Re, Mo, and V. While this implies a baseline shift in atmospheric O_2 levels, it is important to emphasize that the Neoproterozoic oceans were broadly low in O_2 (Sperling et al., 2015b). Against this backdrop, there is evidence for more frequent OOEs relative to the preceding mid-Proterozoic.

Importantly, the Fe speciation record offers little evidence for global redox changes through the Neoproterozoic and even the Paleozoic (Sperling et al., 2015b, Pasquier et al., 2022). Indeed, the protracted timing of change points from the Neoproterozoic through the middle to late Paleozoic (**Figure 15**) lends support to the emerging hypothesis that this was truly a transition to a fully oxygenated deep ocean, and not a geological rapid event isolated to the Neoproterozoic (Sperling et al., 2015b, Wallace et al., 2017, Lu et al., 2018, Cole et al., 2020). The fact that the change points are spread over a temporal range—and do not coincide relatively neatly as for the GOE—and that the order of changes for the redox-sensitive trace elements in our compilation (Re, Mo, V) broadly align with expected redox sensitivities based on **Figure 1**, support a gradual increase in marine oxidation.

In the Phanerozoic—following the OOE-to-OAE transition—increases in trace metal contents are most simply interpreted as changes in basinal restriction that impact the seawater supply of trace elements to marginal anoxic basins (e.g., Hancock et al., 2019). This can also be true in the Neoproterozoic; however, the most parsimonious explanation for higher trace element concentration in **Figure 15** is a secular change in redox-sensitive trace element seawater concentrations. Thus, higher [Re], [Mo], and [V] of black shales is consistent with increases in their marine reservoir size (Tribovillard et al., 2006). These increases in reservoir size are interpreted to be redox-dependent increases in sources and decreases in sinks of these elements to and from the ocean. For example, the main supply of Re and Mo to the ocean are riverine inputs fueled by oxidative weathering of sulfides on land (Miller et al., 2011). Similar to the increases in marine SO_4^{2-} recorded over time, these higher supplies are fundamentally linked to O_2 availability in the atmosphere. However, results from pyrite oxidation experiments at low O_2 indicate that the most prominent increases in supply of trace elements associated with sulfide oxidation likely occurred during the GOE (Johnson et al., 2019), as this process is most sensitive to low levels of O_2 (**Table 1**). This suggests that increases in reservoir size during the Neoproterozoic may be most closely tied to reduced anoxic (ferruginous and/or euxinic) bottom waters which act as a primary sink for these and many other trace elements (**Figure 15**).

The decline of anoxic bottom waters is consistent with the expansion of the eukaryotic fossil record through this interval, which implies O_2 above thresholds necessary for aerobic metabolisms. These thresholds themselves are debated, ranging from <1% PAL to 1-3% PAL, and thus place these redox changes right at the cusp of the threshold for positive Cr isotope fractionations at 1% PAL (Planavsky et al., 2014b). In addition to absolute O_2 thresholds, the timescales of O_2 availability are also expected to increase once the ocean transitions from an oasis

to equilibrium regime. Notably, the 1% PAL threshold for O_2 at 0.8 Ga from Cr isotopes still does not rule out the potential for dynamic O_2 oases, however, considering that as much as 10 μmol kg^{-1} O_2 (or 2.1% PAL) is necessary for this oasis-to-equilibrium regime transition (Reinhard et al., 2016a, Reinhard and Planavsky, 2022). We note, as discussed in more detail in **Table 1**, that records for other proxies with specific O_2 thresholds are limited after the Cr isotope change point. Biological constraints on O_2 (i.e., body size and motility) indicate levels closer to 10% PAL were not reached until the Cambrian (Sperling et al., 2015a). Unlike geochemical proxies, evidence from the fossil record does not rule out higher O_2 prior to these evolutionary events, as the timing of biological innovations can lag behind environmental transitions.

Given that widespread deep-ocean anoxia persisted in the Neoproterozoic and early Paleozoic, the driver of the change point in the shale trace element record in **Figure 15** is an increased frequency of OOEs relative to the mid-Proterozoic. Limited age constraints often make it difficult to correlate geographically disconnected shale stratigraphic sections and can be further complicated by the potential for local basin hydrography as a key player in trace element chemostratigraphy. These OOEs are commonly linked to negative carbon isotope excursions through the Neoproterozoic (Section 4.3.3). Although this can support a link to redox changes, because so many of these carbon isotope records come from carbonate archives, there is also vigorous debate regarding diagenetic vs local vs global carbon cycle origins of geochemical signals (see *Box 1: Linking changes in redox conditions to the carbon isotope record*).

Unique to this stage and controls on redox are 'Snowball Earths.' The Neoproterozoic is notable for two major glaciation episodes—the Sturtian and Marinoan (Kirschivink, 1992, Hoffman, 1998)—that mark the beginning and end of the Cryogenian Period. Sedimentary evidence suggests the presence of glaciers even at equatorial latitudes (Hoffman and Schrag, 2002), although the exact extent of ice is a topic of debate (Runnegar, 2000, Allen and Etienne, 2008). Nonetheless, widespread sea ice and associated climate change likely had an impact on the redox conditions of the ocean. For example, banded iron formations disappear for much of the Proterozoic but make a re-appearance during the Cryogenian glaciations—especially the Sturtian—which suggest anoxic and ferruginous conditions (Tahata et al., 2015), especially in marginal basins that could have maintained high Fe from hydrothermal and detrital sources (Cox et al., 2013). If these glaciations were not truly widespread, then areas of open ocean could have maintained air-sea gas exchange that resulted in O_2-replete surface waters, sustaining life (Pierrehumbert et al., 2011). Evidence for open-ocean conditions during the Marinoan come from N isotope data that indicate an active N cycle and biological production in the surface waters, despite deep waters being ferruginous (Johnson et al., 2017, Sahoo et al., 2012). However, waters with sufficient O_2 are still possible in a regime where the oceans are completely frozen. One possibility is the supply of O_2 from subglacial meltwater, which is inferred from redox proxy gradients from ice-proximal to ice-distal strata in the Sturtian (Lechte et al., 2019). Alternatively, cryoconite holes in ice shelves, resulting from dust-induced melting, could have supported O_2 supply to the surface ocean and small-scale refugia for life, particularly microbial ecosystems (Hoffman, 2016).

The terminations of both Cryogenian glaciations may also have implications for marine redox evolution. Massive weathering that brought the Earth out of a glaciated state (Le Hir et al., 2009, Rooney et al., 2013, Kasemann et al., 2014, Huang et al., 2016) is hypothesized to result in the widespread cap carbonates characteristic of Snowball glaciations (Fabre and Berger, 2012, Hoffman et al., 2017, Higgins and Schrag, 2003). The Cryogenian is also notable for containing several large igneous providences and associated volcanism (Cox et al., 2016, Macdonald and

Wordsworth, 2017). The combination of high weathering rates and widespread fresh basalts may have resulted in large fluxes of P to the oceans (Horton, 2015), which has been suggested as at least one trigger of oxidation of the oceans (Dodd et al., 2023). Support for this hypothesis comes from U isotopes in Mongolian carbonates following the Sturtian (Lau et al., 2017a) and trace element concentrations that imply an OOE directly following deposition of the Marinoan cap carbonate in the lower Doushantuo Formation (Sahoo et al., 2016).

4.3.2 Ocean redox conditions and evolution of complex life

The rise of dissolved O_2 in the Neoproterozoic correlates to changes in the biomarker record that suggests a coupling to the rise of eukaryotes. Similar to the temporal relationship between the appearance of cyanobacteria and the GOE, there is evidence that algae evolved prior to but did not proliferate until the Neoproterozoic (**Figure 13**). Specifically, molecular clock estimates place the last common ancestor of algae from 1.9-1.4 Ga (Parfrey et al., 2011, Sanchez-Baracaldo et al., 2017). The first fossil evidence for red algae is at ~1.2 Ga (Butterfield, 2015) and the first fossil and porphyrin-based evidence for the presence of green algae does not occur until ~1.05 Ga (Gibson et al., 2018, Gueneli et al., 2018). However, sterane biomarkers are not found in the fossil record until 0.9 Ga and sterane/hopane ratios show a pronounced increase during the Cryogenian, 0.72-0.64 Ga (Brocks et al., 2017, Hoshino et al., 2017, Isson et al., 2018). Higher sterane/hopane ratios in the sedimentary biomarker record are interpreted to represent a significant presence of eukaryotes—which produce steranes—relative to bacterially derived hopanes in driving primary productivity in the ocean. The biomarker record thus indicates a rapid and permanent shift in the food chain. Embedded within this shift from bacterial to eukaryotic dominated preservation of primary producers is a shift from a dominance of red to green algae at the Sturtian glaciation (Isson et al., 2018). The establishment of eukaryotes as primary producers in marine systems is hypothesized to lead to ecological pressures at higher trophic levels toward larger grazers, the evolution of predators, and more complex organismal interactions (Brocks, 2018). Further, the establishment of larger primary producers would have also resulted in a more dynamic biological pump (Lenton and Daines, 2018), increasing organic carbon burial fluxes which may be a potential cause for Neoproterozoic O_2 rise.

The causal relationship between Neoproterozoic oxidation and the rise of complex life is highly debated (Cole et al., 2020, Mills et al., 2022, Sperling et al., 2022). Redox conditions in the Neoproterozoic are noted for being highly variable (Section 4.3.1) and O_2 levels did not cause animal to evolve (Knoll and Carroll, 1999). Instability and spatial heterogeneous redox conditions may have hampered metazoan evolution (Johnston et al., 2012, Johnston et al., 2013, Macdonald et al., 2013, Wood et al., 2015, Sahoo et al., 2016). Alternatively, fluctuations in marine redox conditions may provide evolutionary pressures that result in greater diversification and periods of innovation (Wood and Erwin, 2018). Although it is without question that metazoans require O_2 to perform aerobic respiration, the amount of O_2 that is necessary, particularly for basal animals, is not known. Experiments with demosponges—expected to be representative of the physiology and O_2 requirements of the earliest animals that are extant today—indicate that survival is possible even at O_2 levels of 0.5 to 4.0% PAL (Mills et al., 2014), and O_2 as a limitation on multicellular animals has been argued to be unlikely for most of the mid-Proterozoic and later (Sperling et al., 2022). The bilaterian body plan exemplified by the Ediacaran fauna, which, though now extinct, are regarded as the earliest bilaterians (Evans et al., 2020a), would have higher O_2 demands than demosponges depending on the respiratory system of these organisms (reviewed in Sperling et al. (2015a)). Estimates of O_2 demand for small bilaterians, based on calculations of O_2 diffusion and

circulatory systems for a long worm body plan, are <0.5% PAL (Sperling et al., 2013). The ability of bilaterians to tolerate such low O_2 levels is supported by observations of modern animals in waters with dissolved O_2 as low as 0.02 mL L^{-1} (Sperling et al., 2015a) as well as genetic adaptations for anaerobic metabolisms (Mueller et al., 2012, Mentel et al., 2014).

In addition to the low dissolved O_2 threshold for basal animals and bilaterians, whether O_2 is even the limiting factor for animals is debated. Indeed, the argument has been made that higher O_2 is not a precursor requirement for animals but rather the biogeochemical consequence of animal evolution and associated higher organic carbon burial fluxes (Butterfield, 2009). Accompanying the rise of animals and their greater complex behaviors in the Cambrian and early Paleozoic, including substrate-penetrating bioturbation, was also the ability for biological innovation to directly impact redox conditions of the ocean (Butterfield, 2018, Tarhan et al., 2015, Tarhan, 2018, Boyle et al., 2014, Boyle et al., 2018). Additionally, ecophysiological constraints suggest that temperature stability may be more important for Ediacaran biota than the O_2 concentration alone (Boag et al., 2018). Using constraints from modern cnidarians, these authors suggest that deep, colder waters—even if lower in O_2 than warmer surface waters—produced optimal conditions for early animals. Despite this debate, low to moderate O_2 levels of the early Phanerozoic can help to explain the frequency and severity of extinctions in the early Paleozoic compared to the Stage IV interval of Earth's redox history (Sperling et al. (2022); **Figure 13**).

Therefore, although the role of O_2 in directly controlling early bilaterian evolution is debated (Evans et al., 2018), there is support for the hypothesis that O_2 controlled the ecological, physiological, and morphological characteristics of metazoans (Sperling et al., 2022) and even early mass extinctions (Evans et al., 2022). This includes more complex substrate interaction behavior, such as burrowing and other bioirrigation. As a further example, the rise of predation alongside increases in O_2 highlights how greater energy resources available from aerobic respiration may have led to carnivory and the development of more complex trophic structures (Sperling et al., 2013, Sperling et al., 2022). The rise of carnivory may be partially a consequence of the positive relationship between O_2 and body size, which has been argued for early marine animals in the Ediacaran and Cambrian as well as gigantic terrestrial insects in the late Paleozoic and Cretaceous (Dudley, 1998, Knoll and Carroll, 1999, Butterfield, 2007, Harrison et al., 2010, Payne et al., 2011, Clapham and Karr, 2012, Schachat et al., 2018, Zhuravlev and Wood, 2020). Overall, the increase in body size over the Phanerozoic may reflect the increase in oxidation of the atmosphere-ocean system as well (Heim et al., 2015).

An additional biological innovation that is closely tied to ocean redox is the development of increasingly skeletonized phytoplankton and zooplankton. The rise of biomineralization from the late Ediacaran through the early Paleozoic (Knoll, 2003, Porter, 2007, Zhuravlev and Wood, 2008) and the Mesozoic appearance or expansion of skeletonized diatoms, forams, and coccolithophoorids (Ridgwell, 2005) had major impacts on the biological pump. Specifically, skeletonization is hypothesized to increase the depth of remineralization, which Earth system models have shown to effectively oxygenate the oceans, particularly in shelf environments, through the deepening of the OMZ (Meyer et al., 2016, Lu et al., 2018).

This section highlights the "chicken and egg" challenges of linking O_2 with evolutionary and ecological patterns of complex life in Earth's history (see Cole et al. (2020) for a useful point-counterpoint discussion of some of the arguments covered in this section). Ultimately, while there is little doubt that the specific redox conditions of the oceans remain an important consequence of and in some cases, critical necessity, for biospheric evolution, we expect that the why's, how's,

and when's will continue to drive and advance innovative research in geobiology, with major implications for future climate change as well as for astrobiology.

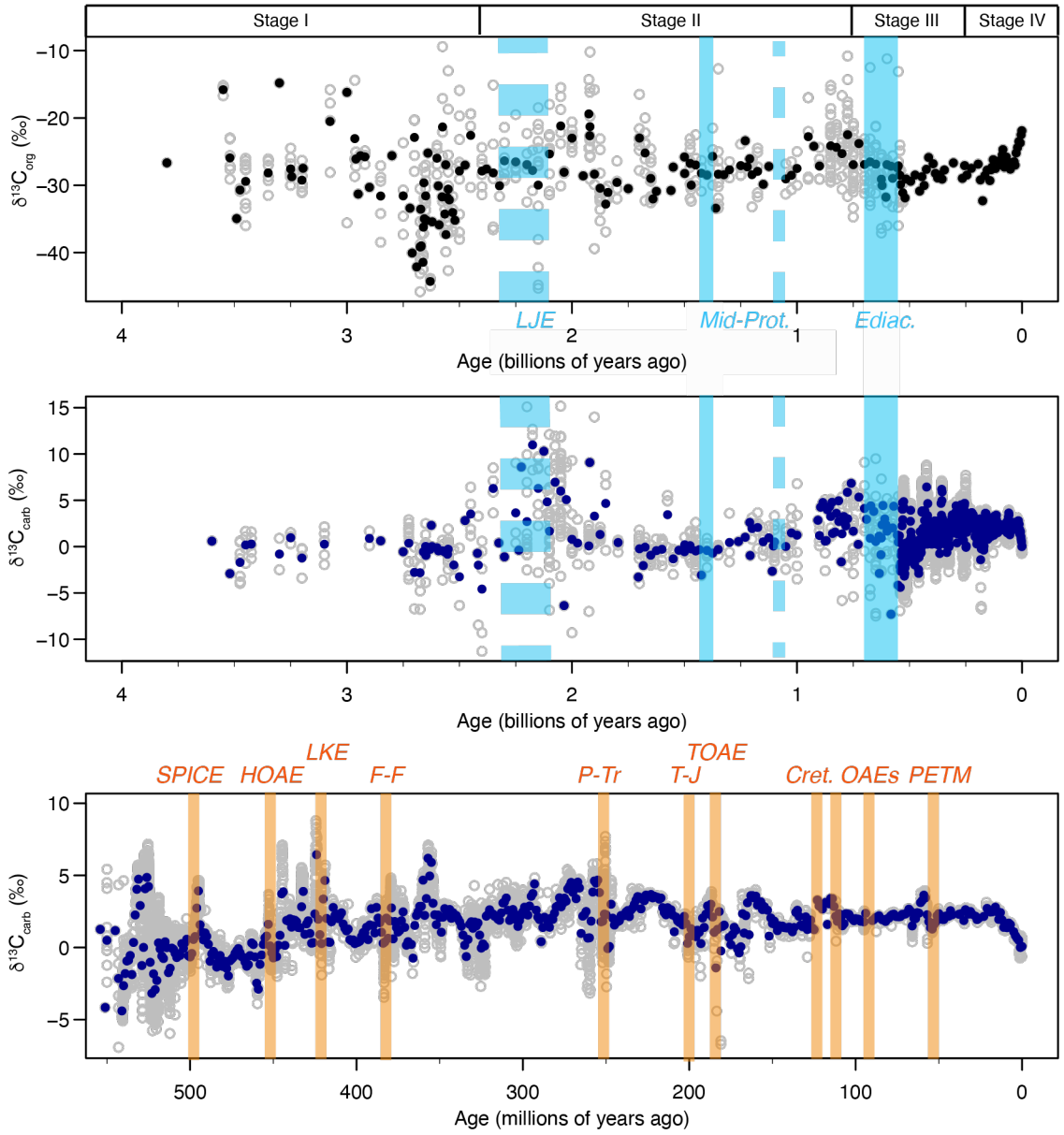

Figure 17. *Compilations of (top) organic carbon isotopes (Krissansen-Totton and Catling, 2017) and (middle) carbonate carbon isotopes (Krissansen-Totton and Catling, 2017, Saltzman and Thomas, 2012). (bottom) Carbonate carbon isotopes for the Phanerozoic only. The solid circles are the binned data (averages for every 1 Myr bins) and the open circles are the entire compilation. Key OOEs (blue bars) and OAEs (orange bars) discussed in Section 4 are marked, with the width of the bar arbitrary. The dashed blue bars indicate proposed (but debated) OOEs. LJE=Lomagundi-Jatuli Event (~2.3 to 2.1 Ma), Mid-Prot=Mid-Proterozoic (~1.4 Ga and ~1.1 Ga), Edia.=multiple Ediacaran OOEs (~640 to 520 Ma), SPICE=Steptoean Positive Carbon Isotope Excursion (~499 Ma), HOAE=Hirnantian Ocean Anoxic Event (~466 Ma), LKE=Late Silurian Lau/Kozlowskii Event (~424 Ma), F-F=Frasnian-Fammenian Lower and Upper Kellwasser events (~372 Ma), P-Tr=Permian-Triassic (~252 Ma), T-J=Triassic-Jurassic (~200 Ma), TOAE=Toarcian Ocean Anoxic Event (~184 Ma), Cret. OAEs=Cretaceous OAEs (OAE-1a, ~120 Ma; OAE-1b, ~111 Ma; OAE-2, ~94 Ma), PETM=Paleocene-Eocene Thermal Maximum (~56 Ma).*

Box 1: Linking changes in redox conditions to the carbon isotope record

Because there are excellent reviews of proxies already published (see **Table 1**), in this Chapter we have focused on the interpretations and implications of redox proxies used to reconstruct past redox conditions. Carbon isotopes are one of the most applied geochemical proxies used to infer changes in O_2 concentrations through Earth history, and so we include this synthesis of recent ideas surrounding if and how carbon isotope records are linked to atmosphere-ocean redox conditions. The link between carbon and redox conditions arises because the proportion of organic carbon burial relative to the total burial of carbon from the ocean-atmosphere system (f_{org}) reflects geological processes that impact redox conditions (Broecker, 1970). Because photosynthesis imparts a large isotope fractionation between inorganic and organic carbon (Hayes and Waldbauer, 2006), buried organic carbon has a lower $\delta^{13}C$ value than inorganic carbon (e.g., carbonate sediments), and therefore increased (decreased) burial of organic carbon would result in a higher (lower) $\delta^{13}C$ of the remaining seawater reservoir of total carbon. Using this framework, the modern mean seawater $\delta^{13}C$ of ~1‰ roughly corresponds to f_{org} = 0.2 (Kump and Arthur, 1999).

The output fluxes of organic carbon burial in terrestrial and marine environments have short-term and long-term implications for O_2 (**Figure 3**; reviewed in Lenton et al. (2016)). Redox conditions in terrestrial and marine settings can be directly linked to organic carbon contents through two non-exclusive mechanisms. First, higher amounts of organic carbon burial can be a direct consequence of greater primary productivity, which leads to greater consumption of O_2 through higher rates of aerobic respiration of sinking organic matter. Triggers for higher primary productivity, including weathering and volcanism-induced delivery of nutrients (Berner, 2006a), can also result in changes in $\delta^{13}C$ via the increase of mantle-derived volcanic CO_2. Second, higher preservation of organic carbon in seafloor sediments corresponds to lower bottom water O_2 concentrations, limiting remineralization pathways to anaerobic metabolisms. Therefore, the direct consequence of lower O_2 (through the production of organic matter and higher preservation) is higher organic carbon burial. On longer time scales, a negative feedback is introduced that results in the opposite relationship (Berner, 2006a, Berner, 2001). Because burial of marine and terrestrial organic carbon removes a major reductant from the ocean-atmosphere system, higher fluxes of organic carbon burial result in a build-up of atmospheric O_2 (e.g., Equation 1). Therefore, the relationship between O_2 and organic carbon, and by extension, $\delta^{13}C$, depends on the spatiotemporal scale of interest.

Based on this long-established framework, a major question is how the C isotope record is representative of global changes in O_2. A compilation of published C isotope records (**Figure 17**) demonstrates that there are major transient and baseline shifts through time, reflected in both the carbonate and organic carbon $\delta^{13}C$ records. The interpretation of these $\delta^{13}C$ compilations has been long investigated, connecting the global carbon and O_2 biogeochemical cycles (Veizer et al., 1999, Saltzman and Thomas, 2012, Krissansen-Totton et al., 2015, Bachan et al., 2017). A major assumption is that the C isotope record is representative of global changes to the ocean-atmosphere C isotope reservoir. This assumption has been challenged, most strikingly by observations in Neogene carbonate sediments (Oehlert and Swart, 2014,

Swart, 2008, Geyman and Maloof, 2019) that highlight the role of diagenesis and local heterogeneity in impacting bulk carbonate $\delta^{13}C$ as well as carbonate paleoredox proxies (**Figure 18**). These factors have also been proposed to impact long-term compilations of $\delta^{13}C$ (Ahm and Husson, 2022), although comparisons of carbonate, marine organic carbon, and terrestrial organic carbon $\delta^{13}C$ can help to support or challenge interpretations of "global" $\delta^{13}C$ signals. Additional caveats to the potential for $\delta^{13}C$ to track redox conditions are other mechanisms that can impact $\delta^{13}C$ independent of O_2 changes, such as the potential for sea-level change and associate weathering/flux changes to impact $\delta^{13}C$ (Saltzman et al., 2015), the release of ^{12}C-enriched sources such as volcanism, organic carbon weathering, or methane (Dickens, 2011, Frieling et al., 2016), and the role of authigenic carbonate precipitation (Higgins et al., 2009, Schrag et al., 2013, Wang et al., 2023). Though these processes have been linked to specific $\delta^{13}C$ excursions, it is currently not clear whether they could play a role in driving the major baseline shifts such as in the Neoproterozoic.

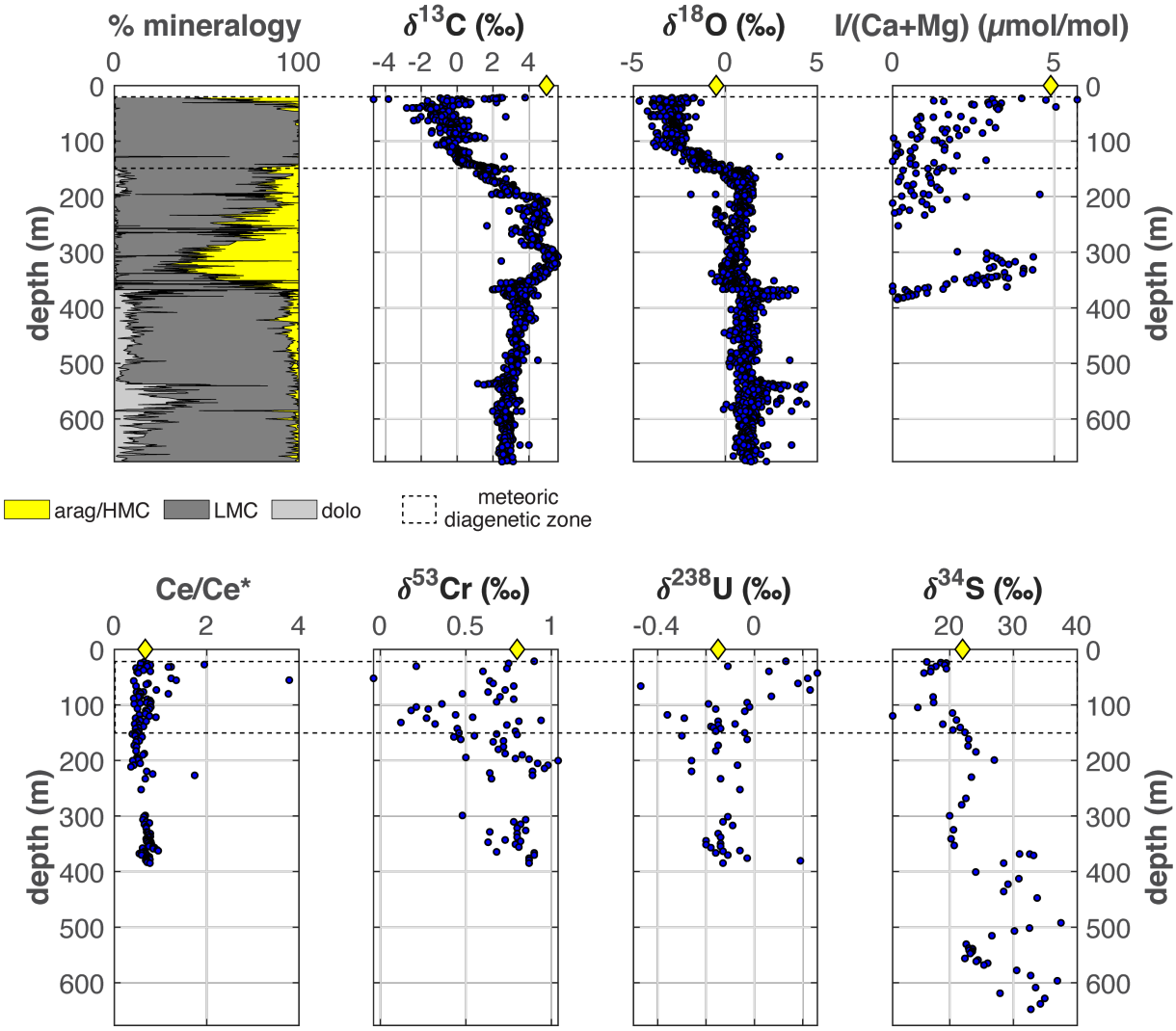

Figure 18. Data from the Neogene to Pleistocene from the Clino core on the Bahamas Bank. The Clino core provides an example of a potential Rosetta's Stone in quantifying paleoredox proxy behavior during carbonate diagenesis, covering a time period

of relatively stable ocean redox but capturing variability in carbon diagenesis, which influences proxy signatures. This includes meteoric diagenesis, driving the negative carbon isotope excursion in the top of the core, and marine burial diagenesis. Data come from multiple sources (Chen et al., 2018, Hardisty et al., 2017, Liu et al., 2019, Wang et al., 2021, Higgins et al., 2018, Melim et al., 1995, Murray et al., 2021, Stewart et al., 2015).

4.3.3 Carbon isotopes and Neoproterozoic OOEs

The relationship between $\delta^{13}C$ and redox change in the Neoproterozoic has been a cause of frequent debate. For example, the negative ~20‰ Shuram excursion (also called the Shuram-Wonoka excursion) that occurred at ca. 574 to 567 Ma appears to correspond to global oxygenation. Specifically, there is evidence for increased SO_4^{2-}, IO_3^-, Mn oxides, U, and other trace metals across this interval (Hardisty et al., 2017, Loyd et al., 2012, Osburn et al., 2015, Zhang et al., 2019, Li et al., 2017, Sahoo et al., 2016, Fike et al., 2006). S and U isotope records hint at a global decrease in pyrite burial (Osburn et al., 2015) and an increase in the extent of oxygenated seafloor at the start of the Shuram (Zhang et al., 2019). That said, the global C cycle interpretations of the Shuram excursion are heavily disputed (Derry, 2010, Husson et al., 2015). Similar to the LJE (Section 4.2.4), explanations for this excursion have been difficult to reconcile with the canonical f_{org} framework linking positive (negative) C isotope changes to higher (lower) organic carbon burial. The nadir $\delta^{13}C_{carb}$ value for the Shuram varies geographically but is consistently below the mantle $\delta^{13}C$ value of ~-6‰ (Kump and Arthur, 1999), ranging from ~-15 to ~-10‰ (see recent compilation in Busch et al. (2022)). The traditional $\delta^{13}C$ interpretative framework of simply a lower f_{org} is not a realistic explanation because the Shuram represents values well below the mantle-input $\delta^{13}C$, and therefore requires alternative explanations including novel carbon pools related to spatial biogeochemical processes, methane addition, or diagenesis (Husson et al., 2015, Tziperman et al., 2011, Rothman et al., 2003, Knauth and Kennedy, 2009, Bjerrum and Canfield, 2011, Busch et al., 2022). Recent arguments even suggest that similar U isotope signals could be generated via euxinic-ferruginous transitions (Gong et al., 2023) and that trace element records from shales provide limited, if any, evidence for oxygenation (Ostrander, 2023).

In contrast to the Shuram, other transient Ediacaran OOEs are not clearly related to systematic shifts in the $\delta^{13}C$, at least within the Doushantuo Formation in South China (Sahoo et al., 2016). Similarly, the Cryogenian Taishir negative $\delta^{13}C$ excursion of ~-15‰, which is best recorded in Mongolian strata spanning the non-glacial interval (Macdonald et al., 2009), has been noted to correspond to a negative shift in U isotopes (Lau et al., 2017b). This has been alternatively interpreted as a long-term expansion of seafloor anoxia or a shift from euxinic to ferruginous conditions (Wei et al., 2021), both of which persist even when the $\delta^{13}C$ record returns to baseline values. In combination, the lack of clear correlation between drivers of $\delta^{13}C$ excursions and transient or long-term redox makes it a challenge to interpret the Neoproterozoic $\delta^{13}C$ record as a consistent recorder of the ocean-marine redox state.

Interestingly, these Precambrian oxygenation "excursions"—that correspond to both positive and negative $\delta^{13}C$ shifts—may be at least in part related to the timescale of these shifts; specifically, if the LJE does indeed represent an oxygenation event of some magnitude, it could be related to the generation of large amounts of organic matter that were subsequently buried, whereas the shorter-lived OOEs could be related to C cycle perturbations that led to temporary oxygenation. Similarly, the Shuram $\delta^{13}C$ has been tied to C cycle dynamics unique to the Ediacaran (Tziperman et al., 2011), and potentially did not reflect organic carbon burial directly but rather the biogeochemical changes that resulted from greater oxygenation.

It is important to note that the baseline redox state of the Precambrian oceans is one with a poorly ventilated, predominantly anoxic deep ocean (**Figure 2**). It is possible that transient shifts to greater anoxia within such an ocean would be difficult to detect given this baseline state. Within this context, a curious observation about the Precambrian C isotopes record, and specifically in the Cryogenian and the Neoproterozoic, are steady-state $\delta^{13}C$ values that are much higher (5 to 10‰) compared to prior and subsequent time intervals. The cause of these high baseline values, and potential implications for both short-term and longer-term redox conditions, remain unexplained (Halverson et al., 2005, Schrag et al., 2013). It is difficult to reconcile how persistently high $\delta^{13}C$ values could be related to long-term higher organic carbon burial as the expectation is that this would be corrected by the negative feedback generating higher atmospheric pO_2. Perhaps these high $\delta^{13}C$ values simply reflect the unique redox stratified ocean and separation of different carbon pools (Bristow and Kennedy, 2008) during the Neoproterozoic (see also Fakraee et al. (2021)).

4.4 Stage IV: OOE to OAE transition

4.4.1 When was the deep ocean oxygenated?

With the Neoproterozoic to Paleozoic transition, the redox structure of the ocean underwent the final change to the present-day configuration shown in **Figure 2** where the deep ocean became fully oxygenated. As discussed in Section 2, this does not signify that O_2 levels in the deep ocean are equivalent to the surface ocean in all locations; the O_2 content of modern bottom waters indicates that regions of water-column productivity, including mouths of rivers and upwelling regions, produce bottom-waters where O_2 is low enough to impact habitability (**Error! Reference source not found.**). However, the vast majority of bottom-water O_2 distribution today is sufficiently high to sustain diverse and abundant metazoan communities. This is possible only when atmospheric O_2 levels were sufficiently high that O_2 consumption through sinking organic carbon (i.e., the biological pump) did not significantly reduce O_2 levels everywhere. The exact atmospheric O_2 level that was required to produce well-oxygenated deep oceans is dependent on parameters of the biological pump, the assumed nutrient availability, as well as ocean configuration. A recent model suggests that the deep ocean is ventilated when atmospheric pO_2 reaches >30% PAL (Reinhard and Planavsky, 2022).

The establishment of modern redox structures can be distinguished by the change in shallow marine carbon redox proxies. Specifically, high I/(Ca+Mg) and low Ce/Ce* bookmark this transition and can both be related to an overall well-oxygenated ocean because globally persistent shallow marine O_2 at high levels can only be sustained (1) when atmospheric O_2 is high and (2) when resupply of well-oxygenated deep oceans to the surface is also high. The change point analysis in **Figure 15** indicates that this likely occurred in the late Paleozoic (Wallace et al., 2017, Lu et al., 2018). Though it may seem paradoxical to utilize proxies for local, shallow redox to represent deep water O_2, recent studies of iodate-iodide dynamics in the modern highlight the fact that the oxidation of I^- to IO_3^- is slow and elevated near-surface IO_3^- likely reflects persistent oxygenation of intermediate and deep ocean masses that resupply IO_3^- to the surface oceans (Hardisty et al., 2020, Hardisty et al., 2021).

Similar to the change points of trace element proxies in the Neoproterozoic, the changes in $\delta^{34}S_{py}$ in the Paleozoic are also closely linked to a decrease in seafloor anoxia (**Figure 15**). Specifically, $\delta^{34}S_{py}$ is a proxy for the degree of pyrite burial, which is intimately linked with the

extent of seafloor anoxia. Increased pyrite burial has the dual effect of acting as a sink for SO_4^{2-}—which is reduced to sulfide in anoxic environments, forming pyrite—and in turn impacting the sulfur isotope composition of both SO_4^{2-} and pyrite. Smaller marine SO_4^{2-} pools, estimated to be <2.5 mM as late as the Cambrian (Gill et al., 2011), ultimately have less buffering capacity and are more sensitive to changes in $\delta^{34}S_{sulfate}$ resulting from sulfate reduction. Together, this means that coupled increases in marine sulfate tied to lower pyrite burial fluxes ushered in a change point for $\delta^{34}S_{py}$ to much more negative values, reflecting changes in the $\Delta^{34}S_{sulfate\text{-}py}$. In comparison, higher seawater SO_4^{2-} in the late Paleozoic (Horita et al., 2002, Lowenstein et al., 2003) resulted in $\delta^{34}S_{sulfate}$ records that are more stable and better buffered against global change. Hence, while the initial $\delta^{34}S_{CAS}$ change point at 2.5 Ga represents an initial increase in seawater SO_4^{2-} linked to increases in atmospheric O_2 and terrestrial weathering of pyrite—i.e., the source of sulfur to the oceans—the later $\delta^{34}S_{py}$ change point at 0.38 Ga represents a stabilization of marine SO_4^{2-} via a decrease in pyrite burial—i.e., the sink of sulfur from the oceans (**Figure 15**). Similarly, the contrast in the change points for $\delta^{238}U_{sh}$ (2.35 Ga), [U] (0.37 Ga), and carbonate associated uranium isotopes ($\delta^{238}U_{CAU}$; 0.39 Ga) can reflect changes in sources and sinks of the U cycle related to redox changes. The change point for $\delta^{238}U_{sh}$ broadly concurrent with the GOE likely reflects an increase in oxidative weathering of uraninite (Partin et al., 2013, Kendall et al., 2013) and the establishment of a seawater U reservoir with seawater $\delta^{238}U$ that could vary from crustal values. Because U reduction in anoxic and euxinic seafloor is the largest sink of seawater U and imparts a significant isotope fractionation (Dunk et al., 2002, Andersen et al., 2014), the Paleozoic change points for [U] and $\delta^{238}U_{CAU}$ reflect a decrease in U removal as seafloor oxygenation spread.

With the establishment of a fully oxygenated ocean, where regions with low O_2 are limited to areas with high productivity, the redox dynamics of the marine realm switched between one where perturbations to the redox state was defined by OAEs and not OOEs. This is not to claim that OAEs are non-existent prior to the late Paleozoic, mainly that short-term (<~1 Myr) perturbations to the atmosphere-ocean O_2 system result in OAEs, whereas such transient perturbations related to O_2 prior to this transition resulted in OOEs, such as in the Ediacaran (Sahoo et al., 2012, Sahoo et al., 2016). In fact, longer-term perturbations (>1 Myr) to the O_2 system prior to this transition result in larger, and more prolonged increases in anoxia (Reershemius and Planavsky, 2021). As discussed in the preceding sections, this transition was likely gradual and/or dynamic.

This general feature of Earth history, where transient perturbations to O_2 go from OOEs to OAEs, hides the complexity of individual events, which occur in distinct biogeochemical contexts such as the biological pump (Ridgwell, 2005, Meyer et al., 2016) or the feedbacks related to bioturbation (Berner and Westrich, 1985, Boyle et al., 2014, Tarhan et al., 2015, Dale et al., 2016) and from different specific triggers leading to anoxia (e.g., exogenous vs. endogenous processes). In other words, the triggers and mechanisms leading to individual OAEs and OOEs were not the same. Nonetheless, this shift from transient OOEs to OAEs overall corresponds to the carbonate U isotope record (Reershemius and Planavsky, 2021), reductions in carbon isotope excursions through the Phanerozoic (Bachan et al., 2017), and the change points in shallow marine redox proxies (carbonate I/(Ca+Mg) and Ce/Ce*; **Figure 15**).

4.4.2 Carbon isotopes and Phanerozoic OAEs

In the Phanerozoic $\delta^{13}C$ record, more anoxia can correspond to either negative or positive $\delta^{13}C$ excursions and reveal the potential roles of external (exogeneous) vs. internal (endogeneous) drivers of C cycle change.

Key examples when deoxygenation is associated with a negative $\delta^{13}C$ excursion (**Figure 17**) include anoxic events that are linked to volcanic (or carbon-input) triggers, including the end-Permian and end-Triassic mass extinctions (Lau et al., 2016, Jost et al., 2017), the Toarcian OAE (Them et al., 2018), and the Paleocene-Eocene Thermal Maximum, or PETM (Clarkson et al., 2021). Most of these events are linked to major volcanic events and specifically Large Igneous Provinces (LIPs), which would have resulted in the addition of volcanic-derived C with low $\delta^{13}C$ values. The potential mechanism between volcanism and anoxia includes global warming-induced changes in ocean circulation (Winguth et al., 2012, Penn et al., 2018), greater weathering and delivery of nutrients (Zhang et al., 2018), and intensification of the biological pump (Meyer et al., 2011, Hülse et al., 2021). The C isotope source for the PETM is also likely related to a C input event (Dickens, 2011), but its transient nature (duration of ~10 kyr) results in a relatively short-lived increase in anoxia (Clarkson et al., 2021). Therefore, negative $\delta^{13}C$ associated with greater anoxia after the oxygenation of the deep ocean is generally a sign of a change in carbon inputs that lead to deoxygenation.

Key examples of intervals where deoxygenation is instead associated with a positive $\delta^{13}C$ (**Figure 17**) include the Cambrian Steptoean Carbon Isotope Excursion (SPICE (Dahl et al., 2014, Gill et al., 2011)), the Lau-Kozlowskii Excursion in the Silurian (Bowman et al., 2021), the Cenomanian-Turonian Ocean Anoxic Event 2 (OAE 2; (Jenkyns et al., 1994, Eldrett et al., 2014)), and the Miocene "Monterey" excursion (White et al., 1992, Flower and Kennett, 1993)—see also (Hess et al., 2023, Li et al., 2023, Auderset et al., 2022). The $\delta^{13}C$ in these examples are often interpreted as a direct recorder of higher organic carbon burial, although the duration of the excursion matters. The early Paleozoic positive $\delta^{13}C$ excursions may be related to the fact that the deep ocean had not fully developed modern levels of oxygenation, with significantly shorter $\delta^{13}C$ excursions in the Mesozoic and Cenozoic reflecting a better ventilated ocean. The SPICE is also complex, with higher anoxia corresponding to the initial positive $\delta^{13}C$ excursion and *more* O_2 associated with the end of the excursion, related to the positive feedback on O_2 from higher organic carbon burial (Dahl et al., 2014). For OAE 2, a combination of S and Tl isotopes suggest seafloor euxinia as extensive as 5%, perhaps initiating up to 54 kyr prior to the carbon isotope excursion itself (Ostrander et al., 2017, Owens et al., 2017). Similar pre-$\delta^{13}C$ excursion initiation of anoxia has also been inferred for the Toarcian OAE (Them et al., 2018). These examples highlight the potential for C isotopes to also record changes in the carbon sinks (compared to the sources that result in negative $\delta^{13}C$ excursions), with the triggers in this case related more to internal, endogenous factors such as reorganization of ocean circulation in the Miocene. The OAE 2 event is an outlier as it has also been linked to LIPs (Turgeon and Creaser, 2008) but a significant negative $\delta^{13}C$ excursion is absent for this event.

Major shifts in the baseline $\delta^{13}C$ in the Devonian or the Carboniferous are absent. A positive shift is expected if greater terrestrial organic carbon burial followed the evolution and proliferation of land plants and coal deposits—an ecological shift that has been linked to great amounts of O_2 in the atmosphere (Algeo et al., 1995, Algeo and Scheckler, 1998, Berner and Canfield, 1989). For example, a +2‰ increase in carbonate $\delta^{13}C$ has been linked to the initial colonization of early plants near the Ordovician/Silurian boundary (Lenton et al., 2016) as higher O_2 levels led to higher continental weathering and increased organic carbon burial. Another

expectation is a change in the carbon isotope fractionation between carbonate and organic carbon with the rise of C3 dominance in land plants, which is hypothesized to explain the increase in the $\delta^{13}C$ of terrestrial organic matter in the Carboniferous (Peters-Kottig et al., 2006). Despite these major changes in the locus of organic carbon burial with the evolution of terrestrial ecosystems, it is possible that the overall net change in organic carbon, and therefore the impact on $\delta^{13}C$, was muted as the terrestrial and marine organic carbon sinks rebalanced due to geographic changes in weathering, nutrients, and productivity.

We return to the original question introduced in *Box 1: Linking changes in redox conditions to the carbon isotope record*: Is there a relationship between $\delta^{13}C$ and redox state of the oceans? Based on this overview, an association between C isotopes and O_2 change is more evident for the Phanerozoic than the Precambrian. However, there is no consistency between increased or decreased anoxia with a $\delta^{13}C$ shift of a given direction, and this demonstrates the complexity of understanding $\delta^{13}C$ excursions as recording either a trigger to anoxia/oxia or the direct effect of the organic carbon cycle itself. There are currently no examples where the redox state of the ocean changed without a concomitant change in $\delta^{13}C$, although this could be a sampling bias issue as these times would appear less interesting biogeochemically. Nonetheless, the many studies that compare $\delta^{13}C$ shifts to redox proxies do indicate support for $\delta^{13}C$ to mark changes in the redox state of the oceans.

5 Future Directions

A range of key insights into marine redox evolution have emerged in the last decade. As always, however, developments in our understanding beget more questions and challenges. It is also humbling to remember that even as our perspectives grow and our constraints are refined, the community is still addressing fundamental questions which were initiated by earlier generations. For paleoceanography—while much has been learned—defining when, where, and how oxygen and associated redox-sensitive elemental cycles were perturbed across key intervals are still heavily debated. For chemical oceanography and diagenesis, quantifying redox-sensitive trace element and isotope relationships to the global carbon and oxygen cycles are still a central challenge. As these fields—which are inherently linked—continue to advance within and beyond these important questions, it is clear from this synthesis and others that we are at the cusp of many important step changes. While there are many, we highlight below important community-wide challenges going forward which leverage recent advances.

- **Integration, curation, and co-analysis of modern and deep time oceanographic data archives:** While new geochemical data from oceanographic transects or sedimentary sections are essential for filling in environmental and temporal gaps, the potential of existing data archives are just beginning to be explored. Indeed, statistical and comprehensive analyses of existing databases and incorporation into models—e.g., data analytics, machine learning, and process-based studies—are the new frontier. Ongoing efforts to curate modern and ancient geochemical databases—e.g., GEOTRACES and SGP—are essential frameworks for these future studies. Importantly, while the differences in geochemical archives may call for different databases, ancient and modern geochemical archives are inherently complimentary and thus should be coordinated and introduced as

such. In this way, future studies can use databases to identify key spatiotemporal gaps, which includes identifying data gaps necessary for constraining palaeoceanographic evolution. For example, many paleoredox studies focus on defined $\delta^{13}C$ excursions, meaning there are important data gaps in defining baseline conditions.

- **Defining O_2 thresholds for redox-sensitive elements:** For both modern chemical and paleoceanography, it is essential to define the O_2 limits associated with oxidation and reduction reactions across redox boundaries. Continued efforts to calibrate redox tracers are necessary for understanding potential variations in metabolic processes within or between ODZs but are also essential for defining O_2 values associated with known redox-transitions in Earth history. For example, comparison of benthic and planktonic C isotopes and I/(Ca+Mg) have been applied to quantify O_2 levels in the Pleistocene and Holocene (Section 3). Further back in Earth history (Section 4), the fractionations associated with $\delta^{53}Cr$ and $\Delta^{33}S$ are associated with well-defined transitions and associated O_2 thresholds, but these constraints are still being determined for other paleoredox proxies. This is an active area of research and, because calibrations should consider modern seawater and sediments, also helps to refine our understanding of the current state of these geochemical cycles. Targeted studies defining O_2 across redox gradients—e.g., depth profiles, experiments—using STOX or other sensors sensitive to sub-μmol kg^{-1} O_2 are essential given the demonstrated importance of these low O_2 levels for aerobic life and most redox-sensitive elemental cycles in the studies to date.

- **Quantifying water mass ages alongside trace element and isotope variations**: As highlighted in this Chapter, determining the relationship between O_2 and water-mass ages provides a mechanistic framework for understanding differences in O_2 abundance and geochemical spatial variation between ODZs. A future challenge is expanding similar approaches to trace element and isotope studies in order to elucidate biogeochemical evolution within and differences between ODZs. The PCA presented in Section 2—based on a relatively limited dataset compared to the broader GEOTRACES compilation—indicates that new insights may emerge with wider efforts at data collection of redox-sensitive elements as well as trace nutrient concentrations.

- **Constraints on trace elements and isotope variations on seasonal and anthropogenic timescales:** Time-series focused projects and databases such as the Ocean Observatory Initiative, Bermuda Atlantic Time Series, Hawaii Ocean Time Series, and the Atlantic Meridional Transect provide unprecedented constraints on temporal variations on daily, seasonal, and annual timescales in key parameters such as C cycling and pH, among others. However, redox-sensitive trace element and isotopes are not routinely measured at the same temporal resolution, limiting our understanding of variations in these geochemical cycles across most timescales. Indeed, our understanding of trace element and isotope variations across geologic time may rival or surpass that across diurnal to anthropogenic timescales. Although logistical constraints play a key role in these gaps—e.g., limited deployable sensors and rigorous/cumbersome sampling requirements—the absence of more detailed modern constraints limit interpretations of these geochemical cycles across modern to geologic timescales.

- **Linking water column and sedimentary redox processes:** The sedimentary geochemical record that forms the basis of redox reconstructions in the past relies on filtering these signals through a myriad of water-column, syn-depositional, and post-depositional processes—including processes broadly included in the theme of "diagenesis." The heterogeneity of water-column geochemistry, including significant variations in trace element compositions even between modern ODZs, was discussed in detail in this synthesis. Interpreting sedimentary geochemistry also requires consideration of interactions across the sediment-water interface that add complexity to what is ultimately recorded in the sedimentary record. Developing nuanced and mechanistic models that link these processes are an area of active research in modern chemical oceanography as well as in deep-time paleoceanography and can be probed with more sediment and porewater sampling as well as reactive-transport modeling and spatially resolved biogeochemical models. The latter in particular can help to reveal whether local changes, including diagenesis, can reflect global climate, tectonic, or geobiological changes.

- **Mechanistic constraints on paleoredox evolution:** While there is a growing arsenal of paleoredox proxies and associated records, a major theme is that the mechanisms driving redox transitions are still debated. For example, as highlighted in this chapter, the mechanisms driving increases in atmospheric and oceanic O_2 at the GOE, in the Neoproterozoic, and within the Paleozoic remain largely unresolved. A future challenge is bolstering ongoing efforts to integrate modern chemical oceanographic observations and experimental constraints into Earth System models aimed at understanding the driving mechanisms for important paleoredox transitions.

- **Temporal constraints on paleoredox evolution:** A major challenge to understanding driving mechanisms for paleoredox evolution is the limited constraints on the timing and tempo associated with these transitions. This is particularly true in the Precambrian where an essential lack of fossil-based correlations means that even determining synchroneity of geochemical records can be contentious. For example, the timing of GOE and LJE remain largely unresolved and the duration and synchronicity of major carbon isotope excursions such as the Shuram-Wonoka in the Ediacaran is highly disputed. A future challenge is bolstering ongoing geochronological studies of these key events/intervals in order to place temporal constraints necessary for stratigraphic correlation and mechanistic models.

- **Relationships between O_2, biological evolution, and habitability:** The geobiological questions posed in this synthesis that link marine redox conditions with the evolution of microscopic and macroscopic life require continued focus on modern constraints. This includes metagenomic analysis of diverse environments that span a range of redox conditions, experiments and models to determine the physiological limits of different extant taxa, and biological oceanographic observations that can improve how biogeochemical processes are integrated into climate models at different levels of complexity. This work will be central to projections of climate change on future marine redox conditions and the impacts on habitability. In Earth history, model-data comparison can help to reveal links between the role that O_2 plays on biotic change (and vice versa) and continued geochronological efforts to refine the rate and timing of both environmental and biotic evolution will test the temporal relationships between redox and life.

6 References

AHM, A.-S. & HUSSON, J. 2022. *Local and Global Controls on Carbon Isotope Chemostratigraphy*, Cambridge University Press.

ALCOTT, L. J., MILLS, B. J. W., BEKKER, A. & POULTON, S. W. 2022. Earth's Great Oxidation Event facilitated by the rise of sedimentary phosphorus recycling. *Nature Geoscience,* 15**,** 210.

ALGEO, T. J., BERNER, R. A., MAYNARD, J. B. & SCHECKLER, S. E. 1995. Late Devonian Oceanic Anoxic Events and Biotic Crises: "Rooted" in the Evolution of Vascular Land Plants? *GSA TODAY***,** 4.

ALGEO, T. J. & LYONS, T. W. 2006. Mo–total organic carbon covariation in modern anoxic marine environments: Implications for analysis of paleoredox and paleohydrographic conditions. *Paleoceanography* [Online], 21.

ALGEO, T. J. & SCHECKLER, S. E. 1998. Terrestrial-marine teleconnections in the Devonian: links between the evolution of land plants, weathering processes, and marine anoxic events. *Philosophical Transactions of the Royal Society of London. Series B: Biological Sciences,* 353**,** 113-130.

ALLEN, P. A. & ETIENNE, J. L. 2008. Sedimentary challenge to Snowball Earth. *Nature Geoscience,* 1**,** 817-825.

ANBAR, A. D., DUAN, Y., LYONS, T. W., ARNOLD, G. L., KENDALL, B., CREASER, R. A., KAUFMAN, A. J., GORDON, G. W., SCOTT, C. & GARVIN, J. 2007. A whiff of oxygen before the great oxidation event? *Science,* 317**,** 1903-1906.

ANDERSEN, M. B., ROMANIELLO, S., VANCE, D., LITTLE, S. H., HERDMAN, R. & LYONS, T. W. 2014. A modern framework for the interpretation of $^{238}U/^{235}U$ in studies of ancient ocean redox. *Earth and Planetary Science Letters,* 400**,** 184-194.

ANDERSON, R. F., ALI, S., BRADTMILLER, L. I., NIELSEN, S. H. H., FLEISHER, M. Q., ANDERSON, B. E. & BURCKLE, L. H. 2009. Wind-Driven Upwelling in the Southern Ocean and the Deglacial Rise in Atmospheric CO2. *Science,* 323**,** 1443-1448.

ARTHUR, M. A., SCHLANGER, S. O. & JENKYNS, H. C. 1987. The Cenomanian-Turonian Oceanic Anoxic Event, II. Palaeoceanographic controls on organic-matter production and preservation. *In:* BROOKS, J. & FLEET, A. J. (eds.) *Marine Petroleum Source Rocks.*

AUDERSET, A., MORETTI, S., TAPHORN, B., EBNER, P. R., KAST, E., WANG, X. T., SCHIEBEL, R., SIGMAN, D. M., HAUG, G. H. & MARTINEZ-GARCIA, A. 2022. Enhanced ocean oxygenation during Cenozoic warm periods. *Nature,* 609**,** 77-+.

BABBIN, A. R., BIANCHI, D., JAYAKUMAR, A. & WARD, B. B. 2015. Rapid nitrous oxide cycling in the suboxic ocean. *Science,* 348**,** 1127-1129.

BACHAN, A., LAU, K. V., SALTZMAN, M. R., THOMAS, E., KUMP, L. R. & PAYNE, J. L. 2017. A model for the decrease in amplitude of carbon isotope excursions across the Phanerozoic. *American Journal of Science,* 317**,** 641-676.

BAKUN, A. & WEEKS, S. J. 2004. Greenhouse gas buildup, sardines, submarine eruptions and the possibility of abrupt degradation of intense marine upwelling ecosystems. *Ecology Letters,* 7**,** 1015-1023.

BANSE, K., NAQVI, S. W. A., NARVEKAR, P. V., POSTEL, J. R. & JAYAKUMAR, D. A. 2014. Oxygen minimum zone of the open Arabian Sea: variability of oxygen and nitrite from daily to decadal timescales. *Biogeosciences,* 11**,** 2237-2261.

BATTLE, M., BENDER, M., SOWERS, T., TANS, P. P., BUTLER, J. H., ELKINS, J. W., ELLIS, J. T., CONWAY, T., ZHANG, N., LANG, P. & CLARKE, A. D. 1996. Atmospheric gas concentrations over the past century measured in air from firn at the South Pole. *Nature,* 383**,** 231-235.

BAYON, G., BINDEMAN, I. N. N., TRINQUIER, A., RETALLACK, G. J. & BEKKER, A. 2022. Long-term evolution of terrestrial weathering and its link to Earth's oxygenation. *Earth and Planetary Science Letters,* 584.

BENDER, M., SOWERS, T. & LABEYRIE, L. 1994a. The Dole Effect and its variations in the last 130,000 years as measured in the Vostok Ice Core. *Global Biogeochemical Cycles,* 8**,** 363-376.

BENDER, M. L., SOWERS, T., BARNOLA, J. M. & CHAPPELLAZ, J. 1994b. Changes in the O_2 /N_2 ratio of the atmosphere during recent decades reflected in the composition of air in the Firn at Vostok Station, Antarctica. *Geophysical Research Letters,* 21**,** 189-192.

BERNER, R. A. 1982. Burial of organic carbon and pyrite sulfur in the modern ocean: its geochemical and environmental significance. *Am. J. Sci,* 282**,** 451-473.

BERNER, R. A. 2001. Modeling atmospheric O_2 over Phanerozoic time. *Geochimica et Cosmochimica Acta,* 65**,** 685-694.

BERNER, R. A. 2006a. GEOCARBSULF: A combined model for Phanerozoic atmospheric O_2 and CO_2. *Geochimica Et Cosmochimica Acta,* 70**,** 5653-5664.

BERNER, R. A. 2006b. GEOCARBSULF: A combined model for Phanerozoic atmospheric O-2 and CO2. *Geochimica Et Cosmochimica Acta,* 70**,** 5653-5664.

BERNER, R. A. & CANFIELD, D. E. 1989. A new model for atmospheric oxygen over Phanerozoic time. *Am. J. Sci,* 289**,** 333-361.

BERNER, R. A. & RAISWELL, R. 1983. Burial of organic carbon and pyrite sulfur in sediments over Phanerozoic time: a new theory. *Geochimica et Cosmochimica Acta,* 47**,** 855-862.

BERNER, R. A. & WESTRICH, J. T. 1985. Bioturbation and the Early Diagenesis of Carbon and Sulfur. *American Journal of Science,* 285**,** 193-206.

BHASKAR, T., SARMA, V. & KUMAR, J. P. 2021. Potential Mechanisms Responsible for Spatial Variability in Intensity and Thickness of Oxygen Minimum Zone in the Bay of Bengal. *Journal of Geophysical Research-Biogeosciences,* 126.

BIAN, X., YANG, S.-C., BOLSTER, K. M., MORIYASU, R., MOFFETT, J. W. & JOHN, S. G. 2023. Biogeochemical cycling of Cd, Mn, and Ce in the Eastern Tropical North Pacific oxygen-deficient zone. *Limnology and Oceanography,* 68**,** 483-497.

BIANCHI, D., WEBER, T. S., KIKO, R. & DEUTSCH, C. 2018. Global niche of marine anaerobic metabolisms expanded by particle microenvironments. *Nature Geoscience,* 11**,** 263-+.

BINDOFF, N. L., CHEUNG, W. W., KAIRO, J. G., ARÍSTEGUI, J., GUINDER, V. A., HALLBERG, R., HILMI, N. J. M., JIAO, N., KARIM, M. S. & LEVIN, L. 2019. Changing ocean, marine ecosystems, and dependent communities. *IPCC special report on the ocean and cryosphere in a changing climate***,** 477-587.

BJERRUM, C. J., BENDTSEN, J. & LEGARTH, J. J. F. 2006. Modeling organic carbon burial during sea level rise with reference to the Cretaceous. *Geochemistry, Geophysics, Geosystems,* 7**,** Q05008.

BJERRUM, C. J. & CANFIELD, D. E. 2011. Towards a quantitative understanding of the late Neoproterozoic carbon cycle. *Proceedings of the National Academy of Sciences,* 108**,** 5542-5547.

BLÄTTLER , C. L., CLAIRE, M. W., PRAVE, A. R., KIRSIMAE, K., HIGGINS, J. A., MEDVEDEV, P. V., ROMASHKIN, A. E., RYCHANCHIK, D. V., ZERKLE, A. L., PAISTE, K., KREITSMANN, T., MILLAR, I. L., HAYLES, J. A., BAO, H., TURCHYN, A. V., WARKE, M. R. & LEPLAND, A. 2018. Two-billion-year-old evaporites capture Earth's great oxidation. *Science,* 360**,** 320.

BOAG, T. H., STOCKEY, R. G., ELDER, L. E., HULL, P. M. & SPERLING, E. A. 2018. Oxygen, temperature and the deep-marine stenothermal cradle of Ediacaran evolution. *Proceedings of the Royal Society B,* 285**,** 1-10.

BOGRAD, S. J., CASTRO, C. G., DI LORENZO, E., PALACIOS, D. M., BAILEY, H., GILLY, W. & CHAVEZ, F. P. 2008. Oxygen declines and the shoaling of the hypoxic boundary in the California Current. *Geophysical Research Letters,* 35.

BOLSTER, K. M., HELLER, M. I., MULHOLLAND, M. R. & MOFFETT, J. W. 2022. Iron and manganese accumulation within the Eastern Tropical North Pacific oxygen deficient zone. *Geochimica Et Cosmochimica Acta,* 334**,** 259-272.

BOSCOLO-GALAZZO, F., CRICHTON, K. A., RIDGWELL, A., MAWBEY, E. M., WADE, B. S. & PEARSON, P. N. 2021. Temperature controls carbon cycling and biological evolution in the ocean twilight zone. *Science,* 371**,** 1148.

BOWMAN, C. N., THEM, T. R., II, KNIGHT, M. D., KALJO, D., ERIKSSON, M. E., HINTS, O., MARTMA, T., OWENS, J. D. & YOUNG, S. A. 2021. A multi-proxy approach to constrain reducing conditions in the Baltic Basin during the late Silurian Lau carbon isotope excursion. *Palaeogeography Palaeoclimatology Palaeoecology,* 581.

BOYER, T., CONKRIGHT, M. E. & LEVITUS, S. 1999. Seasonal variability of dissolved oxygen, percent oxygen saturation, and apparent oxygen utilization in the Atlantic and Pacific Oceans. *Deep-Sea Research Part I-Oceanographic Research Papers,* 46**,** 1593-1613.

BOYER, T. P., GARCÍA, H. E., LOCARNINI, R. A., ZWENG, M. M., MISHONOV, A. V., REAGAN, J. R., WEATHERS, K. A., BARANOVA, O. K., PAVER, C. R. & SEIDOV, D. 2018. World Ocean Atlas.

BOYLE, R. A., DAHL, T. W., BJERRUM, C. J. & CANFIELD, D. E. 2018. Bioturbation and directionality in Earth's carbon isotope record across the Neoproterozoic-Cambrian transition. *Geobiology,* 16**,** 252-278.

BOYLE, R. A., DAHL, T. W., DALE, A. W., SHIELDS-ZHOU, G. A., ZHU, M., BRASIER, M. D., CANFIELD, D. E. & LENTON, T. M. 2014. Stabilization of the coupled oxygen and phosphorus cycles by the evolution of bioturbation. *Nature Geoscience,* 7**,** 671-676.

BREITBURG, D., LEVIN, L. A., OSCHLIES, A., GRÉGOIRE, M., CHAVEZ, F. P., CONLEY, D. J., GARÇON, V., GILBERT, D., GUTIÉRREZ, D., ISENSEE, K., JACINTO, G. S., LIMBURG, K. E., MONTES, I., NAQVI, S. W. A., PITCHER, G. C., RABALAIS, N. N., ROMAN, M. R., ROSE, K. A., SEIBEL, B. A., TELSZEWSKI, M., YASUHARA, M. & ZHANG, J. 2018. Declining oxygen in the global ocean and coastal waters. *Science,* 359**,** eaam7240.

BRISTOW, L. A., CALLBECK, C. M., LARSEN, M., ALTABET, M. A., DEKAEZEMACKER, J., FORTH, M., GAUNS, M., GLUD, R. N., KUYPERS, M. M. M., LAVIK, G., MILUCKA, J., NAQVI, S. W. A.,

PRATIHARY, A., REVSBECH, N. P., THAMDRUP, B., TREUSCH, A. H. & CANFIELD, D. E. 2017. N-2 production rates limited by nitrite availability in the Bay of Bengal oxygen minimum zone. *Nature Geoscience,* 10**,** 24-29.

BRISTOW, L. A., DALSGAARD, T., TIANO, L., MILLS, D. B., BERTAGNOLLI, A. D., WRIGHT, J. J., HALLAM, S. J., ULLOA, O., CANFIELD, D. E. & REVSBECH, N. P. 2016. Ammonium and nitrite oxidation at nanomolar oxygen concentrations in oxygen minimum zone waters. *Proceedings of the National Academy of Sciences,* 113**,** 10601-10606.

BRISTOW, T. F. & KENNEDY, M. J. 2008. Carbon isotope excursions and the oxidant budget of the Ediacaran atmosphere and ocean. *Geology,* 36**,** 863-866.

BROCKS, J. J. 2018. The transition from a cyanobacterial to algal world and the emergence of animals. *Emerging Topics in Life Sciences,* 2**,** 181-190.

BROCKS, J. J., JARRETT, A. J. M., SIRANTOINE, E., HALLMANN, C., HOSHINO, Y. & LIYANAGE, T. 2017. The rise of algae in Cryogenian oceans and the emergence of animals. *Nature,* 548**,** 578-+.

BROCKS, J. J., LOGAN, G. A., BUICK, R. & SUMMONS, R. E. 1999. Archean molecular fossils and the early rise of eukaryotes. *Science,* 285**,** 1033-1036.

BROECKER, W. S. 1970. A boundary condition on the evolution of atmospheric oxygen. *Journal of Geophysical Research (1896-1977),* 75**,** 3553-3557.

BROULLON, D., PEREZ, F. F., VELO, A., HOPPEMA, M., OLSEN, A., TAKAHASHI, T., KEY, R. M., TANHUA, T., MAGDALENA SANTANA-CASIANO, J. & KOZYR, A. 2020. A global monthly climatology of oceanic total dissolved inorganic carbon: a neural network approach. *Earth System Science Data,* 12**,** 1725-1743.

BRUCHERT, V., JORGENSEN, B. B., NEUMANN, K., RIECHMANN, D., SCHLOSSER, M. & SCHULZ, H. 2003. Regulation of bacterial sulfate reduction and hydrogen sulfide fluxes in the central Namibian coastal upwelling zone. *Geochimica Et Cosmochimica Acta,* 67**,** 4505-4518.

BRULAND, K., MIDDAG, R. & LOHAN, M. 2014. Controls of trace metals in seawater. In 'Treatise on Geochemistry'.(Eds H. Holland and K. Turekian.) pp. 19–51. Elsevier: Amsterdam, Netherlands.

BUSCH, J. F., HODGIN, E. B., AHM, A.-S. C., HUSSON, J. M., MACDONALD, F. A., BERGMANN, K. D., HIGGINS, J. A. & STRAUSS, J. V. 2022. Global and local drivers of the Ediacaran Shuram carbon isotope excursion. *Earth and Planetary Science Letters,* 579**,** 117368.

BUTTERFIELD, N. J. 2007. Macroevolution and macroecology through deep time. *Palaeontology,* 50**,** 41-55.

BUTTERFIELD, N. J. 2009. Oxygen, animals and oceanic ventilation: an alternative view. *Geobiology,* 7**,** 1-7.

BUTTERFIELD, N. J. 2015. Early evolution of the eukaryote. *Palaeontology,* 58**,** 5-17.

BUTTERFIELD, N. J. 2018. Oxygen, animals and aquatic bioturbation: An updated account. *Geobiology,* 16**,** 3-16.

CANFIELD, D. 1998. A new model for Proterozoic ocean chemistry. *Nature,* 396**,** 450-453.

CANFIELD, D. E. 2001. Biogeochemistry of sulfur isotopes. *Stable Isotope Geochemistry,* 43**,** 607-636.

CANFIELD, D. E., KRAFT, B., LOSCHER, C., BOYLE, R. A., THAMDRUP, B. & STEWART, F. J. 2019. The regulation of oxygen to low concentrations in marine oxygen-minimum zones. *Journal of Marine Research,* 77**,** 297-324.

CANFIELD, D. E., STEWART, F. J., THAMDRUP, B., DE BRABANDERE, L., DALSGAARD, T., DELONG, E. F., REVSBECH, N. P. & ULLOA, O. 2010. A Cryptic Sulfur Cycle in Oxygen-Minimum-Zone Waters off the Chilean Coast. *Science,* 330**,** 1375-1378.

CANFIELD, D. E. & THAMDRUP, B. 2009. Towards a consistent classification scheme for geochemical environments, or, why we wish the term 'suboxic' would go away. *Geobiology,* 7**,** 385-392.

CANFIELD, D. E., ZHANG, S., FRANK, A. B., WANG, X., WANG, H., SU, J., YE, Y. & FREI, R. 2018. Highly fractionated chromium isotopes in Mesoproterozoic-aged shales and atmospheric oxygen. *Nature Communications,* 9.

CANNARIATO, K. G. & KENNETT, J. P. 1999. Climatically related millennial-scale fluctuations in strength of California margin oxygen-minimum zone during the past 60 k.y. *Geology,* 27**,** 975.

CAROLAN, M. T., SMITH, J. M. & BEMAN, J. M. 2015. Transcriptomic evidence for microbial sulfur cycling in the eastern tropical North Pacific oxygen minimum zone. *Frontiers in Microbiology,* 6.

CATLING, D. C., ZAHNLE, K. J. & MCKAY, C. P. 2001. Biogenic methane, hydrogen escape, and the irreversible oxidation of early Earth. *Science,* 293**,** 839-843.

CHANCE, R., BAKER, A. R., CARPENTER, L. & JICKELLS, T. D. 2014. The distribution of iodide at the sea surface. *Environmental Science-Processes & Impacts,* 16**,** 1841-1859.

CHEN, X., ROMANIELLO, S. J., HERRMANN, A. D., HARDISTY, D., GILL, B. C. & ANBAR, A. D. 2018. Diagenetic effects on uranium isotope fractionation in carbonate sediments from the Bahamas. *Geochimica Et Cosmochimica Acta,* 237**,** 294-311.

CHEN, X., TISSOT, F. L. H., JANSEN, M. F., BEKKER, A., LIU, C. X., NIE, N. X., HALVERSON, G. P., VEIZER, J. & DAUPHAS, N. 2021. The uranium isotopic record of shales and carbonates through geologic time. *Geochimica Et Cosmochimica Acta,* 300**,** 164-191.

CLAPHAM, M. E. & KARR, J. A. 2012. Environmental and biotic controls on the evolutionary history of insect body size. *Proceedings of the National Academy of Sciences,* 109**,** 10927-10930.

CLARKSON, M. O., LENTON, T. M., ANDERSEN, M. B., BAGARD, M.-L., DICKSON, A. J. & VANCE, D. 2021. Upper limits on the extent of seafloor anoxia during the PETM from uranium isotopes. *Nature Communications,* 12**,** 399.

CLEMENT, B. G., LUTHER, G. W. & TEBO, B. M. 2009. Rapid, oxygen-dependent microbial Mn (II) oxidation kinetics at sub-micromolar oxygen concentrations in the Black Sea suboxic zone. *Geochimica et Cosmochimica Acta,* 73**,** 1878-1889.

CODISPOTI, L. A., BRANDES, J., CHRISTENSEN, J. P., DEVOL, A. H., NAQVI, S. W. A., PAERL, H. & YOSHINARI, T. 2001. The oceanic fixed nitrogen and nitrous oxide budgets: moving targets as we enter the anthropocene? *Scientia Marina,* 65**,** 85-105.

COLE, D. B., MILLS, D. B., ERWIN, D. H., SPERLING, E. A., PORTER, S. M., REINHARD, C. T. & PLANAVSKY, N. J. 2020. On the co-evolution of surface oxygen levels and animals. *Geobiology,* 18**,** 260-281.

COLE, D. B., REINHARD, C. T., WANG, X., GUEGUEN, B., HALVERSON, G. P., GIBSON, T., HODGSKISS, M. S., MCKENZIE, N. R., LYONS, T. W. & PLANAVSKY, N. J. 2016. A shale-hosted Cr isotope record of low atmospheric oxygen during the Proterozoic. *Geology***,** G37787. 1.

COLT, J. 1985. American Fisheries Society Special Publication No. 14. Computation of dissolved gas concentrations in water as functions of temperature, salinity, and pressure. *Colt, J. American Fisheries Society Special Publication, No. 14. Computation of Dissolved Gas Concentrations in Water as Functions of Temperature, Salinity, and Pressure. Vi+154p. American Fisheries Society: Bethesda, Md., USA. Illus. Paper*, VI+154P-VI+154P.

COOLEY, S., SCHOEMAN, D., BOPP, L., BOYD, P., DONNER, S., ITO, S.-I., KIESSLING, W., MARTINETTO, P., OJEA, E. & RACAULT, M.-F. 2022. Oceans and coastal ecosystems and their services. *IPCC AR6 WGII.* Cambridge University Press.

COX, G. M., HALVERSON, G. P., MINARIK, W. G., LE HERON, D. P., MACDONALD, F. A., BELLEFROID, E. J. & STRAUSS, J. V. 2013. Neoproterozoic iron formation: An evaluation of its temporal, environmental and tectonic significance. *Chemical Geology,* 362**,** 232-249.

COX, G. M., HALVERSON, G. P., STEVENSON, R. K., VOKATY, M., POIRIER, A., KUNZMANN, M., LI, Z.-X., DENYSZYN, S. W., STRAUSS, J. V. & MACDONALD, F. A. 2016. Continental flood basalt weathering as a trigger for Neoproterozoic Snowball Earth. *Earth and Planetary Science Letters,* 446**,** 89-99.

COX, G. M., LYONS, T. W., MITCHELL, R. N., HASTEROK, D. & GARD, M. 2018. Linking the rise of atmospheric oxygen to growth in the continental phosphorus inventory. *Earth and Planetary Science Letters,* 489**,** 28-36.

CROWE, S. A., DØSSING, L. N., BEUKES, N. J., BAU, M., KRUGER, S. J., FREI, R. & CANFIELD, D. E. 2013. Atmospheric oxygenation three billion years ago. *Nature,* 501**,** 535-538.

CUTTER, G. A. & KRAHFORST, C. F. 1988. Sulfide in surface waters of the Western Atlantic Ocean. *Geophysical Research Letters,* 15**,** 1393-1396.

CUTTER, G. A., MOFFETT, J. G., NIELSDOTTIR, M. C. & SANIAL, V. 2018. Multiple oxidation state trace elements in suboxic waters off Peru: In situ redox processes and advective/diffusive horizontal transport. *Marine Chemistry,* 201**,** 77-89.

CZAJA, A. D., JOHNSON, C. M., RODEN, E. E., BEARD, B. L., VOEGELIN, A. R., NAEGLER, T. F., BEUKES, N. J. & WILLE, M. 2012. Evidence for free oxygen in the Neoarchean ocean based on coupled iron-molybdenum isotope fractionation. *Geochimica Et Cosmochimica Acta,* 86**,** 118-137.

DAHL, T. W., BOYLE, R. A., CANFIELD, D. E., CONNELLY, J. N., GILL, B. C., LENTON, T. M. & BIZZARRO, M. 2014. Uranium isotopes distinguish two geochemically distinct stages during the later Cambrian SPICE event. *Earth and Planetary Science Letters,* 401**,** 313-326.

DALE, A. W., BOYLE, R. A., LENTON, T. M., INGALL, E. D. & WALLMANN, K. 2016. A model for microbial phosphorus cycling in bioturbated marine sediments: Significance for phosphorus burial in the early Paleozoic. *Geochimica et Cosmochimica Acta,* 189**,** 251-268.

DALSGAARD, T., STEWART, F. J., THAMDRUP, B., DE BRABANDERE, L., REVSBECH, N. P., ULLOA, O., CANFIELD, D. E. & DELONG, E. F. 2014. Oxygen at Nanomolar Levels Reversibly Suppresses Process Rates and Gene Expression in Anammox and Denitrification in the Oxygen Minimum Zone off Northern Chile. *Mbio,* 5.

DAVIES, M. H., MIX, A. C., STONER, J. S., ADDISON, J. A., JAEGER, J., FINNEY, B. & WIEST, J. 2011. The deglacial transition on the southeastern Alaska Margin: Meltwater input, sea level rise, marine productivity, and sedimentary anoxia. *Paleoceanography,* 26**,** PA2223.
DE BRABANDERE, L., CANFIELD, D. E., DALSGAARD, T., FRIEDERICH, G. E., REVSBECH, N. P., ULLOA, O. & THAMDRUP, B. 2014. Vertical partitioning of nitrogen-loss processes across the oxic-anoxic interface of an oceanic oxygen minimum zone. *Environmental Microbiology,* 16**,** 3041-3054.
DERRY, L. A. 2010. A burial diagenesis origin for the Ediacaran Shuram–Wonoka carbon isotope anomaly. *Earth and Planetary Science Letters,* 294**,** 152-162.
DEUTSCH, C., BERELSON, W., THUNELL, R., WEBER, T., TEMS, C., MCMANUS, J., CRUSIUS, J., ITO, T., BAUMGARTNER, T., FERREIRA, V., MEY, J. & VAN GEEN, A. 2014. Centennial changes in North Pacific anoxia linked to tropical trade winds. *Science,* 345**,** 665-668.
DEUTSCH, C., EMERSON, S. & THOMPSON, L. 2006. Physical-biological interactions in North Pacific oxygen variability. *Journal of Geophysical Research: Oceans,* 111.
DIAMOND, C. W. & LYONS, T. W. 2018. Mid-Proterozoic redox evolution and the possibility of transient oxygenation events. *Emerging Topics in Life Sciences,* 2**,** 235-245.
DICKENS, G. R. 2011. Down the Rabbit Hole: toward appropriate discussion of methane release from gas hydrate systems during the Paleocene-Eocene thermal maximum and other past hyperthermal events. *Climate of the Past,* 7**,** 831-846.
DODD, M. S., SHI, W., LI, C., ZHANG, Z. H., CHENG, M., GU, H. D., HARDISTY, D. S., LOYD, S. J., WALLACE, M. W., HOOD, A. V., LAMOTHE, K., MILLS, B. J. W., POULTON, S. W. & LYONS, T. W. 2023. Uncovering the Ediacaran phosphorus cycle. *Nature,* 618**,** 974-+.
DU, J., MIX, A. C., HALEY, B. A., BELANGER, C. L. & SHARON 2022. Volcanic trigger of ocean deoxygenation during Cordilleran ice sheet retreat. *Nature,* 611**,** 74-80.
DUAN, Y., ANBAR, A. D., ARNOLD, G. L., LYONS, T. W., GORDON, G. W. & KENDALL, B. 2010. Molybdenum isotope evidence for mild environmental oxygenation before the Great Oxidation Event. *Geochimica Et Cosmochimica Acta,* 74**,** 6655-6668.
DUDLEY, R. 1998. Atmospheric oxygen, giant Paleozoic insects and the evolution of aerial locomotor performance. *The Journal of Experimental Biology,* 201**,** 1043-1050.
DUNCAN, M. S. & DASGUPTA, R. 2017. Rise of Earth's atmospheric oxygen controlled by efficient subduction of organic carbon. *Nature Geoscience,* 10**,** 387-+.
DUNK, R. M., MILLS, R. A. & JENKINS, W. J. 2002. A reevaluation of the oceanic uranium budget for the Holocene. *Chemical Geology,* 190**,** 45-67.
ELDERFIELD, H. & TRUESDALE, V. W. 1980. On the biophilic nature of iodine in seawater. *Earth and Planetary Science Letters,* 50**,** 105-114.
ELDRETT, J. S., MINISINI, D. & BERGMAN, S. C. 2014. Decoupling of the carbon cycle during Ocean Anoxic Event 2. *Geology,* 42**,** 567-570.
EPPLEY, R. W. 1972. Temperature and phytoplankton growth in the sea. *Fish. bull,* 70**,** 1063-1085.
EVANS, S. D., DIAMOND, C. W., DROSER, M. L. & LYONS, T. W. 2018. Dynamic oxygen and coupled biological and ecological innovation during the second wave of the Ediacara Biota. *Emerging Topics in Life Sciences,* 2**,** 223-233.

EVANS, S. D., HUGHES, I. V., GEHLING, J. G. & DROSER, M. L. 2020a. Discovery of the oldest bilaterian from the Ediacaran of South Australia. *Proceedings of the National Academy of Sciences,* 117**,** 7845-7850.

EVANS, S. D., TU, C., RIZZO, A., SURPRENANT, R. L., BOAN, P. C., MCCANDLESS, H., MARSHALL, N., XIAO, S. & DROSER, M. L. 2022. Environmental drivers of the first major animal extinction across the Ediacaran White Sea-Nama transition. *Proceedings of the National Academy of Sciences of the United States of America,* 119**,** e2207475119-e2207475119.

EVANS, Z. C., BOLES, E., KWIECINSKI, J. V., MULLEN, S., WOLF, M., DEVOL, A. H., MORIYASU, R., NAM, S., BABBIN, A. R. & MOFFETT, J. W. 2020b. The role of water masses in shaping the distribution of redox active compounds in the Eastern Tropical North Pacific oxygen deficient zone and influencing low oxygen concentrations in the eastern Pacific Ocean. *Limnology and Oceanography*.

FABRE, S. & BERGER, G. 2012. How tillite weathering during the snowball Earth aftermath induced cap carbonate deposition. *Geology,* 40**,** 1027-1030.

FAKHRAEE, M., TARHAN, L. G., PLANAVSKY, N. J. & REINHARD, C. T. 2021. A largely invariant marine dissolved organic carbon reservoir across Earth's history. *Proceedings of the National Academy of Sciences of the United States of America,* 118.

FAKHRAEE, M., TARHAN, L. G., REINHARD, C. T., CROWE, S. A., LYONS, T. W. & PLANAVSKY, N. J. 2023. Earth's surface oxygenation and the rise of eukaryotic life: Relationships to the Lomagundi positive carbon isotope excursion revisited. *Earth-Science Reviews,* 240.

FARQUHAR, J., ZERKLE, A. L. & BEKKER, A. 2011. Geological constraints on the origin of oxygenic photosynthesis. *Photosynthesis Research,* 107**,** 11-36.

FARRELL, U. C., SAMAWI, R., ANJANAPPA, S., KLYKOV, R., ADEBOYE, O. O., AGIC, H., AHM, A.-S. C., BOAG, T. H., BOWYER, F., BROCKS, J. J., BRUNOIR, T. N., CANFIELD, D. E., CHEN, X., CHENG, M., CLARKSON, M. O., COLE, D. B., CORDIE, D. R., CROCKFORD, P. W., CUI, H., DAHL, T. W., MOURO, L. D., DEWING, K., DORNBOS, S. Q., DRABON, N., DUMOULIN, J. A., EMMINGS, J. F., ENDRIGA, C. R., FRASER, T. A., GAINES, R. R., GASCHNIG, R. M., GIBSON, T. M., GILLEAUDEAU, G. J., GILL, B. C., GOLDBERG, K., GUILBAUD, R., HALVERSON, G. P., HAMMARLUND, E. U., HANTSOO, K. G., HENDERSON, M. A., HODGSKISS, M. S. W., HORNER, T. J., HUSSON, J. M., JOHNSON, B., KABANOV, P., BRENHIN KELLER, C., KIMMIG, J., KIPP, M. A., KNOLL, A. H., KREITSMANN, T., KUNZMANN, M., KURZWEIL, F., LEROY, M. A., LI, C., LIPP, A. G., LOYDELL, D. K., LU, X., MACDONALD, F. A., MAGNALL, J. M., MAND, K., MEHRA, A., MELCHIN, M. J., MILLER, A. J., MILLS, N. T., MWINDE, C. N., O'CONNELL, B., OCH, L. M., OSSA OSSA, F., PAGES, A., PAISTE, K., PARTIN, C. A., PETERS, S. E., PETROV, P., PLAYTER, T. L., PLAZA-TORRES, S., PORTER, S. M., POULTON, S. W., PRUSS, S. B., RICHOZ, S., RITZER, S. R., ROONEY, A. D., SAHOO, S. K., SCHOEPFER, S. D., SCLAFANI, J. A., SHEN, Y., SHORTTLE, O., SLOTZNICK, S. P., SMITH, E. F., SPINKS, S., STOCKEY, R. G., STRAUSS, J. V., STUEKEN, E. E., TECKLENBURG, S., THOMSON, D., TOSCA, N. J., UHLEIN, G. J., VIZCAINO, M. N., WANG, H., WHITE, T., WILBY, P. R., WOLTZ, C. R., et al. 2021. The Sedimentary Geochemistry and Paleoenvironments Project. *Geobiology,* 19**,** 545-556.

FIKE, D. A., GROTZINGER, J. P., PRATT, L. M. & SUMMONS, R. E. 2006. Oxidation of the Ediacaran Ocean. *Nature,* 444**,** 744-747.

FISCHER, A. G. 1965. Fossils, early life, and atmospheric history. *Proceedings of the National Academy of Sciences,* 53**,** 1205-1215.
FISCHER, W. W., HEMP, J. & JOHNSON, J. E. 2016. Evolution of Oxygenic Photosynthesis. *In:* JEANLOZ, R. & FREEMAN, K. H. (eds.) *Annual Review of Earth and Planetary Sciences, Vol 44.*
FITZSIMMONS, J. N., BOYLE, E. A. & JENKINS, W. J. 2014. Distal transport of dissolved hydrothermal iron in the deep South Pacific Ocean. *Proceedings of the National Academy of Sciences,* 111**,** 16654-16661.
FITZSIMMONS, J. N. & CONWAY, T. M. 2023. Novel insights into marine iron biogeochemistry from iron isotopes. *Annual Review of Marine Science,* 15**,** 383-406.
FITZSIMMONS, J. N., CONWAY, T. M., LEE, J. M., KAYSER, R., THYNG, K. M., JOHN, S. G. & BOYLE, E. A. 2016. Dissolved iron and iron isotopes in the southeastern Pacific Ocean. *Global Biogeochemical Cycles,* 30**,** 1372-1395.
FLOWER, B. P. & KENNETT, J. P. 1993. Relations between Monterey Formation deposition and middle Miocene global cooling: Naples Beach section, California. *Geology,* 21**,** 877-880.
FOURNIER, G. P., MOORE, K. R., RANGEL, L. T., PAYETTE, J. G., MOMPER, L. & BOSAK, T. 2021. The Archean origin of oxygenic photosynthesis and extant cyanobacterial lineages. *Proceedings of the Royal Society B-Biological Sciences,* 288.
FRENCH, K. L., HALLMANN, C., HOPE, J. M., SCHOON, P. L., ZUMBERGE, J. A., HOSHINO, Y., PETERS, C. A., GEORGE, S. C., LOVE, G. D., BROCKS, J. J., BUICK, R. & SUMMONS, R. E. 2015. Reappraisal of hydrocarbon biomarkers in Archean rocks. *Proceedings of the National Academy of Sciences of the United States of America,* 112**,** 5915-5920.
FRIEDRICH, T., OSCHLIES, A. & EDEN, C. 2006. Role of wind stress and heat fluxes in interannual-to-decadal variability of air-sea CO2 and O-2 fluxes in the North Atlantic. *Geophysical Research Letters,* 33.
FRIELING, J., SVENSEN, H. H., PLANKE, S., CRAMWINCKEL, M. J., SELNES, H. & SLUIJS, A. 2016. Thermogenic methane release as a cause for the long duration of the PETM. *Proceedings of the National Academy of Sciences of the United States of America,* 113**,** 12059-12064.
FROELICH, P. N., KLINKHAMMER, G., BENDER, M. A. A., LUEDTKE, N., HEATH, G. R., CULLEN, D., DAUPHIN, P., HAMMOND, D., HARTMAN, B. & MAYNARD, V. 1979. Early oxidation of organic matter in pelagic sediments of the eastern equatorial Atlantic: suboxic diagenesis. *Geochimica et Cosmochimica Acta,* 43**,** 1075-1090.
GAILLARD, F., SCAILLET, B. & ARNDT, N. T. 2011. Atmospheric oxygenation caused by a change in volcanic degassing pressure. *Nature,* 478**,** 229-U112.
GALBRAITH, E. D. & KIENAST, M. 2013. The acceleration of oceanic denitrification during deglacial warming. *Nature Geoscience,* 6**,** 579-584.
GALLOWAY, J. N., DENTENER, F. J., CAPONE, D. G., BOYER, E. W., HOWARTH, R. W., SEITZINGER, S. P., ASNER, G. P., CLEVELAND, C. C., GREEN, P. A., HOLLAND, E. A., KARL, D. M., MICHAELS, A. F., PORTER, J. H., TOWNSEND, A. R. & VOROSMARTY, C. J. 2004. Nitrogen cycles: past, present, and future. *Biogeochemistry,* 70**,** 153-226.
GARCIA-ROBLEDO, E., PADILLA, C. C., ALDUNATE, M., STEWART, F. J., ULLOA, O., PAULMIER, A., GREGORI, G. & REVSBECH, N. P. 2017. Cryptic oxygen cycling in anoxic marine zones.

Proceedings of the National Academy of Sciences of the United States of America, 114**,** 8319-8324.
GARVIN, J., BUICK, R., ANBAR, A. D., ARNOLD, G. L. & KAUFMAN, A. J. 2009. Isotopic Evidence for an Aerobic Nitrogen Cycle in the Latest Archean. *Science,* 323**,** 1045-1048.
GAZITUA, M. C., VIK, D. R., ROUX, S., GREGORY, A. C., BOLDUC, B., WIDNER, B., MULHOLLAND, M. R., HALLAM, S. J., ULLOA, O. & SULLIVAN, M. B. 2021. Potential virus-mediated nitrogen cycling in oxygen-depleted oceanic waters. *Isme Journal,* 15**,** 981-998.
GEOTRACES INTERMEDIATE DATA PRODUCT GROUP 2021. The GEOTRACES Intermediate Data Product 2021 (IDP2021). NERC EDS British Oceanographic Data Centre NOC.
GEYMAN, E. C. & MALOOF, A. C. 2019. A diurnal carbon engine explains ^{13}C-enriched carbonates without increasing the global production of oxygen. *Proceedings of the National Academy of Sciences,* 116**,** 24433-24439.
GIBSON, T. M., SHIH, P. M., CUMMING, V. M., FISCHER, W. W., CROCKFORD, P. W., HODGSKISS, M. S. W., WORNDLE, S., CREASER, R. A., RAINBIRD, R. H., SKULSKI, T. M. & HALVERSON, G. P. 2018. Precise age of Bangiomorpha pubescens dates the origin of eukaryotic photosynthesis. *Geology,* 46**,** 135-138.
GILL, B. C., LYONS, T. W. & FRANK, T. D. 2008. Behavior of carbonate-associated sulfate during meteoric diagenesis and implications for the sulfur isotope paleoproxy. *Geochimica et Cosmochimica Acta,* 72**,** 4699-4711.
GILL, B. C., LYONS, T. W., YOUNG, S. A., KUMP, L. R., KNOLL, A. H. & SALTZMAN, M. R. 2011. Geochemical evidence for widespread euxinia in the Later Cambrian ocean. *Nature,* 469**,** 80-83.
GILLEAUDEAU, G., FREI, R., KAUFMAN, A., KAH, L., AZMY, K., BARTLEY, J., CHERNYAVSKIY, P. & KNOLL, A. 2016. Oxygenation of the mid-Proterozoic atmosphere: clues from chromium isotopes in carbonates.
GODFREY, L. V. & FALKOWSKI, P. G. 2009. The cycling and redox state of nitrogen in the Archaean ocean. *Nature Geoscience,* 2**,** 725-729.
GOLDBLATT, C., LENTON, T. M. & WATSON, A. J. 2006. Bistability of atmospheric oxygen and the Great Oxidation. *Nature,* 443**,** 683-686.
GONG, Z., WEI, G.-Y., FAKHRAEE, M., ALCOTT, L. J., JIANG, L., ZHAO, M. & PLANAVSKY, N. J. 2023. Revisiting marine redox conditions during the Ediacaran Shuram carbon isotope excursion. *Geobiology*.
GROOTES, P. M. & STUIVER, M. 1997. Oxygen 18/16 variability in Greenland snow and ice with 10^{-3}- to 10^{5}- year time resolution. *Journal of Geophysical Research-Oceans,* 102**,** 26455-26470.
GUENELI, N., MCKENNA, A. M., OHKOUCHI, N., BOREHAM, C. J., BEGHIN, J., JAVAUX, E. J. & BROCKS, J. J. 2018. 1.1-billion-year-old porphyrins establish a marine ecosystem dominated by bacterial primary producers. *Proceedings of the National Academy of Sciences of the United States of America,* 115**,** E6978-E6986.
GUMSLEY, A. P., CHAMBERLAIN, K. R., BLEEKER, W., SOEDERLUND, U., DE KOCK, M. O., LARSSON, E. R. & BEKKER, A. 2017. Timing and tempo of the Great Oxidation Event. *Proceedings of the National Academy of Sciences of the United States of America,* 114**,** 1811-1816.

HALLAM, A. 1989. The case for sea-level change as a dominant causal factor in mass extinction of marine invertebrates. *Philosophical Transactions of the Royal Society of London B.,* 325**,** 437-455.
HALLAM, A. & WIGNALL, P. B. 1999. Mass extinctions and sea-level changes. *Earth-Science Reviews,* 48**,** 217-250.
HALVERSON, G. P., HOFFMAN, P. F., SCHRAG, D. P., MALOOF, A. C. & RICE, A. H. N. 2005. Toward a Neoproterozoic composite carbon-isotope record. *Geological Society of America Bulletin,* 117**,** 1181-1207.
HANSARD, S. P., EASTER, H. D. & VOELKER, B. M. 2011. Rapid Reaction of Nanomolar Mn(II) with Superoxide Radical in Seawater and Simulated Freshwater. *Environmental Science & Technology,* 45**,** 2811-2817.
HANSEL, C. M. & DIAZ, J. M. 2021. Production of Extracellular Reactive Oxygen Species by Marine Biota. *In:* CARLSON, C. A. & GIOVANNONI, S. J. (eds.) *Annual Review of Marine Science, Vol 13, 2021.*
HAQ, B. U., HARDENBOL, J. & VAIL, P. R. 1987. Chronology of Fluctuating Sea Levels Since the Triassic. *Science,* 235**,** 1156-1167.
HARDISTY, D., HORNER, T., WANKEL, S., BLUSZTAJN, J. & NIELSEN, S. 2020. Experimental observations of marine iodide oxidation using a novel sparge-interface MC-ICP-MS technique. *Chemical Geology,* 532.
HARDISTY, D. S., HORNER, T. J., EVANS, N., MORIYASU, R., BABBIN, A. R., WANKEL, S. D., MOFFETT, J. W. & NIELSEN, S. G. 2021. Limited iodate reduction in shipboard seawater incubations from the Eastern Tropical North Pacific oxygen deficient zone. *Earth and Planetary Science Letters,* 554.
HARDISTY, D. S., LU, Z., BEKKER, A., DIAMOND, C. W., GILL, B. C., JIANG, G., KAH, L. C., KNOLL, A. H., LOYD, S. J., OSBURN, M. R., PLANAVSKY, N. J., WANG, C., ZHOU, X. & LYONS, T. W. 2017. Perspectives on Proterozoic surface ocean redox from iodine contents in ancient and recent carbonate. *Earth and Planetary Science Letters,* 463**,** 159-170.
HARDISTY, D. S., LU, Z., PLANAVSKY, N. J., BEKKER, A., PHILIPPOT, P., ZHOU, X. & LYONS, T. W. 2014. An iodine record of Paleoproterozoic surface ocean oxygenation. *Geology,* 42**,** 619-622.
HARRISON, J. F., KAISER, A. & VANDENBROOKS, J. M. 2010. Atmospheric oxygen level and the evolution of insect body size. *Proceedings of the Royal Society B-Biological Sciences,* 277**,** 1937-1946.
HAYES, J. 1994. Global methanotrophy at the Archean-Proterozoic transition. *Earky Life on Earth, Nobel Symposiin No. 84***,** 220-236.
HAYES, J. M. & WALDBAUER, J. R. 2006. The carbon cycle and associated redox processes through time. *Philosophical Transactions of the Royal Society B: Biological Sciences,* 361**,** 931-950.
HEARD, A. W., DAUPHAS, N., GUILBAUD, R., ROUXEL, O. J., BUTLER, I. B., NIE, N. X. & BEKKER, A. 2020. Triple iron isotope constraints on the role of ocean iron sinks in early atmospheric oxygenation. *Science,* 370**,** 446-449.
HEDGES, J. I. & KEIL, R. G. 1995. Sedimentary organic-matter preservation - an assessment and speculative synthesis. *Marine Chemistry,* 49**,** 81-115.

HEIM, N. A., KNOPE, M. L., SCHAAL, E. K., WANG, S. C. & PAYNE, J. L. 2015. Cope's rule in the evolution of marine animals. *Science,* 347**,** 867-870.
HELLER, M. I. & CROOT, P. L. 2010. Superoxide Decay Kinetics in the Southern Ocean. *Environmental Science & Technology,* 44**,** 191-196.
HELLER, M. I., LAM, P. J., MOFFETT, J. W., TILL, C. P., LEE, J.-M., TONER, B. M. & MARCUS, M. A. 2017. Accumulation of Fe oxyhydroxides in the Peruvian oxygen deficient zone implies non-oxygen dependent Fe oxidation. *Geochimica Et Cosmochimica Acta,* 211**,** 174-193.
HELLY, J. J. & LEVIN, L. A. 2004. Global distribution of naturally occurring marine hypoxia on continental margins. *Deep-Sea Research Part I-Oceanographic Research Papers,* 51**,** 1159-1168.
HELM, K. P., BINDOFF, N. L. & CHURCH, J. A. 2011. Observed decreases in oxygen content of the global ocean. *Geophysical Research Letters,* 38.
HEPBURN, L. E., BUTLER, I. B., BOYCE, A. & SCHRÖDER, C. 2020. The use of operationally-defined sequential Fe extraction methods for mineralogical applications: A cautionary tale from Mössbauer spectroscopy. *Chemical Geology,* 543**,** 119584.
HESS, A. V., AUDERSET, A., ROSENTHAL, Y., MILLER, K. G., ZHOU, X. L., SIGMAN, D. M. & MARTINEZ-GARCIA, A. 2023. A well-oxygenated eastern tropical Pacific during the warm Miocene. *Nature,* 619**,** 521-+.
HIGGINS, J. A., BLÄTTLER, C.L., LUNDSTRON, E. A., SANTIAGO-RAMOS, D. P., AKHTAR, A. A., AHM, A. S. C., BIALIK, O., HOLMDEN, C., BRADBURY, H. J., MURRAY, S. T. & SWART, P. K. 2018. Mineralogy, early marine diagenesis, and the chemistry of shallow water carbonate sediments. *Geochimica et Cosmochimica Acta*.
HIGGINS, J. A., FISCHER, W. W. & SCHRAG, D. P. 2009. Oxygenation of the ocean and sediments: Consequences for the seafloor carbonate factory. *Earth and Planetary Science Letters,* 284**,** 25-33.
HIGGINS, J. A. & SCHRAG, D. P. 2003. Aftermath of a snowball Earth. *Geochemistry Geophysics Geosystems,* 4.
HLOHOWSKYJ, S. R., CHAPPAZ, A. & DICKSON, A. J. 2021. Molybdenum as a Paleoredox Proxy: Past, Present, and Future. *Elements in Geochemical Tracers in Earth System Science*.
HO, T. Y., QUIGG, A., FINKEL, Z. V., MILLIGAN, A. J., WYMAN, K., FALKOWSKI, P. G. & MOREL, F. M. 2003. The elemental composition of some marine phytoplankton 1. *Journal of phycology,* 39**,** 1145-1159.
HODGSKISS, M. S. W., CROCKFORD, P. W., PENG, Y., WING, B. A. & HORNER, T. J. 2019. A productivity collapse to end Earth's Great Oxidation. *Proceedings of the National Academy of Sciences of the United States of America,* 116**,** 17207-17212.
HODGSKISS, M. S. W. & SPERLING, E. A. 2022. A prolonged, two-step oxygenation of Earth's early atmosphere: Support from confidence intervals. *Geology,* 50**,** 158-162.
HOEGH-GULDBERG, O., CAI, R., POLOCZANSKA, E. S., BREWER, P. G., SUNDBY, S., HILMI, K., FABRY, V. J., JUNG, S., SKIRVING, W., STONE, D., BURROWS, M. T., BELL, J., CAO, L., DONNER, S., EAKIN, C. M., EIDE, A., HALPERN, B., MCCLAIN, C. R., O'CONNOR, M. I., PARMESAN, C., PERRY, R. I., RICHARDSON, A. J., BROWN, C. J., SCHOEMAN, D., SIGNORINI, S., SYDEMAN, W., ZHANG, R., VAN HOOIDONK, R. & MCKINNELL, S. M. 2014. The Ocean. *In:* BARROS, V. R., FIELD, C. B., DOKKEN, D. J., MASTRANDREA, M. D., MACH, K. J., BILIR, T. B., CHATTERJEE, M., EBI, K. L., ESTRADA, Y. O., GENOVA, R. C., GIRMA, B.,

KISSEL, E. S., LEVY, A. N., MACCRACKEN, S., MASTRANDREA, P. R. & WHITE, L. L. (eds.) *Climate Change 2014: Impacts, Adaptation, and Vulnerability, Pt B: Regional Aspects: Working Group Ii Contribution to the Fifth Assessment Report of the Intergovernmental Panel on Climate Change.*

HOFFMAN, P. F. 1998. A Neoproterozoic Snowball Earth. *Science,* 281**,** 1342-1346.

HOFFMAN, P. F. 2016. Cryoconite pans on Snowball Earth: supraglacial oases for Cryogenian eukaryotes? *Geobiology,* 14**,** 531-542.

HOFFMAN, P. F., ABBOT, D. S., ASHKENAZY, Y., BENN, D. I., BROCKS, J. J., COHEN, P. A., COX, G. M., CREVELING, J. R., DONNADIEU, Y., ERWIN, D. H., FAIRCHILD, I. J., FERREIRA, D., GOODMAN, J. C., HALVERSON, G. P., JANSEN, M. F., LE HIR, G., LOVE, G. D., MACDONALD, F. A., MALOOF, A. C., PARTIN, C. A., RAMSTEIN, G., ROSE, B. E. J., ROSE, C. V., SADLER, P. M., TZIPERMAN, E., VOIGT, A. & WARREN, S. G. 2017. Snowball Earth climate dynamics and Cryogenian geology-geobiology. *Science Advances,* 3**,** e1600983.

HOFFMAN, P. F. & SCHRAG, D. P. 2002. The snowball Earth hypothesis: testing the limits of global change. *Terra Nova,* 14**,** 129-155.

HOFMANN, A. F., PELTZER, E. T., WALZ, P. M. & BREWER, P. G. 2011. Hypoxia by degrees: Establishing definitions for a changing ocean. *Deep-Sea Research Part I-Oceanographic Research Papers,* 58**,** 1212-1226.

HOLLAND, H. D. 2009. Why the atmosphere became oxygenated: A proposal. *Geochimica Et Cosmochimica Acta,* 73**,** 5241-5255.

HOOGAKKER, B. A. A., ELDERFIELD, H., SCHMIEDL, G., MCCAVE, I. N. & RICKABY, R. E. M. 2015. Glacial-interglacial changes in bottom-water oxygen content on the Portuguese margin. *Nature Geoscience,* 8**,** 40-43.

HOOGAKKER, B. A. A., LU, Z., UMLING, N., JONES, L., ZHOU, X., RICKABY, R. E. M., THUNELL, R., CARTAPANIS, O. & GALBRAITH, E. 2018. Glacial expansion of oxygen-depleted seawater in the eastern tropical Pacific. *Nature,* 562**,** 410-413.

HOOGAKKER, B. A. A., THORNALLEY, D. J. R. & BARKER, S. 2016. Millennial changes in North Atlantic oxygen concentrations. *Biogeosciences,* 13**,** 211-221.

HOPKINSON, B. M. & BARBEAU, K. A. 2007. Organic and redox speciation of iron in the eastern tropical North Pacific suboxic zone. *Marine Chemistry,* 106**,** 2-17.

HORITA, J., ZIMMERMANN, H. & HOLLAND, H. D. 2002. Chemical evolution of seawater during the Phanerozoic: Implications from the record of marine evaporites. *Geochimica et Cosmochimica Acta,* 66**,** 3733-3756.

HORNER, T. J., LITTLE, S. H., CONWAY, T. M., FARMER, J. R., HERTZBERG, J. E., JANSSEN, D. J., LOUGH, A. J. M., MCKAY, J. L., TESSIN, A., GALER, S. J. G., JACCARD, S. L., LACAN, F., PAYTAN, A., WUTTIG, K. & PRODUCTIVITY, G. P. B. 2021. Bioactive Trace Metals and Their Isotopes as Paleoproductivity Proxies: An Assessment Using GEOTRACES-Era Data. *Global Biogeochemical Cycles,* 35.

HORNER, T. J., WILLIAMS, H. M., HEIN, J. R., SAITO, M. A., BURTON, K. W., HALLIDAY, A. N. & NIELSEN, S. G. 2015. Persistence of deeply sourced iron in the Pacific Ocean. *Proceedings of the National Academy of Sciences of the United States of America,* 112**,** 1292-1297.

HORTON, F. 2015. Did phosphorus derived from the weathering of large igneous provinces fertilize the Neoproterozoic ocean? *Geochemistry Geophysics Geosystems,* 16**,** 1723-1738.
HOSHINO, Y., POSHIBAEVA, A., MEREDITH, W., SNAPE, C., POSHIBAEV, V., VERSTEEGH, G. J. M., KUZNETSOV, N., LEIDER, A., VAN MALDEGEM, L., NEUMANN, M., NAEHER, S., MOCZYDLOWSKA, M., BROCKS, J. J., JARRETT, A. J. M., TANG, Q., XIAO, S., MCKIRDY, D., DAS, S. K., ALVARO, J. J., SANSJOFRE, P. & HALLMANN, C. 2017. Cryogenian evolution of stigmasteroid biosynthesis. *Science Advances,* 3.
HOWELL, E. A., DONEY, S. C., FINE, R. A. & OLSON, D. B. 1997. Geochemical estimates of denitrification in the Arabian Sea and the Bay of Bengal during WOCE. *Geophysical Research Letters,* 24**,** 2549-2552.
HUANG, K.-J., TENG, F.-Z., SHEN, B., XIAO, S., LANG, X., MA, H.-R., FU, Y. & PENG, Y. 2016. Episode of intense chemical weathering during the termination of the 635 Ma Marinoan glaciation. *Proceedings of the National Academy of Sciences,* 113**,** 14904-14909.
HUANG, Y., NICHOLSON, D., HUANG, B. & CASSAR, N. 2021. Global Estimates of Marine Gross Primary Production Based on Machine Learning Upscaling of Field Observations. *Global Biogeochemical Cycles,* 35.
HUSSON, J. M., HIGGINS, J. A., MALOOF, A. C. & SCHOENE, B. 2015. Ca and Mg isotope constraints on the origin of Earth's deepest $\delta^{13}C$ excursion. *Geochimica et Cosmochimica Acta,* 160**,** 243-266.
HÜLSE, D., LAU, K. V., VAN DE VELDE, S. J., ARNDT, S., MEYER, K. M. & RIDGWELL, A. 2021. End-Permian marine extinction due to temperature-driven nutrient recycling and euxinia. *Nature Geoscience,* 14**,** 862-867.
ISSON, T. T., LOVE, G. D., DUPONT, C. L., REINHARD, C. T., ZUMBERGE, A. J., ASAEL, D., GUEGUEN, B., MCCROW, J., GILL, B. C., OWENS, J., RAINBIRD, R. H., ROONEY, A. D., ZHAO, M.-Y., STUEEKEN, E. E., KONHAUSER, K. O., JOHN, S. G., LYONS, T. W. & PLANAVSKY, N. J. 2018. Tracking the rise of eukaryotes to ecological dominance with zinc isotopes. *Geobiology,* 16**,** 341-352.
JACCARD, S., GALBRAITH, E., FRÖLICHER, T. & GRUBER, N. 2014. Ocean (De)oxygenation Across the Last Deglaciation: Insights for the Future. *Oceanography,* 27**,** 26-35.
JACCARD, S. L. & GALBRAITH, E. D. 2011. Large climate-driven changes of oceanic oxygen concentrations during the last deglaciation. *Nature Geoscience,* 5**,** 151-156.
JACCARD, S. L., GALBRAITH, E. D., MARTINEZ-GARCIA, A. & ANDERSON, R. F. 2016. Covariation of deep Southern Ocean oxygenation and atmospheric CO_2 through the last ice age. *Nature,* 530**,** 207.
JACCARD, S. L., GALBRAITH, E. D., SIGMAN, D. M., HAUG, G. H., FRANCOIS, R., PEDERSEN, T. F., DULSKI, P. & THIERSTEIN, H. R. 2009. Subarctic Pacific evidence for a glacial deepening of the oceanic respired carbon pool. *Earth and Planetary Science Letters,* 277**,** 156-165.
JANSSEN, D. J., RICKLI, J., QUAY, P. D., WHITE, A. E., NASEMANN, P. & JACCARD, S. L. 2020. Biological Control of Chromium Redox and Stable Isotope Composition in the Surface Ocean. *Global Biogeochemical Cycles,* 34.
JENKINS, W. J., SMETHIE, W. M., JR., BOYLE, E. A. & CUTTER, G. A. 2015. Water mass analysis for the US GEOTRACES (GA03) North Atlantic sections. *Deep-Sea Research Part Ii-Topical Studies in Oceanography,* 116**,** 6-20.

JENKYNS, H. C. 1980. Cretaceous anoxic events: from continents to oceans. *Journal of the Geological Society,* 137**,** 171-188.
JENKYNS, H. C., DICKSON, A. J., RUHL, M. & VAN DEN BOORN, S. H. J. M. 2017. Basalt-seawater interaction, the Plenus Cold Event, enhanced weathering and geochemical change: deconstructing Oceanic Anoxic Event 2 (Cenomanian-Turonian, Late Cretaceous). *Sedimentology,* 64**,** 16-43.
JENKYNS, H. C., GALE, A. S. & CORFIELD, R. M. 1994. Carbon- and oxygen-isotope stratigraphy of the English Chalk and Italian Scaglia and its palaeoclimatic significance. *Geological Magazine,* 131**,** 1-34.
JIA-ZHONG, Z. & WHITFIELD, M. 1986. Kinetics of inorganic redox reactions in seawater: I. The reduction of iodate by bisulphide. *Marine Chemistry,* 19**,** 121-137.
JOHNSON, A. C., OSTRANDER, C. M., ROMANIELLO, S. J., REINHARD, C. T., GREANEY, A. T., LYONS, T. W. & ANBAR, A. D. 2021. Reconciling evidence of oxidative weathering and atmospheric anoxia on Archean Earth. *Science Advances,* 7.
JOHNSON, A. C., ROMANIELLO, S. J., REINHARD, C. T., GREGORY, D. D., GARCIA-ROBLEDO, E., REVSBECH, N. P., CANFIELD, D. E., LYONS, T. W. & ANBAR, A. D. 2019. Experimental determination of pyrite and molybdenite oxidation kinetics at nanomolar oxygen concentrations. *Geochimica Et Cosmochimica Acta,* 249**,** 160-172.
JOHNSON, B. W., POULTON, S. W. & GOLDBLATT, C. 2017. Marine oxygen production and open water supported an active nitrogen cycle during the Marinoan Snowball Earth. *Nature Communications,* 8.
JOHNSON, J. E., GERPHEIDE, A., LAMB, M. P. & FISCHER, W. W. 2014. O_2 constraints from Paleoproterozoic detrital pyrite and uraninite. *Geological Society of America Bulletin,* 126**,** 813-830.
JOHNSTON, D. T., POULTON, S. W., GOLDBERG, T., SERGEEV, V. N., PODKOVYROV, V., VOROB'EVA, N. G., BEKKER, A. & KNOLL, A. H. 2012. Late Ediacaran redox stability and metazoan evolution. *Earth and Planetary Science Letters,* 335-336**,** 25-35.
JOHNSTON, D. T., POULTON, S. W., TOSCA, N. J., O'BRIEN, T., HALVERSON, G. P., SCHRAG, D. P. & MACDONALD, F. A. 2013. Searching for an oxygenation event in the fossiliferous Ediacaran of northwestern Canada. *Chemical Geology,* 362**,** 273-286.
JORGENSEN, B. B. 1977. Bacterial sulfate reduction within reduced microfiches of oxidized marine sediments. *Marine Biology,* 41**,** 7-17.
JOST, A. B., BACHAN, A., VAN DE SCHOOTBRUGGE, B., LAU, K. V., WEAVER, K. L., MAHER, K. & PAYNE, J. L. 2017. Uranium isotope evidence for an expansion of marine anoxia during the end-Triassic extinction. *Geochemistry, Geophysics, Geosystems,* 18**,** 3093-3108.
KADOYA, S., CATLING, D. C., NICKLAS, R. W., PUCHTEL, I. S. & ANBAR, A. D. 2020. Mantle cooling causes more reducing volcanic gases and gradual reduction of the atmosphere. *Geochemical Perspectives Letters,* 13**,** 25-29.
KAH, L. C., LYONS, T. W. & FRANK, T. D. 2004. Low marine sulphate and protracted oxygenation of the proterozoic biosphere. *Nature,* 431**,** 834-838.
KALVELAGE, T., LAVIK, G., JENSEN, M. M., REVSBECH, N. P., LOESCHER, C., SCHUNCK, H., DESAI, D. K., HAUSS, H., KIKO, R., HOLTAPPELS, M., LAROCHE, J., SCHMITZ, R. A., GRACO, M. I. & KUYPERS, M. M. M. 2015. Aerobic microbial respiration In oceanic oxygen minimum zones. *Plos One,* 10.

KARHU, J. A. & HOLLAND, H. D. 1996. Carbon isotopes and the rise of atmospheric oxygen. *Geology,* 24**,** 867-870.
KARSTENSEN, J., STRAMMA, L. & VISBECK, M. 2008. Oxygen minimum zones in the eastern tropical Atlantic and Pacific oceans. *Progress in Oceanography,* 77**,** 331-350.
KASEMANN, S. A., POGGE VON STRANDMANN, P. A. E., PRAVE, A. R., FALLICK, A. E., ELLIOTT, T. & HOFFMANN, K.-H. 2014. Continental weathering following a Cryogenian glaciation: Evidence from calcium and magnesium isotopes. *Earth and Planetary Science Letters,* 396**,** 66-77.
KASTING, J. 1992. Models relating to Proterozoic atmospheric and ocean chemistry. *The Proterozoic Biosphere: A Multidisciplinary Study***,** 1185-1187.
KASTING, J. F., EGGLER, D. H. & RAEBURN, S. P. 1993. Mantle Redox Evolution and the Oxidation State of the Archean Atmosphere. *The Journal of Geology,* 101**,** 245-257.
KAUFMAN, A. J., JOHNSTON, D. T., FARQUHAR, J., MASTERSON, A. L., LYONS, T. W., BATES, S., ANBAR, A. D., ARNOLD, G. L., GARVIN, J. & BUICK, R. 2007. Late Archean biospheric oxygenation and atmospheric evolution. *Science,* 317**,** 1900-1903.
KEELING, R. & MANNING, A. 2014. Studies of recent changes in atmospheric O2 content. *Treatise on Geochemistry: Second Edition.*
KEELING, R. F., KOERTZINGER, A. & GRUBER, N. 2010. Ocean Deoxygenation in a Warming World. *Annual Review of Marine Science.*
KEELING, R. F., NAJJAR, R. P., BENDER, M. L. & TANS, P. P. 1993. What atmospheric oxygen measurements can tell us about the global carbon cycle. *Global Biogeochemical Cycles,* 7**,** 37-67.
KENDALL, B., BRENNECKA, G. A., WEYER, S. & ANBAR, A. D. 2013. Uranium isotope fractionation suggests oxidative uranium mobilization at 2.50 Ga. *Chemical Geology,* 362**,** 105-114.
KIRSCHIVINK, J. L. 1992. Late Proterozoic Low-Latitude Global Glaciation: the Snowball Earth. *In:* SCHOPF, J. W. & KLEIN, C. (eds.) *The Proterozoic Biosphere.* New York: Cambridge University Press.
KNAUTH, L. P. & KENNEDY, M. J. 2009. The late Precambrian greening of the Earth. *Nature,* 460**,** 728-732.
KNOLL, A. H. 2003. Biomineralization and Evolutionary History. *Reviews in Mineralogy and Geochemistry,* 54**,** 329-356.
KNOLL, A. H. & CARROLL, S. B. 1999. Early Animal Evolution: Emerging Views from Comparative Biology and Geology. *Science,* 284**,** 2129-2137.
KOEHLER, M. C., BUICK, R., KIPP, M. A., STUEKEN, E. E. & ZALOUMIS, J. 2018. Transient surface ocean oxygenation recorded in the similar to 2.66-Ga Jeerinah Formation, Australia. *Proceedings of the National Academy of Sciences of the United States of America,* 115**,** 7711-7716.
KOHFELD, K. E., QUÉRÉ, C. L., HARRISON, S. P. & ANDERSON, R. F. 2005. Role of Marine Biology in Glacial-Interglacial CO_2 Cycles. *Science,* 308**,** 74-78.
KRAFT, B., JEHMLICH, N., LARSEN, M., BRISTOW, L. A., KONNEKE, M., THAMDRUP, B. & CANFIELD, D. E. 2022. Oxygen and nitrogen production by an ammonia-oxidizing archaeon. *Science,* 375**,** 97.

KRISSANSEN-TOTTON, J., BUICK, R. & CATLING, D. C. 2015. A statistical analysis of the carbon isotope record from the Archean to Phanerozoic and implications for the rise of oxygen. *American Journal of Science,* 315**,** 275-316.

KRISSANSEN-TOTTON, J. & CATLING, D. C. 2017. Constraining climate sensitivity and continental versus seafloor weathering using an inverse geological carbon cycle model. *Nature Communications,* 8.

KUMP, L. R. & ARTHUR, M. A. 1999. Interpreting carbon-isotope excursions: carbonates and organic matter. *Chemical Geology,* 161**,** 181-198.

KUMP, L. R. & BARLEY, M. E. 2007. Increased subaerial volcanism and the rise of atmospheric oxygen 2.5 billion years ago. *Nature,* 448**,** 1033-1036.

KVENVOLDEN, K. A. & ROGERS, B. W. 2005. Gaia's breath - global methane exhalations. *Marine and Petroleum Geology,* 22**,** 579-590.

KWIATKOWSKI, L., TORRES, O., BOPP, L., AUMONT, O., CHAMBERLAIN, M., CHRISTIAN, J. R., DUNNE, J. P., GEHLEN, M., ILYINA, T., JOHN, J. G., LENTON, A., LI, H., LOVENDUSKI, N. S., ORR, J. C., PALMIERI, J., SANTANA-FALCON, Y., SCHWINGER, J., SEFERIAN, R., STOCK, C. A., TAGLIABUE, A., TAKANO, Y., TJIPUTRA, J., TOYAMA, K., TSUJINO, H., WATANABE, M., YAMAMOTO, A., YOOL, A. & ZIEHN, T. 2020. Twenty-first century ocean warming, acidification, deoxygenation, and upper-ocean nutrient and primary production decline from CMIP6 model projections. *Biogeosciences,* 17**,** 3439-3470.

LALONDE, S. V. & KONHAUSER, K. O. 2015. Benthic perspective on Earth's oldest evidence for oxygenic photosynthesis. *Proceedings of the National Academy of Sciences of the United States of America,* 112**,** 995-1000.

LAM, P. J., HELLER, M. I., LERNER, P. E., MOFFETT, J. W. & BUCK, K. N. 2020. Unexpected Source and Transport of Iron from the Deep Peru Margin. *Acs Earth and Space Chemistry,* 4**,** 977-992.

LANDING, W. M. & BRULAND, K. W. 1987. The contrasting biogeochemistry of iron and manganese in the Pacific Ocean. *Geochimica et Cosmochimica Acta,* 51**,** 29-43.

LARSEN, M., LEHNER, P., BORISOV, S. M., KLIMANT, I., FISCHER, J. P., STEWART, F. J., CANFIELD, D. E. & GLUD, R. N. 2016. In situ quantification of ultra-low O-2 concentrations in oxygen minimum zones: Application of novel optodes. *Limnology and Oceanography-Methods,* 14**,** 784-800.

LAU, K. V. & HARDISTY, D. S. 2022. Modeling the impacts of diagenesis on carbonate paleoredox proxies. *Geochimica Et Cosmochimica Acta,* 337**,** 123-139.

LAU, K. V., LYONS, T. W. & MAHER, K. 2020. Uranium reduction and isotopic fractionation in reducing sediments: Insights from reactive transport modeling. *Geochimica et Cosmochimica Acta,* 287**,** 65-92.

LAU, K. V., MACDONALD, F. A., MAHER, K. & PAYNE, J. L. 2017a. Uranium isotope evidence for temporary ocean oxygenation in the aftermath of the Sturtian Snowball Earth. *Earth and Planetary Science Letters,* 458**,** 282-292.

LAU, K. V., MAHER, K., ALTINER, D., KELLEY, B. M., KUMP, L. R., LEHRMANN, D. J., SILVA-TAMAYO, J. C., WEAVER, K. L., YU, M. Y. & PAYNE, J. L. 2016. Marine anoxia and delayed Earth system recovery after the end-Permian extinction. *Proceedings of the National Academy of Sciences of the United States of America,* 113**,** 2360-2365.

LAU, K. V., MAHER, K., BROWN, S. T., JOST, A. B., ALTINER, D., DEPAOLO, D. J., EISENHAUER, A., KELLEY, B. M., LEHRMANN, D. J., PAYTAN, A., YU, M., SILVA-TAMAYO, J. C. & PAYNE, J. L. 2017b. The influence of seawater carbonate chemistry, mineralogy, and diagenesis on calcium isotope variations in Lower-Middle Triassic carbonate rocks. *Chemical Geology,* 471**,** 13-37.

LAU, K. V., ROMANIELLO, S. J. & ZHANG, F. 2019. *The uranium isotope paleoredox proxy*, Cambridge University Press.

LAVIK, G., STÜHRMANN, T., BRÜCHERT, V., VAN DER PLAS, A., MOHRHOLZ, V., LAM, P., MUßMANN, M., FUCHS, B. M., AMANN, R. & LASS, U. 2009. Detoxification of sulphidic African shelf waters by blooming chemolithotrophs. *Nature,* 457**,** 581-584.

LE HIR, G., DONNADIEU, Y., GODDÉRIS, Y., PIERREHUMBERT, R. T., HALVERSON, G. P., MACOUIN, M., NÉDÉLEC, A. & RAMSTEIN, G. 2009. The snowball Earth aftermath: Exploring the limits of continental weathering processes. *Earth and Planetary Science Letters,* 277**,** 453-463.

LE ROY, E., SANIAL, V., CHARETTE, M. A., VAN BEEK, P., LACAN, F., JACQUET, S. H. M., HENDERSON, P. B., SOUHAUT, M., GARCIA-IBANEZ, M. I., JEANDEL, C., PEREZ, F. F. & SARTHOU, G. 2018. The Ra-226-Ba relationship in the North Atlantic during GEOTRACES-GA01. *Biogeosciences,* 15**,** 3027-3048.

LEARMAN, D. R., VOELKER, B. M., VAZQUEZ-RODRIGUEZ, A. I. & HANSEL, C. M. 2011. Formation of manganese oxides by bacterially generated superoxide. *Nature Geoscience,* 4**,** 95-98.

LECHTE, M. A., WALLACE, M. W., HOOD, A. V. S., LI, W., JIANG, G., HALVERSON, G. P., ASAEL, D., MCCOLL, S. L. & PLANAVSKY, N. J. 2019. Subglacial meltwater supported aerobic marine habitats during Snowball Earth. *Proceedings of the National Academy of Sciences,* 116**,** 25478-25483.

LECKIE, R. M., BRALOWER, T. J. & CASHMAN, R. 2002. Oceanic anoxic events and plankton evolution: Biotic response to tectonic forcing during the mid-Cretaceous. *Paleoceanography,* 17**,** 13-1-13-29.

LENTON, T. M., DAHL, T. W., DAINES, S. J., MILLS, B. J. W., OZAKI, K., SALTZMAN, M. R. & PORADA, P. 2016. Earliest land plants created modern levels of atmospheric oxygen. *Proceedings of the National Academy of Sciences of the United States of America,* 113**,** 9704-9709.

LENTON, T. M. & DAINES, S. J. 2018. The effects of marine eukaryote evolution on phosphorus, carbon and oxygen cycling across the Proterozoic–Phanerozoic transition. *Emerging Topics in Life Sciences,* 2**,** 267-278.

LENTON, T. M., DAINES, S. J. & MILLS, B. J. 2018. COPSE reloaded: An improved model of biogeochemical cycling over Phanerozoic time. *Earth-Science Reviews,* 178**,** 1-28.

LEONG, J. A. M., ELY, T. & SHOCK, E. L. 2021. Decreasing extents of Archean serpentinization contributed to the rise of an oxidized atmosphere. *Nature Communications,* 12.

LI, C., HARDISTY, D. S., LUO, G., HUANG, J., ALGEO, T. J., CHENG, M., SHI, W., AN, Z., TONG, J. & XIE, S. 2017. Uncovering the spatial heterogeneity of Ediacaran carbon cycling. *Geobiology,* 15**,** 211-224.

LI, H.-P., DANIEL, B., CREELEY, D., GRANDBOIS, R., ZHANG, S., XU, C., HO, Y.-F., SCHWEHR, K. A., KAPLAN, D. I. & SANTSCHI, P. H. 2014. Superoxide production by a manganese-oxidizing

bacterium facilitates iodide oxidation. *Applied and environmental microbiology,* 80**,** 2693-2699.
LI, Z. Y., ZHANG, Y. G., TORRES, M. & MILLS, B. J. W. 2023. Neogene burial of organic carbon in the global ocean. *Nature,* 613**,** 90-+.
LISIECKI, L. E. & STERN, J. V. 2016. Regional and global benthic δ<sup>18<sup>O stacks for the last glacial cycle. *Paleoceanography,* 31**,** 1368-1394.
LIU, T., KRISCH, S., XIE, R. C., HOPWOOD, M. J., DENGLER, M. & ACHTERBERG, E. P. 2022. Sediment Release in the Benguela Upwelling System Dominates Trace Metal Input to the Shelf and Eastern South Atlantic Ocean. *Global Biogeochemical Cycles,* 36.
LIU, X.-M., HARDISTY, D. S., LYONS, T. W. & SWART, P. K. 2019. Evaluating the fidelity of the cerium paleoredox tracer during variable carbonate diagenesis on the Great Bahamas Bank. *Geochimica Et Cosmochimica Acta,* 248**,** 25-42.
LOVENDUSKI, N. S., GRUBER, N. & DONEY, S. C. 2008. Toward a mechanistic understanding of the decadal trends in the Southern Ocean carbon sink. *Global Biogeochemical Cycles,* 22.
LOWENSTEIN, T. K., HARDIE, L. A., TIMOFEEFF, M. N. & DEMICCO, R. V. 2003. Secular variation in seawater chemistry and the origin of calcium chloride basinal brines. *Geology,* 31**,** 857-860.
LOWENSTEIN, T. K., KENDALL, B. & ANBAR, A. 2013. The geologic history of seawater. *The Oceans and Marine Geochemistry.* Elsevier Inc.
LOYD, S. J., MARENCO, P. J., HAGADORN, J. W., LYONS, T. W., KAUFMAN, A. J., SOUR-TOVAR, F. & CORSETTI, F. A. 2012. Sustained low marine sulfate concentrations from the Neoproterozoic to the Cambrian: Insights from carbonates of northwestern Mexico and eastern California. *Earth and Planetary Science Letters,* 339-340**,** 79-94.
LU, W., RICKABY, R. E. M., HOOGAKKER, B. A. A., RATHBURN, A. E., BURKETT, A. M., DICKSON, A. J., MARTINEZ-MENDEZ, G., HILLENBRAND, C.-D., ZHOU, X., THOMAS, E. & LU, Z. 2020a. I/Ca in epifaunal benthic foraminifera: A semi-quantitative proxy for bottom water oxygen in a multi-proxy compilation for glacial ocean deoxygenation. *Earth and Planetary Science Letters,* 533.
LU, W., RIDGWELL, A., THOMAS, E., HARDISTY, D. S., LUO, G., ALGEO, T.J., SALTZMAN, M. R., GILL, B. C., SHEN, Y., LING, H. F., EDWARDS, C. T., WHALEN, M. T., ZHOU, X., GUTCHESS, K. M., JIN, L., RICKABY, R. E. M., JENKYNS, H. C., LYONS, T. W., LENTON, T. M., KUMP, L. R. & LU, Z. 2018. Late inception of a resiliently oxygenated upper ocean. *Science,* in press.
LU, W., WANG, Y., OPPO, D. W., NIELSEN, S. G. & COSTA, K. M. 2022. Comparing paleo-oxygenation proxies (benthic foraminiferal surface porosity, I/Ca, authigenic uranium) on modern sediments and the glacial Arabian Sea. *Geochimica Et Cosmochimica Acta,* 331**,** 69-85.
LU, Z., HOOGAKKER, B. A. A., HILLENBRAND, C.-D., ZHOU, X., THOMAS, E., GUTCHESS, K. M., LU, W., JONES, L. & RICKABY, R. E. M. 2016. Oxygen depletion recorded in upper waters of the glacial Southern Ocean. *Nature Communications,* 7.
LU, Z., LU, W., RICKABY, R. E. & THOMAS, E. 2020b. *Earth History of Oxygen and the iprOxy*, Cambridge University Press.
LUO, G., ONO, S., BEUKES, N. J., WANG, D. T., XIE, S. & SUMMONS, R. E. 2016. Rapid oxygenation of Earth's atmosphere 2.33 billion years ago. *Science Advances,* 2.

LUYTEN, J. R., PEDLOSKY, J. & STOMMEL, H. 1983. THE VENTILATED THERMOCLINE. *Journal of Physical Oceanography,* 13**,** 292-309.
LYONS, T. W., REINHARD, C. T. & PLANAVSKY, N. J. 2014. The rise of oxygen in Earth/'s early ocean and atmosphere. *Nature,* 506**,** 307-315.
LÜTHI, D., LE FLOCH, M., BEREITER, B., BLUNIER, T., BARNOLA, J.-M., SIEGENTHALER, U., RAYNAUD, D., JOUZEL, J., FISCHER, H., KAWAMURA, K. & STOCKER, T. F. 2008. High-resolution carbon dioxide concentration record 650,000–800,000 years before present. *Nature,* 453**,** 379-382.
MACDONALD, F. A., JONES, D. S. & SCHRAG, D. P. 2009. Stratigraphic and tectonic implications of a newly discovered glacial diamictite–cap carbonate couplet in southwestern Mongolia. *Geology,* 37**,** 123-126.
MACDONALD, F. A., STRAUSS, J. V., SPERLING, E. A., HALVERSON, G. P., NARBONNE, G. M., JOHNSTON, D. T., KUNZMANN, M., SCHRAG, D. P. & HIGGINS, J. A. 2013. The stratigraphic relationship between the Shuram carbon isotope excursion, the oxygenation of Neoproterozoic oceans, and the first appearance of the Ediacara biota and bilaterian trace fossils in northwestern Canada. *Chemical Geology,* 362**,** 250-272.
MACDONALD, F. A. & WORDSWORTH, R. 2017. Initiation of Snowball Earth with volcanic sulfur aerosol emissions. *Geophysical Research Letters*.
MARCHI, S., DRABON, N., SCHULZ, T., SCHAEFER, L., NESVORNY, D., BOTTKE, W. F., KOEBERL, C. & LYONS, T. 2021. Delayed and variable late Archaean atmospheric oxidation due to high collision rates on Earth. *Nature Geoscience,* 14**,** 827.
MARGOLSKEE, A., FRENZEL, H., EMERSON, S. & DEUTSCH, C. 2019. Ventilation Pathways for the North Pacific Oxygen Deficient Zone. *Global Biogeochemical Cycles,* 33**,** 875-890.
MARTIN, J. H., COALE, K. H., JOHNSON, K. S., FITZWATER, S. E., GORDON, R. M., TANNER, S. J., HUNTER, C. N., ELROD, V. A., NOWICKI, J. L., COLEY, T. L., BARBER, R. T., LINDLEY, S., WATSON, A. J., VAN SCOY, K., LAW, C. S., LIDDICOAT, M. I., LING, R., STANTON, T., STOCKEL, J., COLLINS, C., ANDERSON, A., BIDIGARE, R., ONDRUSEK, M., LATASA, M., MILLERO, F. J., LEE, K., YAO, W., ZHANG, J. Z., FRIEDERICH, G., SAKAMOTO, C., CHAVEZ, F., BUCK, K., KOLBER, Z., GREENE, R., FALKOWSKI, P., CHISHOLM, S. W., HOGE, F., SWIFT, R., YUNGEL, J., TURNER, S., NIGHTINGALE, P., HATTON, A., LISS, P. & TINDALE, N. W. 1994. Testing the iron hypothesis in ecosystems of the equatorial Pacific Ocean. *Nature,* 371**,** 123-129.
MARTIN, J. H. & KNAUER, G. A. 1973. Elemental composition of plankton. *Geochimica Et Cosmochimica Acta,* 37**,** 1639-1653.
MATEAR, R. J. & HIRST, A. C. 2003. Long-term changes in dissolved oxygen concentrations in the ocean caused by protracted global warming. *Global Biogeochemical Cycles,* 17.
MATSUMOTO, K. 2007. Biology-mediated temperature control on atmospheric pCO₂ and ocean biogeochemistry. *Geophysical Research Letters,* 34.
MELIM, L. A., SWART, P. K. & MALIVA, R. G. 1995. Meteoric-like fabrics forming in marine waters: implications for the use of petrography to identify diagenetic environments. *Geology,* 23**,** 755-758.
MENG, X., SIMON, A. C., KLEINSASSER, J. M., MOLE, D. R., KONTAK, D. J., JUGO, P. J., MAO, J. & RICHARDS, J. P. 2022. Formation of oxidized sulfur-rich magmas in Neoarchaean subduction zones. *Nature Geoscience,* 15**,** 1064-+.

MENTEL, M., ROETTGER, M., LEYS, S., TIELENS, A. G. M. & MARTIN, W. F. 2014. Of early animals, anaerobic mitochondria, and a modern sponge. *Bioessays,* 36**,** 924-932.
METE, Ö., SUBHAS, A., KIM, H., DUNLEA, A., WHITMORE, L., SHILLER, A., GILBERT, M., LEAVITT, W. & HORNER, T. 2023. Barium in seawater: Dissolved distribution, relationship to silicon, and barite saturation state determined using machine learning. *Earth System Science Data Discussions,* 2023**,** 1-42.
MEYER, K. M., RIDGWELL, A. & PAYNE, J. L. 2016. The influence of the biological pump on ocean chemistry: implications for long-term trends in marine redox chemistry, the global carbon cycle, and marine animal ecosystems. *Geobiology,* 14**,** 207-219.
MEYER, K. M., YU, M., JOST, A. B., KELLEY, B. M. & PAYNE, J. L. 2011. $\delta^{13}C$ evidence that high primary productivity delayed recovery from end-Permian mass extinction. *Earth and Planetary Science Letters,* 302**,** 378-384.
MILLER, C. A., PEUCKER-EHRENBRINK, B., WALKER, B. D. & MARCANTONIO, F. 2011. Re-assessing the surface cycling of molybdenum and rhenium. *Geochimica et Cosmochimica Acta,* 75**,** 7146-7179.
MILLS, D. B., BOYLE, R. A., DAINES, S. J., SPERLING, E. A., PISANI, D., DONOGHU, I. C. J. & LENTON, T. M. 2022. Eukaryogenesis and oxygen in Earth history. *Nature Ecology & Evolution,* 6**,** 520-532.
MILLS, D. B., WARD, L. M., JONES, C., SWEETEN, B., FORTH, M., TREUSCH, A. H. & CANFIELD, D. E. 2014. Oxygen requirements of the earliest animals. *Proceedings of the National Academy of Sciences,* 111**,** 4168-4172.
MOFFETT, J. W. & GERMAN, C. R. 2020. Distribution of iron in the Western Indian Ocean and the Eastern tropical South pacific: An inter-basin comparison. *Chemical Geology,* 532.
MOFFETT, J. W., GOEFFERT, T. J. & NAQVI, S. W. A. 2007. Reduced iron associated with secondary nitrite maxima in the Arabian Sea. *Deep-Sea Research Part I-Oceanographic Research Papers,* 54**,** 1341-1349.
MOFFITT, S. E., MOFFITT, R. A., SAUTHOFF, W., DAVIS, C. V., HEWETT, K. & HILL, T. M. 2015. Paleoceanographic Insights on Recent Oxygen Minimum Zone Expansion: Lessons for Modern Oceanography. *Plos One,* 10.
MOLLENHAUER, G., SCHNEIDER, R. R., MULLER, P. J., SPIESS, V. & WEFER, G. 2002. Glacial/interglacial variablity in the Benguela upwelling system: Spatial distribution and budgets of organic carbon accumulation. *Global Biogeochemical Cycles,* 16.
MONNIN, E., INDERMUHLE, A., DALLENBACH, A., FLUCKIGER, J., STAUFFER, B., STOCKER, T. F., REYNAUD, D. & BARNOLA, J.-M. 2001. Atmospheric CO_2 Concentrations over the Last Glacial Termination. *Science,* 291**,** 112-114.
MONTES, I., DEWITTE, B., GUTKNECHT, E., PAULMIER, A., DADOU, I., OSCHLIES, A. & GARCON, V. 2014. High-resolution modeling of the Eastern Tropical Pacific oxygen minimum zone: Sensitivity to the tropical oceanic circulation. *Journal of Geophysical Research-Oceans,* 119**,** 5515-5532.
MORIYASU, R., EVANS, Z. C., BOLSTER, K. M., HARDISTY, D. S. & MOFFETT, J. W. 2020. The Distribution and Redox Speciation of Iodine in the Eastern Tropical North Pacific Ocean. Global Biogeochemical Cycles.
MUELLER, M., MENTEL, M., VAN HELLEMOND, J. J., HENZE, K., WOEHLE, C., GOULD, S. B., YU, R.-Y., VAN DER GIEZEN, M., TIELENS, A. G. M. & MARTIN, W. F. 2012. Biochemistry and

Evolution of Anaerobic Energy Metabolism in Eukaryotes. *Microbiology and Molecular Biology Reviews,* 76**,** 444-495.
MURRAY, S. T., HIGGINS, J. A., HOLMDEN, C., LU, C. J. & SWART, P. K. 2021. Geochemical fingerprints of dolomitization in Bahamian carbonates: Evidence from sulphur, calcium, magnesium and clumped isotopes. *Sedimentology,* 68**,** 1-29.
MÄND, K., PLANAVSKY, N. J., PORTER, S. M., ROBBINS, L. J., WANG, C., KREITSMANN, T., PAISTE, K., PAISTE, P., ROMASHKIN, A. E., DEINES, Y. E., KIRSIMÄE, K., LEPLAND, A. & KONHAUSER, K. O. 2022. Chromium evidence for protracted oxygenation during the Paleoproterozoic. *Earth and Planetary Science Letters,* 584**,** 117501.
NAJJAR, R. G. & KEELING, R. F. 2000. Mean annual cycle of the air-sea oxygen flux: A global view. *Global Biogeochemical Cycles,* 14**,** 573-584.
NANA YOBO, L., HOLMDEN, C., BRANDON, A. D., LAU, K. V., ELDRETT, J. S. & BERGMAN, S. 2022. LIP volcanism (not anoxia) tracked by Cr isotopes during Ocean Anoxic Event 2 in the proto-North Atlantic region. *Geochimica et Cosmochimica Acta,* 332**,** 138-155.
NIELSEN, S. G. 2020. *Vanadium Isotopes: A Proxy for Ocean Oxygen Variations*, Cambridge University Press.
NOBLE, A. E., LAMBORG, C. H., OHNEMUS, D. C., LAM, P. J., GOEPFERT, T. J., MEASURES, C. I., FRAME, C. H., CASCIOTTI, K. L., DITULLIO, G. R., JENNINGS, J. & SAITO, M. A. 2012. Basin-scale inputs of cobalt, iron, and manganese from the Benguela-Angola front to the South Atlantic Ocean. *Limnology and Oceanography,* 57**,** 989-1010.
NOFFKE, A., HENSEN, C., SOMMER, S., SCHOLZ, F., BOHLEN, L., MOSCH, T., GRACO, M. & WALLMANN, K. 2012. Benthic iron and phosphorus fluxes across the Peruvian oxygen minimum zone. *Limnology and Oceanography,* 57**,** 851-867.
OEHLERT, A. M. & SWART, P. K. 2014. Interpreting carbonate and organic carbon isotope covariance in the sedimentary record. *Nature Communications,* 5**,** 1-7.
OHDE, T. & DADOU, I. 2018. Seasonal and annual variability of coastal sulphur plumes in the northern Benguela upwelling system. *Plos One,* 13.
OLSON, S. L., KUMP, L. R. & KASTING, J. F. 2013. Quantifying the areal extent and dissolved oxygen concentrations of Archean oxygen oases. *Chemical Geology,* 362**,** 35-43.
OSBURN, M. R., OWENS, J., BERGMANN, K. D., LYONS, T. W. & GROTZINGER, J. P. 2015. Dynamic changes in sulfate sulfur isotopes preceding the Ediacaran Shuram Excursion. *Geochimica et Cosmochimica Acta,* 170**,** 204-224.
OSCHLIES, A., BRANDT, P., STRAMMA, L. & SCHMIDTKO, S. 2018. Drivers and mechanisms of ocean deoxygenation. *Nature Geoscience,* 11**,** 467-473.
OSMAN, M. B., TIERNEY, J. E., ZHU, J., TARDIF, R., HAKIM, G. J., KING, J. & POULSEN, C. J. 2021. Globally resolved surface temperatures since the Last Glacial Maximum. *Nature,* 599**,** 239-244.
OSSA, F. O., HOFMANN, A., WILLE, M., SPANGENBERG, J. E., BEKKER, A., POULTON, S. W., EICKMANN, B. & SCHOENBERG, R. 2018. Aerobic iron and manganese cycling in a redox-stratified Mesoarchean epicontinental sea. *Earth and Planetary Science Letters,* 500**,** 28-40.
OSTRANDER, C. M. 2023. Mulling and nulling the coeval rise of Ediacaran oxygen and animals. *Earth and Planetary Science Letters,* 614.

OSTRANDER, C. M., NIELSEN, S. G., OWENS, J. D., KENDALL, B., GORDON, G. W., ROMANIELLO, S. J. & ANBAR, A. D. 2019. Fully oxygenated water columns over continental shelves before the Great Oxidation Event. *Nature Geoscience,* 12**,** 186.

OSTRANDER, C. M., OWENS, J. D. & NIELSEN, S. G. 2017. Constraining the rate of oceanic deoxygenation leading up to a Cretaceous Oceanic Anoxic Event (OAE-2: ~94 Ma). *Science Advances,* 3**,** e1701020.

OWENS, J. D., LYONS, T. W., HARDISTY, D. S., LOWERY, C. M., LU, Z., LEE, B. & JENKYNS, H. C. 2017. Patterns of local and global redox variability during the Cenomanian–Turonian Boundary Event (Oceanic Anoxic Event 2) recorded in carbonates and shales from central Italy. *Sedimentology***,** 168-185.

OZAKI, K., COLE, D. B., REINHARD, C. T. & TAJIKA, E. 2022. CANOPS-GRB v1.0: a new Earth system model for simulating the evolution of ocean-atmosphere chemistry over geologic timescales. *Geoscientific Model Development,* 15**,** 7593-7639.

OZAKI, K. & REINHARD, C. T. 2021. The future lifespan of Earth's oxygenated atmosphere. *Nature Geoscience,* 14**,** 138.

OZAKI, K. & TAJIKA, E. 2013. Biogeochemical effects of atmospheric oxygen concentration, phosphorus weathering, and sea-level stand on oceanic redox chemistry: Implications for greenhouse climates. *Earth and Planetary Science Letters,* 373**,** 129-139.

OZAKI, K., THOMPSON, K. J., SIMISTER, R. L., CROWE, S. A. & REINHARD, C. T. 2019. Anoxygenic photosynthesis and the delayed oxygenation of Earth's atmosphere. *Nature Communications,* 10.

PADILLA, C. C., BRISTOW, L. A., SARODE, N., GARCIA-ROBLEDO, E., GOMEZ RAMIREZ, E., BENSON, C. R., BOURBONNAIS, A., ALTABET, M. A., GIRGUIS, P. R., THAMDRUP, B. & STEWART, F. J. 2016. NC10 bacteria in marine oxygen minimum zones. *Isme Journal,* 10**,** 2067-2071.

PALEVSKY, H. I. & NICHOLSON, D. P. 2018. The North Atlantic Biological Pump: Insights from the ocean observatories initiative Irminger Sea array. *Oceanography,* 31**,** 42-49.

PARFREY, L. W., LAHR, D. J. G., KNOLL, A. H. & KATZ, L. A. 2011. Estimating the timing of early eukaryotic diversification with multigene molecular clocks. *Proceedings of the National Academy of Sciences of the United States of America,* 108**,** 13624-13629.

PARTIN, C. A., BEKKER, A., PLANAVSKY, N. J., SCOTT, C. T., GILL, B. C., LI, C., PODKOVYROV, V., MASLOV, A., KONHAUSER, K. O., LALONDE, S. V., LOVE, G. D., POULTON, S. W. & LYONS, T. W. 2013. Large-scale fluctuations in Precambrian atmospheric and oceanic oxygen levels from the record of U in shales. *Earth and Planetary Science Letters,* 369-370**,** 284-293.

PASQUIER, V., FIKE, D. A., REVILLON, S. & HALEVY, I. 2022. A global reassessment of the controls on iron speciation in modern sediments and sedimentary rocks: A dominant role for diagenesis. *Geochimica Et Cosmochimica Acta,* 335**,** 211-230.

PAULMIER, A. & RUIZ-PINO, D. 2009. Oxygen minimum zones (OMZs) in the modern ocean. *Progress in Oceanography,* 80**,** 113-128.

PAVLOV, A. A., KASTING, J. F., BROWN, L. L., RAGES, K. A. & FREEDMAN, R. 2000. Greenhouse warming by CH4 in the atmosphere of early Earth. *Journal of Geophysical Research: Planets,* 105**,** 11981-11990.

PAYNE, J. L., MCCLAIN, C. R., BOYER, A. G., BROWN, J. H., FINNEGAN, S., KOWALEWSKI, M., KRAUSE, R. A., LYONS, S. K., MCSHEA, D. W., NOVACK-GOTTSHALL, P. M., SMITH, F. A., SPAETH, P., STEMPIEN, J. A. & WANG, S. C. 2011. The evolutionary consequences of oxygenic photosynthesis: a body size perspective. *Photosynthesis Research,* 107**,** 37-57.

PENN, J., WEBER, T. & DEUTSCH, C. 2016. Microbial functional diversity alters the structure and sensitivity of oxygen deficient zones. *Geophysical Research Letters,* 43**,** 9773-9780.

PENN, J. L., DEUTSCH, C., PAYNE, J. L. & SPERLING, E. A. 2018. Temperature-dependent hypoxia explains biogeography and severity of end-Permian marine mass extinction. *Science,* 362**,** 1-6.

PETERS, B. D., JENKINS, W. J., SWIFT, J. H., GERMAN, C. R., MOFFETT, J. W., CUTTER, G. A., BRZEZINSKI, M. A. & CASCIOTTI, K. L. 2018. Water mass analysis of the 2013 US GEOTRACES eastern Pacific zonal transect (GP16). *Marine Chemistry,* 201**,** 6-19.

PETERS-KOTTIG, W., STRAUSS, H. & KERP, H. 2006. The land plant δ¹³C record and plant evolution in the Late Palaeozoic. *Palaeogeography, Palaeoclimatology, Palaeoecology,* 240**,** 237-252.

PETIT, J. R., JOUZEL, J., RAYNAUD, D., BARKOV, N. I., BARNOLA, J. M., BASILE, I., BENDER, M., CHAPPELLAZ, J., DAVIS, M., DELAYGUE, G., DELMOTTE, M., KOTLYAKOV, V. M., LEGRAND, M., LIPENKOV, V. Y., LORIUS, C., PEPIN, L., RITZ, C., SALTZMAN, E. & STIEVENARD, M. 1999. Climate and atmospheric history of the past 420,000 years from the Vostok ice core, Antarctica. *Nature,* 399**,** 429-436.

PETSCH, S. T. 2014. The global oxygen cycle. Treatise in Geochemistry (2nd Edition).

PIERREHUMBERT, R. T., ABBOT, D. S., VOIGT, A. & KOLL, D. 2011. Climate of the Neoproterozoic. *Annual Review of Earth and Planetary Sciences,* 39**,** 417-460.

PLANAVSKY, N. J., ASAEL, D., HOFMANN, A., REINHARD, C. T., LALONDE, S. V., KNUDSEN, A., WANG, X., OSSA, F. O., PECOITS, E. & SMITH, A. J. 2014a. Evidence for oxygenic photosynthesis half a billion years before the Great Oxidation Event. *Nature geoscience,* 7**,** 283-286.

PLANAVSKY, N. J., BEKKER, A., HOFMANN, A., OWENS, J. D. & LYONS, T. W. 2012. Sulfur record of rising and falling marine oxygen and sulfate levels during the Lomagundi event. *Proceedings of the National Academy of Sciences,* 109**,** 18300-18305.

PLANAVSKY, N. J., CROWE, S. A., FAKHRAEE, M., BEATY, B., REINHARD, C. T., MILLS, B. J. W., HOLSTEGE, C. & KONHAUSER, K. O. 2021. Evolution of the structure and impact of Earth's biosphere. *Nature Reviews Earth & Environment,* 2**,** 123-139.

PLANAVSKY, N. J., MCGOLDRICK, P., SCOTT, C. T., LI, C., REINHARD, C. T., KELLY, A. E., CHU, X., BEKKER, A., LOVE, G. D. & LYONS, T. W. 2011. Widespread iron-rich conditions in the mid-Proterozoic ocean. *Nature,* 477**,** 448-451.

PLANAVSKY, N. J., REINHARD, C. T., WANG, X., THOMSON, D., MCGOLDRICK, P., RAINBIRD, R. H., JOHNSON, T., FISCHER, W. W. & LYONS, T. W. 2014b. Low Mid-Proterozoic atmospheric oxygen levels and the delayed rise of animals. *Science,* 346**,** 635-638.

PORTER, S. M. 2007. Seawater Chemistry and Early Carbonate Biomineralization. *Science,* 316**,** 1302-1302.

POULTON, S. W., BEKKER, A., CUMMING, V. M., ZERKLE, A. L., CANFIELD, D. E. & JOHNSTON, D. T. 2021. A 200-million-year delay in permanent atmospheric oxygenation. *Nature,* 592**,** 232-+.

PRAETORIUS, S. K., MIX, A. C., WALCZAK, M. H., WOLHOWE, M. D., ADDISON, J. A. & PRAHL, F. G. 2015. North Pacific deglacial hypoxic events linked to abrupt ocean warming. *Nature,* 527**,** 362-366.

PRAVE, A. R., KIRSIMAE, K., LEPLAND, A., FALLICK, A. E., KREITSMANN, T., DEINES, Y. E., ROMASHKIN, A. E., RYCHANCHIK, D. V., MEDVEDEV, P. V., MOUSSAVOU, M., BAKAKAS, K. & HODGSKISS, M. S. W. 2022. The grandest of them all: the Lomagundi-Jatuli Event and Earth's oxygenation. *Journal of the Geological Society,* 179.

PRESENT, T. M., ADKINS, J. F. & FISCHER, W. W. 2020. Variability in Sulfur Isotope Records of Phanerozoic Seawater Sulfate. *Geophysical Research Letters,* 47.

QUADFASEL, D. R. & SCHOTT, F. 1982. Water-mass distributions at intermediate layers off the Somali Coast during the onset of the southwest monsoon, 1979. *Journal of Physical Oceanography,* 12**,** 1358-1372.

RAISWELL, R., HARDISTY, D., LYONS, T., CANFIELD, D., OWENS, J., PLANAVSKY, N., POULTON, S. & REINHARD, C. 2018. The iron paleoredox proxies: A guide to the pitfalls, problems and proper practice. *American Journal of Science*.

RAPP, I., SCHLOSSER, C., BARRAQUETA, J. L. M., WENZEL, B., LUDKE, J., SCHOLTEN, J., GASSER, B., REICHERT, P., GLEDHILL, M., DENGLER, M. & ACHTERBERG, E. P. 2019. Controls on redox-sensitive trace metals in the Mauritanian oxygen minimum zone. *Biogeosciences,* 16**,** 4157-4182.

RAPP, I., SCHLOSSER, C., BROWNING, T. J., WOLF, F., LE MOIGNE, F. A. C., GLEDHILL, M. & ACHTERBERG, E. P. 2020. El Nino-Driven Oxygenation Impacts Peruvian Shelf Iron Supply to the South Pacific Ocean. *Geophysical Research Letters,* 47.

RASHBY, S. E., SESSIONS, A. L., SUMMONS, R. E. & NEWMAN, D. K. 2007. Biosynthesis of 2-methylbacteriohopanepolyols by an anoxygenic phototroph. *Proceedings of the National Academy of Sciences of the United States of America,* 104**,** 15099-15104.

RAVEN, M. R., KEIL, R. G. & WEBB, S. M. 2021. Microbial sulfate reduction and organic sulfur formation in sinking marine particles. *Science,* 371**,** 178.

REERSHEMIUS, T. & PLANAVSKY, N. J. 2021. What controls the duration and intensity of ocean anoxic events in the Paleozoic and the Mesozoic? *Earth-Science Reviews,* 221**,** 103787.

REICHART, G. J., LOURENS, L. J. & ZACHARIASSE, W. J. 1998. Temporal variability in the northern Arabian Sea oxygen minimum zone (OMZ) during the last 225,000 years. *Paleoceanography,* 13**,** 607-621.

REINHARD, C., PLANAVSKY, N., OLSON, S., LYONS, T. & ERWIN, D. 2016a. Earth's oxygen cycle and the evolution of metazoan life. *Proceedings of the National Academy of Sciences*.

REINHARD, C. T., LALONDE, S. V. & LYONS, T. W. 2013a. Oxidative sulfide dissolution on the early Earth. *Chemical Geology,* 362**,** 44-55.

REINHARD, C. T. & PLANAVSKY, N. J. 2022. The History of Ocean Oxygenation. *Annual Review of Marine Science,* 14**,** 331-353.

REINHARD, C. T., PLANAVSKY, N. J. & LYONS, T. W. 2013b. Long-term sedimentary recycling of rare sulphur isotope anomalies. *Nature,* 497**,** 100-103.

REINHARD, C. T., PLANAVSKY, N. J., OLSON, S. L., LYONS, T. W. & ERWIN, D. H. 2016b. Earth's oxygen cycle and the evolution of animal life. *Proceedings of the National Academy of Sciences,* 113**,** 8933-8938.

REINHARD, C. T., PLANAVSKY, N. J., ROBBINS, L. J., PARTIN, C. A., GILL, B. C., LALONDE, S. V., BEKKER, A., KONHAUSER, K. O. & LYONS, T. W. 2013c. Proterozoic ocean redox and biogeochemical stasis. *Proceedings of the National Academy of Sciences,* 110**,** 5357-5362.

REINHARD, C. T., RAISWELL, R., SCOTT, C., ANBAR, A. D. & LYONS, T. W. 2009. A late Archean sulfidic sea stimulated by early oxidative weathering of the continents. *Science,* 326**,** 713-716.

RESING, J. A., SEDWICK, P. N., GERMAN, C. R., JENKINS, W. J., MOFFETT, J. W., SOHST, B. M. & TAGLIABUE, A. 2015. Basin-scale transport of hydrothermal dissolved metals across the South Pacific Ocean. *Nature,* 523**,** 200-U140.

REVSBECH, N. P., LARSEN, L. H., GUNDERSEN, J., DALSGAARD, T., ULLOA, O. & THAMDRUP, B. 2009. Determination of ultra-low oxygen concentrations in oxygen minimum zones by the STOX sensor. *Limnol. Oceanogr. Methods,* 7**,** 371-381.

REYES-UMANA, V., HENNING, Z., LEE, K., BARNUM, T. P. & COATES, J. D. 2022. Genetic and phylogenetic analysis of dissimilatory iodate-reducing bacteria identifies potential niches across the world's oceans. *Isme Journal,* 16**,** 38-49.

RIDGWELL, A. 2005. A Mid Mesozoic Revolution in the regulation of ocean chemistry. *Marine Geology,* 217**,** 339-357.

RIDING, R., FRALICK, P. & LIANG, L. 2014. Identification of an Archean marine oxygen oasis. *Precambrian Research,* 251**,** 232-237.

RIDING, R., LIANG, L. & FRALICK, P. 2022. Oxygen-induced chemocline precipitation between Archean Fe-rich and Fe-poor carbonate seas. *Precambrian Research,* 383.

RIEDINGER, N., SCHOLZ, F., ABSHIRE, M. L. & ZABEL, M. 2021. Persistent deep water anoxia in the eastern South Atlantic during the last ice age. *Proceedings of the National Academy of Sciences of the United States of America,* 118.

ROONEY, A. D., MACDONALD, F. A., STRAUSS, J. V., DUDAS, F. O., HALLMANN, C. & SELBY, D. 2013. Re-Os geochronology and coupled Os-Sr isotope constraints on the Sturtian snowball Earth. *Proceedings of the National Academy of Sciences,* 111**,** 51-56.

ROSE, A. L. 2012. The influence of extracellular superoxide on iron redox chemistry and bioavailability to aquatic microorganisms. *Frontiers in Microbiology,* 3.

ROSHAN, S. & WU, J. F. 2015a. Cadmium regeneration within the North Atlantic. *Global Biogeochemical Cycles,* 29**,** 2082-2094.

ROSHAN, S. & WU, J. F. 2015b. Water mass mixing: The dominant control on the zinc distribution in the North Atlantic Ocean. *Global Biogeochemical Cycles,* 29**,** 1060-1074.

ROTHMAN, D. H., HAYES, J. M. & SUMMONS, R. E. 2003. Dynamics of the Neoproterozoic carbon cycle. *Proceedings of the National Academy of Sciences of the United States of America,* 100**,** 8124-8129.

RUE, E. L., SMITH, G. J., CUTTER, G. A. & BRULAND, K. W. 1997. The response of trace element redox couples to suboxic conditions in the water column. *Deep-Sea Research Part I-Oceanographic Research Papers,* 44**,** 113-134.

RUNNEGAR, B. 2000. Loophole for snowball Earth. *Nature,* 405**,** 403-404.

SAHOO, S. K., PLANAVSKY, N. J., JIANG, G., KENDALL, B., OWENS, J. D., WANG, X., SHI, X., ANBAR, A. D. & LYONS, T. W. 2016. Oceanic oxygenation events in the anoxic Ediacaran ocean. *Geobiology,* 14**,** 457-468.

SAHOO, S. K., PLANAVSKY, N. J., KENDALL, B., WANG, X., SHI, X., SCOTT, C., ANBAR, A. D., LYONS, T. W. & JIANG, G. 2012. Ocean oxygenation in the wake of the Marinoan glaciation. *Nature,* 489**,** 546-549.

SALTZMAN, M. R., EDWARDS, C. T., ADRAIN, J. M. & WESTROP, S. R. 2015. Persistent oceanic anoxia and elevated extinction rates separate the Cambrian and Ordovician radiations. *Geology,* 43**,** 807-810.

SALTZMAN, M. R. & THOMAS, E. 2012. Carbon Isotope Stratigraphy. *The Geologic Time Scale.* Elsevier.

SANCHEZ-BARACALDO, P., RAVEN, J. A., PISANI, D. & KNOLL, A. H. 2017. Early photosynthetic eukaryotes inhabited low-salinity habitats. *Proceedings of the National Academy of Sciences of the United States of America,* 114**,** E7737-E7745.

SAUNDERS, J. K., MCILVIN, M. R., DUPONT, C. L., KAUL, D., MORAN, D. M., HORNER, T., LAPERRIERE, S. M., WEBB, E. A., BOSAK, T., SANTORO, A. E. & SAITO, M. A. 2022. Microbial functional diversity across biogeochemical provinces in the central Pacific Ocean. *Proceedings of the National Academy of Sciences of the United States of America,* 119**,** e2200014119-e2200014119.

SCHACHAT, S. R., LABANDEIRA, C. C., SALTZMAN, M. R., CRAMER, B. D., PAYNE, J. L. & BOYCE, C. K. 2018. Phanerozoic pO_2 and the early evolution of terrestrial animals. *Proceedings of the Royal Society B: Biological Sciences,* 285**,** 20172631.

SCHIRRMEISTER, B. E., DE VOS, J. M., ANTONELLI, A. & BAGHERI, H. C. 2013. Evolution of multicellularity coincided with increased diversification of cyanobacteria and the Great Oxidation Event. *Proceedings of the National Academy of Sciences of the United States of America,* 110**,** 1791-1796.

SCHLITZER, R., ANDERSON, R. F., DODAS, E. M., LOHAN, M., GEIBERE, W., TAGLIABUE, A., BOWIE, A., JEANDEL, C., MALDONADO, M. T., LANDING, W. M., COCKWELL, D., ABADIE, C., ABOUCHAMI, W., ACHTERBERG, E. P., AGATHER, A., AGULIAR-ISLAS, A., VAN AKEN, H. M., ANDERSEN, M., ARCHER, C., AURO, M., DE BAAR, H. J., BAARS, O., BAKER, A. R., BAKKER, K., BASAK, C., BASKARAN, M., BATES, N. R., BAUCH, D., VAN BEEK, P., BEHRENS, M. K., BLACK, E., BLUHM, K., BOPP, L., BOUMAN, H., BOWMAN, K., BOWN, J., BOYD, P., BOYE, M., BOYLE, E. A., BRANELLEC, P., BRIDGESTOCK, L., BRISSEBRAT, G., BROWNING, T., BRULAND, K. W., BRUMSACK, H.-J., BRZEZINSKI, M., BUCK, C. S., BUCK, K. N., BUESSELER, K., BULL, A., BUTLER, E., CAI, P., CAMARA MOR, P., CARDINAL, D., CARLSON, C., CARRASCO, G., CASACUBERTA, N., CASCIOTTI, K. L., CASTRILLEJO, M., CHAMIZO, E., CHANCE, R., CHARETTE, M. A., CHAVES, J. E., CHENG, H., CHEVER, F., CHRISTL, M., CHURCH, T. M., CLOSSET, I., COLMAN, A., CONWAY, T. M., COSSA, D., CROOT, P., CULLEN, J. T., CUTTER, G. A., DANIELS, C., DEHAIRS, F., DENG, F., DIEU, H. T., DUGGAN, B., DULAQUAIS, G., DUMOUSSEAUD, C., ECHEGOYEN-SANZ, Y., EDWARDS, R. L., ELLWOOD, M., FAHRBACH, E., FITZSIMMONS, J. N., FLEGAL, A. R., FLEISHER, M. Q., VAN DE FLIERDT, T., FRANK, M., FRIEDRICH, J., FRIPIAT, F., FROELLJE, H., GALER, S. J. G., GAMO, T., GANESHRAM, R. S., GARCIA-ORELLANA, J., GARCIA-SOLSONA, E., GAULT-RINGOLD, M., GEORGE, E., et al. 2018. The GEOTRACES Intermediate Data Product 2017. *Chemical Geology,* 493**,** 210-223.

SCHLOSSER, C., STREU, P., FRANK, M., LAVIK, G., CROOT, P. L., DENGLER, M. & ACHTERBERG, E. P. 2018. H2S events in the Peruvian oxygen minimum zone facilitate enhanced dissolved Fe concentrations. *Scientific Reports,* 8.

SCHMIDT, H., CZESCHEL, R. & VISBECK, M. 2020. Seasonal variability of the Arabian Sea intermediate circulation and its impact on seasonal changes of the upper oxygen minimum zone. *Ocean Science,* 16**,** 1459-1474.

SCHMIDTKO, S., STRAMMA, L. & VISBECK, M. 2017. Decline in global oceanic oxygen content during the past five decades. *Nature,* 542**,** 335-339.

SCHOLZ, F., HENSEN, C., NOFFKE, A., ROHDE, A., LIEBETRAU, V. & WALLMANN, K. 2011. Early diagenesis of redox-sensitive trace metals in the Peru upwelling area - response to ENSO-related oxygen fluctuations in the water column. *Geochimica Et Cosmochimica Acta,* 75**,** 7257-7276.

SCHOLZ, F., SEVERMANN, S., MCMANUS, J. & HENSEN, C. 2014a. Beyond the Black Sea paradigm: The sedimentary fingerprint of an open-marine iron shuttle. *Geochimica Et Cosmochimica Acta,* 127**,** 368-380.

SCHOLZ, F., SEVERMANN, S., MCMANUS, J., NOFFKE, A., LOMNITZ, U. & HENSEN, C. 2014b. On the isotope composition of reactive iron in marine sediments: Redox shuttle versus early diagenesis. *Chemical Geology,* 389**,** 48-59.

SCHRAG, D. P., HIGGINS, J. A., MACDONALD, F. A. & JOHNSTON, D. T. 2013. Authigenic Carbonate and the History of the Global Carbon Cycle. *Science,* 339**,** 540-543.

SCOTT, C. T., BEKKER, A., REINHARD, C. T., SCHNETGER, B., KRAPEŽ, B., RUMBLE III, D. & LYONS, T. W. 2011. Late Archean euxinic conditions before the rise of atmospheric oxygen. *Geology,* 39**,** 119-122.

SEVERMANN, S., JOHNSON, C. M., BEARD, B. L. & MCMANUS, J. 2006. The effect of early diagenesis on the Fe isotope compositions of porewaters and authigenic minerals in continental margin sediments. *Geochimica et Cosmochimica Acta,* 70**,** 2006-2022.

SHANKLE, M. G., BURLS, N. J., FEDOROV, A. V., THOMAS, M. D., LIU, W., PENMAN, D. E., FORD, H. L., JACOBS, P. H., PLANAVSKY, N. J. & HULL, P. M. 2021. Pliocene decoupling of equatorial Pacific temperature and pH gradients. *Nature,* 598**,** 457-+.

SHANKS, A. L. & REEDER, M. L. 1993. REDUCING MICROZONES AND SULFIDE PRODUCTION IN MARINE SNOW. *Marine Ecology Progress Series,* 96**,** 43-47.

SHEEN, A. I., KENDALL, B., REINHARD, C. T., CREASER, R. A., LYONS, T. W., BEKKER, A., POULTON, S. W. & ANBAR, A. D. 2018. A model for the oceanic mass balance of rhenium and implications for the extent of Proterozoic ocean anoxia. *Geochimica Et Cosmochimica Acta,* 227**,** 75-95.

SHERWEN, T., CHANCE, R. J., TINEL, L., ELLIS, D., EVANS, M. J. & CARPENTER, L. J. 2019. A machine-learning-based global sea-surface iodide distribution. *Earth System Science Data,* 11**,** 1239-1262.

SHRIKUMAR, A., LAWRENCE, R. & CASCIOTTI, K. L. 2022. PYOMPA version 0.3. *Authorea Preprints*.

SIANI, G., MICHEL, E., DE POL-HOLZ, R., DEVRIES, T., LAMY, F., CAREL, M., ISGUDER, G., DEWILDE, F. & LOURANTOU, A. 2013. Carbon isotope records reveal precise timing of enhanced Southern Ocean upwelling during the last deglaciation. *Nature Communications,* 4.

SINGH, N. D., SINGH, S. K., MALLA, N. & CHINNI, V. 2023. Biogeochemical cycling of dissolved manganese in the Arabian Sea. *Geochimica et Cosmochimica Acta*.

SLOTZNICK, S. P., JOHNSON, J. E., RASMUSSEN, B., RAUB, T. D., WEBB, S. M., ZI, J.-W., KIRSCHVINK, J. L. & FISCHER, W. W. 2022. Reexamination of 2.5-Ga "whiff" of oxygen interval points to anoxic ocean before GOE. *Science Advances,* 8.

SLOTZNICK, S. P., SPERLING, E. A., TOSCA, N. J., MILLER, A. J., CLAYTON, K. E., VAN HELMOND, N. A. G. M., SLOMP, C. P. & SWANSON-HYSELL, N. L. 2020. Unraveling the Mineralogical Complexity of Sediment Iron Speciation Using Sequential Extractions. *Geochemistry Geophysics Geosystems,* 21.

SPERLING, E. A., BOAG, T. H., DUNCAN, M. I., ENDRIGA, C. R., MARQUEZ, J. A., MILLS, D. B., MONARREZ, P. M., SCLAFANI, J. A., STOCKEY, R. G. & PAYNE, J. L. 2022. Breathless through Time: Oxygen and Animals across Earth's History. *Biological Bulletin*.

SPERLING, E. A., FRIEDER, C. A., RAMAN, A. V., GIRGUIS, P. R., LEVIN, L. A. & KNOLL, A. H. 2013. Oxygen, ecology, and the Cambrian radiation of animals. *Proceedings of the National Academy of Sciences,* 110**,** 13446-13451.

SPERLING, E. A., KNOLL, A. H. & GIRGUIS, P. R. 2015a. The Ecological Physiology of Earth's Second Oxygen Revolution. *Annual Review of Ecology, Evolution, and Systematics,* 46**,** 215-235.

SPERLING, E. A., WOLOCK, C. J., MORGAN, A. S., GILL, B. C., KUNZMANN, M., HALVERSON, G. P., MACDONALD, F. A., KNOLL, A. H. & JOHNSTON, D. T. 2015b. Statistical analysis of iron geochemical data suggests limited late Proterozoic oxygenation. *Nature,* 523**,** 451-454.

SPINKS, S. C., SPERLING, E. A., THORNE, R. L., LAFOUNTAIN, F., WHITE, A. J. R., ARMSTRONG, J., WOLTERING, M. & TYLER, I. M. 2023. Mesoproterozoic surface oxygenation accompanied major sedimentary manganese deposition at 1.4 and 1.1 Ga. *Geobiology,* 21**,** 28-43.

STEWART, J. A., GUTJAHR, M., PEARCE, F., SWART, P. K. & FOSTER, G. L. 2015. Boron during meteoric diagenesis and its potential implications for Marinoan snowball Earth δ11B-pH excursions. *Geology,* 43**,** 627-630.

STRAMMA, L., JOHNSON, G. C., SPRINTALL, J. & MOHRHOLZ, V. 2008. Expanding Oxygen-Minimum Zones in the Tropical Oceans. *Science,* 320**,** 655-658.

STUEEKEN, E. E., BUICK, R. & ANBAR, A. D. 2015. Selenium isotopes support free O-2 in the latest Archean. *Geology,* 43**,** 259-262.

SUN, D., ITO, T. & BRACCO, A. 2017. Oceanic Uptake of Oxygen During Deep Convection Events Through Diffusive and Bubble-Mediated Gas Exchange. *Global Biogeochemical Cycles,* 31**,** 1579-1591.

SUN, X., FREY, C., GARCIA-ROBLEDO, E., JAYAKUMAR, A. & WARD, B. B. 2021. Microbial niche differentiation explains nitrite oxidation in marine oxygen minimum zones. *Isme Journal,* 15**,** 1317-1329.

SUNDA, W. G., HUNTSMAN, S. A. & HARVEY, G. R. 1983. Photoreduction of manganese oxides in seawater and its geochemical and biological implications. *Nature,* 301**,** 234-236.

SUTHERLAND, K. M., WANKEL, S. D. & HANSEL, C. M. 2020. Dark biological superoxide production as a significant flux and sink of marine dissolved oxygen. *Proceedings of the National Academy of Sciences of the United States of America,* 117**,** 3433-3439.

SWANNER, E. D., LAMBRECHT, N., WITTKOP, C., HARDING, C., KATSEV, S., TORGESON, J. & POULTON, S. W. 2020. The biogeochemistry of ferruginous lakes and past ferruginous oceans. *Earth-Science Reviews,* 211.

SWART, P. K. 2008. Global synchronous changes in the carbon isotopic composition of carbonate sediments unrelated to changes in the global carbon cycle. *Proceedings of the National Academy of Sciences of the United States of America,* 105**,** 13741-13745.

SWART, P. K. & EBERLI, G. 2005. The nature of the δ 13 C of periplatform sediments: implications for stratigraphy and the global carbon cycle. *Sedimentary Geology,* 175**,** 115-129.

TAHATA, M., SAWAKI, Y., YOSHIYA, K., NISHIZAWA, M., KOMIYA, T., HIRATA, T., YOSHIDA, N., MARUYAMA, S. & WINDLEY, B. F. 2015. The marine environments encompassing the Neoproterozoic glaciations: Evidence from C, Sr and Fe isotope ratios in the Hecla Hoek Supergroup in Svalbard. *Precambrian Research,* 263**,** 19-42.

TANG, W., LI, Z. & CASSAR, N. 2019. Machine Learning Estimates of Global Marine Nitrogen Fixation. *Journal of Geophysical Research-Biogeosciences,* 124**,** 717-730.

TARHAN, L. G. 2018. The early Paleozoic development of bioturbation—Evolutionary and geobiological consequences. *Earth-Science Reviews,* 178**,** 177-207.

TARHAN, L. G., DROSER, M. L., PLANAVSKY, N. J. & JOHNSTON, D. T. 2015. Protracted development of bioturbation through the early Palaeozoic Era. *Nature Geoscience,* 8**,** 865-869.

THAMDRUP, B., DALSGAARD, T. & REVSBECH, N. P. 2012. Widespread functional anoxia in the oxygen minimum zone of the Eastern South Pacific. *Deep Sea Research Part I: Oceanographic Research Papers,* 65**,** 36-45.

THAMDRUP, B., STEINSDOTTIR, H. G. R., BERTAGNOLLI, A., PADILLA, C., PATIN, N. V., GARCIA-ROBLEDO, E., BRISTOW, L. A. & STEWART, F. J. 2019. Anaerobic methane oxidation is an important sink for methane in the ocean's largest oxygen minimum zone. *Limnology and Oceanography,* 64**,** 2569-2585.

THEM, T. R., GILL, B. C., CARUTHERS, A. H., GERHARDT, A. M., GRÖCKE, D. R., LYONS, T. W., MARROQUÍN, S. M., NIELSEN, S. G., TRABUCHO ALEXANDRE, J. P. & OWENS, J. D. 2018. Thallium isotopes reveal protracted anoxia during the Toarcian (Early Jurassic) associated with volcanism, carbon burial, and mass extinction. *Proceedings of the National Academy of Sciences,* 115**,** 6596-6601.

TIANO, L., GARCIA-ROBLEDO, E., DALSGAARD, T., DEVOL, A. H., WARD, B. B., ULLOA, O., CANFIELD, D. E. & REVSBECH, N. P. 2014. Oxygen distribution and aerobic respiration in the north and south eastern tropical Pacific oxygen minimum zones. *Deep-Sea Research Part I-Oceanographic Research Papers,* 94**,** 173-183.

TOMCZAK, M. & GODFREY, J. S. 2003. *Regional oceanography: an introduction*, Daya books.

TRIBOVILLARD, N., ALGEO, T. J., LYONS, T. & RIBOULLEAU, A. 2006. Trace metals as paleoredox and paleoproductivity proxies: An update. *Chemical Geology,* 232**,** 12-32.

TSANDEV, I., SLOMP, C. P. & VAN CAPPELLEN, P. 2008. Glacial-interglacial variations in marine phosphorus cycling: Implications for ocean productivity. *Global Biogeochemical Cycles,* 22.

TSEMENTZI, D., WU, J., DEUTSCH, S., NATH, S., RODRIGUEZ-R, L. M., BURNS, A. S., RANJAN, P., SARODE, N., MALMSTROM, R. R., PADILLA, C. C., STONE, B. K., BRISTOW, L. A., LARSEN,

M., GLASS, J. B., THAMDRUP, B., WOYKE, T., KONSTANTINIDIS, K. T. & STEWART, F. J. 2016. SAR11 bacteria linked to ocean anoxia and nitrogen loss. *Nature,* 536**,** 179-+.
TURGEON, S. C. & CREASER, R. A. 2008. Cretaceous oceanic anoxic event 2 triggered by a massive magmatic episode. *Nature,* 454**,** 323-326.
TZIPERMAN, E., HALEVY, I., JOHNSTON, D. T., KNOLL, A. H. & SCHRAG, D. P. 2011. Biologically induced initiation of Neoproterozoic snowball-Earth events. *Proceedings of the National Academy of Sciences,* 108**,** 15091-15096.
ULLOA, O., CANFIELD, D. E., DELONG, E. F., LETELIER, R. M. & STEWART, F. J. 2012. Microbial oceanography of anoxic oxygen minimum zones. *Proceedings of the National Academy of Sciences of the United States of America,* 109**,** 15996-16003.
UVEGES, B. T., IZON, G., ONO, S., BEUKES, N. J. & SUMMONS, R. E. 2023. Reconciling discrepant minor sulfur isotope records of the Great Oxidation Event. *Nature communications,* 14**,** 279-279.
VAIL, P. R., HARDENBOL, J. & TODD, R. G. 1984. Jurassic Unconformities, Chronostratigraphy, and Sea-Level Changes from Seismic Stratigraphy and Biostratigraphy. *AAPG Special Bulletin***,** 129-144.
VAN DE VELDE, S. J., HÜLSE, D., REINHARD, C. T. & RIDGWELL, A. 2021. Iron and sulfur cycling in the cGENIE. muffin Earth system model (v0. 9.21). *Geoscientific Model Development,* 14**,** 2713-2745.
VEDAMATI, J., GOEPFERT, T. & MOFFETT, J. W. 2014. Iron speciation in the eastern tropical South Pacific oxygen minimum zone off Peru. *Limnology and Oceanography,* 59**,** 1945-1957.
VEIZER, J., ALA, D., AZMY, K., BRUCKSCHEN, P., BUHL, D., BRUHN, F., CARDEN, G. A. F., DIENER, A., EBNETH, S., GODDERIS, Y., JASPER, T., KORTE, C., PAWELLEK, F., PODLAHA, O. G. & STRAUSS, H. 1999. $^{87}Sr/^{86}Sr$, $\delta^{13}C$ and $\delta^{18}O$ evolution of Phanerozoic seawater. *Chemical Geology,* 161**,** 59-88.
VERGARA, O., DEWITTE, B., MONTES, I., GARCON, V., RAMOS, M., PAULMIER, A. & PIZARRO, O. 2016. Seasonal variability of the oxygen minimum zone off Peru in a high-resolution regional coupled model. *Biogeosciences,* 13**,** 4389-4410.
VOELKER, B. M. & SEDLAK, D. L. 1995. Iron reduction by photoproduced superoxide in seawater. *Marine Chemistry,* 50**,** 93-102.
VOELKER, B. M., SEDLAK, D. L. & ZAFIRIOU, O. C. 2000. Chemistry of superoxide radical in seawater: Reactions with organic Cu complexes. *Environmental Science & Technology,* 34**,** 1036-1042.
VOIGT, S., GALE, A. S. & VOIGT, T. 2006. Sea-level change, carbon cycling and palaeoclimate during the Late Cenomanian of northwest Europe; an integrated palaeoenvironmental analysis. *Cretaceous Research,* 27**,** 836-858.
WALLACE, M. W., HOOD, A. V., SHUSTER, A., GREIG, A., PLANAVSKY, N. J. & REED, C. P. 2017. Oxygenation history of the Neoproterozoic to early Phanerozoic and the rise of land plants. *Earth and Planetary Science Letters,* 466**,** 12-19.
WALLMANN, K. 2003. Feedbacks between oceanic redox states and marine productivity: A model perspective focused on benthic phosphorus cycling. *Global Biogeochemical Cycles,* 17.

WANG, C. L., REINHARD, C. T., RYBACKI, K. S., HARDISTY, D. S., OSSA, F. O., WANG, X. L., HOFMANN, A., ASAEL, D., ROBBINS, L. J., ZHANG, L. C. & PLANAVSKY, N. J. 2021. Chromium isotope systematics and the diagenesis of marine carbonates. *Earth and Planetary Science Letters,* 562.

WANG, D., GOUHIER, T. C., MENGE, B. A. & GANGULY, A. R. 2015. Intensification and spatial homogenization of coastal upwelling under climate change. *Nature,* 518**,** 390-394.

WANG, J., TARHAN, L. G., JACOBSON, A. D., OEHLERT, A. M. & PLANAVSKY, N. J. 2023. The evolution of the marine carbonate factory. *Nature*.

WANG, S.-J., RUDNICK, R. L., GASCHNIG, R. M., WANG, H. & WASYLENKI, L. E. 2019. Methanogenesis sustained by sulfide weathering during the Great Oxidation Event. *Nature Geoscience,* 12**,** 296-+.

WEI, G.-Y., PLANAVSKY, N. J., HE, T., ZHANG, F., STOCKEY, R. G., COLE, D. B., LIN, Y.-B. & LING, H.-F. 2021. Global marine redox evolution from the late Neoproterozoic to the early Paleozoic constrained by the integration of Mo and U isotope records. *Earth-Science Reviews,* 214.

WHITE, L. D., GARRISON, R. E. & BARRON, J. A. 1992. Miocene intensification of upwelling along the California margin as recorded in siliceous facies of the Monterey Formation and offshore DSDP sites. *Geological Society, London, Special Publications,* 64**,** 429-442.

WILMETH, D. T., LALONDE, S. V., BERELSON, W. M., PETRYSHYN, V., CELESTIAN, A. J., BEUKES, N. J., AWRAMIK, S. M., SPEAR, J. R., MAHSEREDJIAN, T. & CORSETTI, F. A. 2022. Evidence for benthic oxygen production in Neoarchean lacustrine stromatolites. *Geology,* 50**,** 907-911.

WINCKLER, G., ANDERSON, R. F., FLEISHER, M. Q., MCGEE, D. & MAHOWALD, N. M. 2008. Covariant Glacial-Interglacial Dust Fluxes in the Equatorial Pacific and Antarctica | Science. *Science,* 320**,** 93-96.

WINGUTH, A. M. E., THOMAS, E. & WINGUTH, C. 2012. Global decline in ocean ventilation, oxygenation, and productivity during the Paleocene-Eocene Thermal Maximum: Implications for the benthic extinction. *Geology,* 40**,** 263-266.

WISHNER, K. F., OUTRAM, D. M., SEIBEL, B. A., DALY, K. L. & WILLIAMS, R. L. 2013. Zooplankton in the eastern tropical north Pacific: Boundary effects of oxygen minimum zone expansion. *Deep-Sea Research Part I-Oceanographic Research Papers,* 79**,** 122-140.

WOOD, R. & ERWIN, D. H. 2018. Innovation not recovery: dynamic redox promotes metazoan radiations: Dynamic redox promotes radiations. *Biological Reviews,* 93**,** 863-873.

WOOD, R. A., POULTON, S. W., PRAVE, A. R., HOFFMANN, K. H., CLARKSON, M. O., GUILBAUD, R., LYNE, J. W., TOSTEVIN, R., BOWYER, F., PENNY, A. M., CURTIS, A. & KASEMANN, S. A. 2015. Dynamic redox conditions control late Ediacaran metazoan ecosystems in the Nama Group, Namibia. *Precambrian Research,* 261**,** 252-271.

WUTTIG, K., HELLER, M. I. & CROOT, P. L. 2013. Pathways of Superoxide (O-2(-)) Decay in the Eastern Tropical North Atlantic. *Environmental Science & Technology,* 47**,** 10249-10256.

ZEEBE, R. E. 2012. LOSCAR: Long-term ocean-atmosphere-sediment carbon cycle reservoir model v2. 0.4. *Geoscientific Model Development,* 5**,** 149.

ZERKLE, A. L., POULTON, S. W., NEWTON, R. J., METTAM, C., CLAIRE, M. W., BEKKER, A. & JUNIUM, C. K. 2017. Onset of the aerobic nitrogen cycle during the Great Oxidation Event. *Nature,* 542**,** 465-+.

ZHANG, F., LENTON, T. M., DEL REY, A., ROMANIELLO, S. J., CHEN, X., PLANAVSKY, N. J., CLARKSON, M. O., DAHL, T. W., LAU, K. V., WANG, W., LI, Z., ZHAO, M., ISSON, T., ALGEO, T. J. & ANBAR, A. D. 2020. Uranium isotopes in marine carbonates as a global ocean paleoredox proxy: A critical review. *Geochimica Et Cosmochimica Acta,* 287**,** 27-49.

ZHANG, F., XIAO, S., ROMANIELLO, S. J., HARDISTY, D., LI, C., MELEZHIK, V., POKROVSKY, B., CHENG, M., SHI, W., LENTON, T. M. & ANBAR, A. D. 2019. Global marine redox changes drove the rise and fall of the Ediacara biota. *Geobiology,* 17**,** 594-610.

ZHANG, F. F., ROMANIELLO, S. J., ALGEO, T. J., LAU, K. V., CLAPHAM, M. E., RICHOZ, S., HERRMANN, A. D., SMITH, H., HORACEK, M. & ANBAR, A. D. 2018. Multiple episodes of extensive marine anoxia linked to global warming and continental weathering following the latest Permian mass extinction. *Science Advances,* 4.

ZHAO, M., MILLS, B. J., HOMOKY, W. B. & PEACOCK, C. L. 2023. Oxygenation of the Earth aided by mineral–organic carbon preservation. *Nature Geoscience***,** 1-6.

ZHURAVLEV, A. Y. & WOOD, R. 2020. Dynamic and synchronous changes in metazoan body size during the Cambrian Explosion. *Scientific Reports,* 10.

ZHURAVLEV, A. Y. & WOOD, R. A. 2008. Eve of biomineralization: Controls on skeletal mineralogy. *Geology,* 36**,** 923.